SYNTHESIS AND CHARACTERIZATION OF MECHANICAL PROPERTIES OF A NOVEL BIOCERAMIC COMPOSITE MATERIAL FOR BIOLOGICAL APPLICATIONS

By

Jillian Ladegard B.A., B.E.

RECOMMENDED:

Advisory Committee Chair

Chair, Department of Mechanical Engineering

APPROVED:

Dean, College of Engineering and Mines

Dean of the Graduate School

Aug 9, 2010

Date

SYNTHESIS AND CHARACTERIZATION OF MECHANICAL PROPERTIES OF A NOVEL BIOCERAMIC COMPOSITE MATERIAL FOR BIOLOGICAL APPLICATIONS

A

THESIS

Presented to the Faculty

of the University of Alaska Fairbanks

in Partial Fulfillment of the Requirements

for the Degree of

MASTER OF SCIENCE

By

Jillian Ladegard

Fairbanks, Alaska

August 2010

ABSTRACT

Bioceramics are used in a wide range of human skeletal repair and restoration applications as a synthetic bone substitute. 45S5 Bioglass, a bioactive ceramic, exhibits poor mechanical properties limiting the potential of the material and preventing its use in major load bearing applications. This investigation evaluated the synthesis and mechanical properties of a 45S5 Bioglass composite reinforced with different weight percentages of multi-wall carbon nanotubes. The material was analyzed using an X-Ray Diffractometer and a scanning electron microscope to determine the crystal structure, microstructural homogeneity, and surface texture of the composite material. The material was evaluated during the synthesis process to observe the evolution of the composite. Samples were sintered at 1000°C and 850°C to determine the effect of the sintering temperature on the mechanical properties of the composite. Once synthesized, the material was tested using the Vickers hardness indentation test to determine the mechanical properties of the ceramic, as defined by hardness and fracture toughness values. Hardness of the composite decreased with increasing nanotube concentration for all samples. A maximum fracture toughness value of 47.6 $GPa \cdot m^{1/2}$ corresponded to the addition of 1 weight percent multi-wall carbon nanotubes in the composite samples sintered at 1000°C. All of the composite samples sintered at 850°C reported lower fracture toughness values than the pure bioglass samples indicating that sintering temperature affects bonding between the composite components. These results prove that a Bioglass-multi-wall carbon nanotube composite has the potential for use as a synthetic material to restore function in load bearing bones.

TABLE OF CONTENTS

LIST OF FIGURES

Page

LIST OF TABLES

Page

LIST OF APPENDICES

Page

LIST OF EQUATIONS

Page

ACKNOWLEDGEMENTS

I thank my advisor, Dr. Jing Zhang, for his support and guidance of this work. I also thank Dr. Ken Severin, Dr. Tom Trainor, and Eric Johansen, for their help and guidance to use the scanning electron microscope, x-ray Diffractometer, and Engineering Machine Shop equipment. I extend my gratitude to Lily Zhang and Jenny Gu for their post processing ideas regarding sample mounts, grinding procedures, and hardness testing.

I am also grateful for Dr. Jing Zhang's National Science Foundation/Experimental Program to Stimulate Competitive Research Early Career Award, which provided funding to support this research. I thank and recognize the Mechanical Engineering department and the Advanced Instrumentation Laboratory for providing the equipment and facilities to conduct this research as well as the University of Alaska Fairbanks.

CHAPTER 1: Introduction

Bioceramics are used in a wide range of human skeletal repair and restoration applications and are an important synthetic bone substitute. 45S5 Bioglass (Bioglass), a successful bioactive ceramic, exhibits poor mechanical properties limiting the usability of the material and preventing its use in major load bearing applications. This investigation evaluated the mechanical properties of a Bioglass composite reinforced with different weight percentages of multi-wall carbon nanotubes (MWCNTs). The material was analyzed using an X-Ray Diffractometer (XRD) and a scanning electron microscope (SEM) to determine the crystal structure, homogeneity, and surface texture of the composite material. The material was also evaluated during the synthesis process to observe the evolution of the composite. Once synthesized, the mechanical properties of the composite material were measured using the Vickers hardness indentation test to determine composite hardness and fracture toughness. As a conclusion to this investigation, a comparison was established between the weight percentage of MWCNTs present in the composite and the fracture toughness of the material.

1.1. Motivation and Objectives

Substantial research has been completed on carbon nanotubes (CNT)-ceramic composites, however, no investigations have developed a CNT-composite with Bioglass as the ceramic matrix using a mixing, compaction, and sintering process. The objectives of this thesis are to:

- Synthesize and characterize a novel Bioglass-MWCNT composite material
- Characterize the mechanical properties, microstructure, and phase of the composite
- Evaluate the effect of MWCNT concentration on the composite mechanical properties of hardness and fracture toughness
- Determine the optimal weight percent of MWCNTs in the composite

The ultimate goal of this thesis is to determine the potential of this composite for use as a synthetic bone material that can effectively replace and restore function to load bearing bone structures in the human body.

1.2. Thesis Structure

A literature review of biocomposite materials including Bioglass and MWCNTs, synthesis of CNT-composites, and mechanical testing techniques is included in Chapter 2. An overview of the raw materials and synthesis processes utilized in this thesis is presented in Chapter 3. Chapter 4 discusses the experimental procedures and evaluation techniques used to characterize the composite material during and after synthesis. Chapter 5 presents a summary and discussion of results obtained during this thesis investigation. The final conclusions of this thesis are presented and summarized in Chapter 6. The following appendices include additional material, background information, equipment procedures, experimental data, and investigation photographs as identified below:

Appendix A – Material Data Sheets

Appendix B – Equipment Standard Operating Procedures

Appendix C – Experimental Data and Calculations

Appendix D – Photographic Log

CHAPTER 2: Literature Review

For over 40 years scientists and engineers have investigated the use and application of bioactive ceramics, glasses, and glass ceramics to repair and restore human skeletal functionality. During that time, the field of bioceramics has seen major improvements in the diverse range of materials used for clinical applications and also improvements in the quality of bone repair that they offer.

2.1. Research to Date

Bioceramics are defined as a class of ceramic materials used for skeletal repair and reconstruction. These materials have been investigated for many applications including hard tissue replacement and hard tissue regeneration as well as thin coatings for metallic and polymer based implants. Bioceramics are used for numerous applications in the body and can be broken down into two groups, bioinert or bioactive and further into resorbable or non-resorbable [1]. Initial efforts to repair and restore basic structural functions using biomaterials in the 1960's, caused by injury or disease, endeavored to develop and integrate a bioinert material into the body. These first generation materials invoked a minimal biological response from the physiological environment and are classified as bioinert. Materials that are bioinert still induce a physiological response resulting in the encapsulation of the implant in a thin fibrous non-adherent layer, however, the response is considered minimal and is nontoxic [1, 2]. Inert ceramics such as zirconia and alumina were used primarily as femoral heads and were encapsulated as part of an immunoresponse to the foreign body [3].

Researchers soon realized that the success of bioceramic materials was dependent on their ability to achieve a stable attachment to the existing connective tissue through a bioactive response [3]. This prompted an investigation into the physiological structure of bone and the implant environment.

Bone is a living composite made of hard tissue built off a collagen based organic phase embedded with calcium–containing inorganic crystals. Hard tissue is formed from

amorphous calcium phosphate, which evolves towards a noncrystalline calcium-deficient apatite in the presence of carbonate ions [4]. By weight bone contains 10% water, 20% organic material, and 70% mineral matter [3]. The collagen fibrils are a few nanometers (nm) in diameter. The organic material is also composed of other proteins, a cement-like component, and a cellular component, comprised of osteocytes, osteoblasts, and osteoclasts, which aid in dissolution, deposition, and nourishment of the bone [5]. The inorganic component is an apatite which contains calcium and phosphate ions, similar in structure and composition to hydroxyapatite $Ca_{10}(PO_4)_6(OH)_2$, a commonly used bioceramic [6]. The structure of apatite has the ability to accommodate several different ions in its three sub lattice structures. Hydroxyapatite structures are approximately 25-50 nm in size [4]. Bones are formed based on a hierarchical structure and contain a variety of substructures at many different scales. This enables bone to maintain porosity on a micron scale allowing cells to perform formation and regeneration tasks. Many composite materials have been developed to mimic natural bone structure in an attempt to develop a nanoceramic material that enables cell activity and is biocompatible [3].

Several bioglass materials were developed to improve the bioresponse between an implant and the body. Metal and polymer based implants used during the Vietnam War caused the growth of interfacial scar tissue highlighting the need for a material that could bond to existing connective tissues. Bioglass was developed to meet that need in 1967 [1].

A glass is defined as a solid matter without a crystal structure that is arranged as a disordered solid [4]. Bioglass is highly reactive to human tissue and responds similarly to bone when placed in a physiological environment. Through the formation of calcium and phosphorus bonds, bioglass generates the precursors to a carbonated and crystallized apatite coating [4]. The formation of a biologically active hydroxy-carbon apatite layer, chemically and structurally similar to the mineral phase in bone, establishes the bonding interface between the material and living tissues [3]. This surface reaction enables the material to bond with the host tissue and bone [1]. Bioglass is generally composed of a

Na_2O-CaO-P_2O_5-SiO_2 system [3]. Later research showed that bioglass not only bonded with bone, but, also with soft connective tissues [3].

The mechanical properties of bioglass are poor and prevent the material from being used in major load bearing applications or to repair large skeletal defects. Due to the poor mechanical properties, these materials are used to fill small defects, where the rate of regeneration is the main concern, and where mechanical strength is not required. In several cases bioglass materials were used to provide structural support, however, the high-strength implants were so dense that fluids could not penetrate the structure and the biological reaction was limited to the implant surface [4].

Many of the mechanical properties of current bioceramics fail to match the tensile strength and fracture toughness of bone. Experiments with hydroxyapatite, a bioactive ceramic, reported fracture toughness results around 0.32 $GPa \cdot m^{1/2}$, significantly lower than the fracture toughness of load bearing bone at 2 $GPa \cdot m^{1/2}$ [5, 7, 8]. Several efforts to develop a biomaterial with increased bending strength; fracture toughness and Young's modulus properties resulted in the development of several different ceramics. An understanding of ceramic fracture mechanisms is required to prevent catastrophic failure of a composite material under the application of external stresses.

Fracture toughness is a fundamental design property of materials containing cracks that undergo fracture as a result of unstable crack propagation. Toughness is a measure of the maximum energy a material can absorb before fracture takes place. Fracture toughness can be determined by using one of two general methods. The first method, the standardized fracture toughness test, uses a standard pre-formed crack which is either molded into the ceramic or cut into the material using a diamond bit. This crack is then subjected to tensile loading conditions that include three and four point flexural bending to induce failure [9]. The second method utilizes the Vickers indentation fracture test (VIF) and is indented by a pyramidal microhardness indenter. The standardized test using a pre-formed crack is widely utilized for its consistently

reproducible data [10]. The VIF tests are easier to perform, but, produce toughness data that can have a degree of variability associated with the results. Proposed reasons for discrepancies in VIF results include the dependence of crack geometry on the applied load and microstructural properties, along with the effects of non-ideal indentation deformation and fracture behavior.

A large number of empirical equations are available for fracture toughness evaluation in each case involving a range of crack parameters and geometric factors as well as testing conditions and material response. Both test methods employ a stress intensity factor to define the magnitude of stress at a crack tip during mechanical loading. At failure, the stress intensity factor is defined as fracture toughness.

It is virtually impossible to create ceramics without flaws because of pores in the material. Material flaws are both intrinsic and extrinsic manifesting as grain corners, pores, and cracks forming during densification, sintering and machining, and from the material properties and microstructure, respectively. These flaws are the dominant cause of brittle fracture and failure of the material and explain the substantially lower strength of ceramic materials than predicted by theory from interatomic bonding forces. Fracture toughness describes the property of a material containing cracks that experiences fracture as a result of unstable crack propagation [11]. Fracture toughness is affected by the microstructure, grain size, intergranular phases, and residual stresses influencing crack propagation. When cracks exist within material above a critical crack size they are characterized as unstable, cracks smaller than the critical crack size are contained by the surface energy of the material and are considered stable [12]. The critical stress intensity factor for uniaxial loading, K_{IC}, is obtained by assuming that the applied stress of the indentation load is equal to the critical stress intensity factor caused by crack propagation which results in the final tensile mode failure of the material. Tensile mode cracking is one of three defined modes of crack surface displacement including tensile, sliding, and tearing modes. The uniaxial tensile mode is identified by the I in K_{IC} and is a standard parameter used to evaluate the fracture toughness of ceramic materials [9]. The Vickers

indentation fracture test is widely used to determine the fracture toughness of ceramic composites. The use of indentation techniques to determine fracture toughness was introduced by Lawn and Wilshaw in 1975 [12]. This indirect method requires the follow up use of strength determination using a bending test to verify the cracks do not increase in size following the bending test.

Ceramic materials are not tough and fracture in a brittle mode. A greater Young's modulus of elasticity corresponds to a stiffer material with a smaller elastic strain in response to applied stress; most ceramics only experience elastic deformation. On an atomic scale, elastic strain is manifested as small changes in the atomic spacing and the stretching of ineratomic bonding forces [13]. The modulus of elasticity is a measure of the resistance to the separation of adjacent atoms. Most ceramic materials fracture before they experience plastic deformation [9, 12]. The brittleness of ceramics is attributed to their resistance to dislocation slip and inability to deform plastically [13].

Several other bioceramic materials have been investigated in an attempt to mimic the chemical similarities to bone. Synthetic calcium phosphate ceramics like hydroxyapatite (HA) mimic the chemical inorganic component of the mineral component of bone [14]. Many different types of calcium phosphate ceramics have been developed through variations in the Ca/P ratio, which affect the biological response to the implant in vivo [1]. Several of these materials are classified as biodegradable and dissolve in the body and can be replaced by bone during implantation. However, the solubility rate of the calcium phosphate is important and cannot exceed the rate of tissue regeneration for use as an implant. In situations where the implant is intended to initially assist in bone repair until it is resorbed and replaced by natural tissue, it is important to match the rate of resorption with the expected rate of tissue regeneration [3, 14].

Several modifications to hydroxyapatite are possible due to its hexagonal crystal structure, which can support substitutions of other ions on the Ca_2^{+}, PO_4^{3-} and OH^- groups [5]. These substitutions affect lattice parameters, crystal morphology, crystalline structure, solubility, and thermal stability of the composite.

Hydroxyapatite has been used for over 25 years for clinical bone graft procedures. One of the major advances in bioceramics in the last 20 years was the use of hydroxyapatite as a coating for prostheses to extend the usable life of an implant. Clinical studies evaluated hydroxyapatite-coated femoral stems of hip prostheses to non-coated prostheses and found that they extended the life of the implant and was beneficial for implants in younger patients [1]. However due to inferior mechanical properties, hydroxyapatite use was limited to non-major load bearing applications.

Recent studies have investigated materials to improve the strength of many popular bioceramics. For example, an apatite-wollastonite glass-ceramic consisting of small apatite particles reinforced by wollastonite was able to achieve a higher bending strength, fracture toughness and Young's modulus for bioactive ceramics. Because of these excellent mechanical properties, these materials can be used to fabricate vertebral prostheses, iliac crest replacements, and other major load bearing components [1]. Investigations also identified that combinations of hydroxyapatite with carbon MWCNTs and other materials can improve the mechanical properties of the resulting composite. The fracture toughness of bone is measured between 2 and 12 $GPa \cdot m^{1/2}$ and the fracture toughness of dense pure hydroxyapatite is approximately 1 $GPa \cdot m^{1/2}$ [5]. Carbon MWCNTs provide excellent mechanical properties including high strength and stiffness and act as an ideal reinforcement material that may not compromise the bioactivity of the material.

MWCNTs are composed of a graphene sheet with hemispherical, half fullerene end caps. Single-wall carbon nanotubes (SWCNTs) have just one sheet while MWCNTs consist of many graphene sheets concentrically rolled up within one another. SWCNTs have diameters ranging from 0.7 to 2 nm and lengths from several micrometers to several millimeters [5]. The mechanical properties of MWCNTs in composites depend on the amount of interfacial bonding between the two phases and the orientation of the MWCNTs in the composite. These factors are largely affected by manufacturing techniques. The driver behind creating ceramic composites is to improve the material's

ability to resist fracture when a crack is present. Improvements in fracture toughness also lead to improvement in material strength and stiffness. The high aspect ratio of the MWCNTs, and long thin morphology help to reinforce the material and reinforce better than particulates [5]. In order to optimally reinforce the composite, the volume fraction of MWCNTs must be optimized and a homogeneous mixture must be obtained in order to ensure homogeneous properties in the material.

Several procedures are used to prepare carbon nanotube composite materials. Physical blending, including ball milling and dry mixing, and in-situ formation such as carbon nanotube or matrix synthesis are a few of the mixing procedures used. Once the two phases are mixed, the composite is sintered to obtain a dense and cohesive material [15]. Sintering methodologies are under review and are shown in several studies to reduce the number of MWCNTs in the composite matrix [16]. Sintering is usually conducted between 1200° and 1300°C and has been performed in a vacuum and using various gas environments to help reduce the degradation of MWCNTs [1].

Very little mechanical testing has been performed on these composite materials. A recent study [5] investigated bulk composites and the effect of carbon nanotube loading on hardness and Young's modulus values. The study showed that at a concentration of 2 weight percent (wt%) MWCNTs, a 38% increase in compressive strength was observed for oxidized MWCNTs [5]. Another study investigating a silicon carbide matrix found a 10% improvement in fracture toughness by incorporating MWCNTs [5]. Vickers hardness and facture toughness results for pure alumina with a 5.7% weight by volume of SWCNTs, proved to be more than twice as high as pure alumina with almost no decrease in material hardness. Toughness was improved by a factor of three over pure alumina through the addition of a 10% weight by volume mixture of SWCNTs [17]. Another study by Jiang [17] showed a 24% increase in toughness for a composite with SWCNTs in a 10% weight by volume composite with Al_2O_3.

From these studies, it is apparent that the incorporation of SWCNTs can significantly increase fracture toughness of a composite material [16]. However, fracture toughness of composite ceramics is difficult to conduct because of the heterogeneous nature of the material. The goal driving the incorporation of MWCNTs into bioactive ceramic materials is to achieve mechanical properties similar to those of bone for use in major load bearing situations [18]. The natural mechanical properties of bone exhibit a tensile strength of approximately 50 MPa, a hardness of 0.396 GPa [19], and a fracture toughness of at least 2 $GPa \cdot m^{1/2}$ [5].

Several attempts have been made to improve the mechanical properties of bioglass materials. A heat treatment process was used to improve the structural properties of bioglass by producing a glass ceramic. The mechanical properties of the material are improved as the microstructure of the glass reinforces the structure, however bioactivity is only partly maintained. Other research is branching into the development organic-inorganic hybrids, magnetic glasses and glass ceramics, calcium phosphate cements, ordered mesoporous silica materials, and fabricated glasses.

Calcium phosphate cements do not have strong mechanical properties, however, the material is widely used to restore skeletal function including spinal fusion, craniomaxillofacial reconstruction, treatment of bone defects, fracture treatment, total joint replacement and bone augmentation, and revision surgery [1, 20]. Current research is investigating composite materials to improve the mechanical strength of calcium phosphate cements [4].

Ordered mesoporous silica materials are composed of an amorphous silica network of well ordered and arranged pore systems and cavities. This material behaves as a bioglass and is able to form biological type apatite coatings, but has the added benefit of an appropriately sized pore channel system to allow the passage and inclusion of molecules promoting additional bioactivity [4]. Templated or fabricated glasses exhibit many of the same characteristics as other silica based biomaterials, but with a specific surface that is double that of other materials. These materials have a much

higher contact surface area for physiological fluid and show excellent bioactivity and apatite formation faster than many other materials [4]. Biological interactions showed that material porosity is an important bioceramic parameter. Pores in the 20 to 400 micron range is required to support cellular activity and regeneration, however mechanical properties are sacrificed [4]. Future bioceramic research is directed towards the improvement of the mechanical performance of bioactive hydroxyapatite ceramics and bioglass materials through the incorporation of carbon nanotubes. The future of bioceramics includes improvements in the mechanical performance of existing bioactive ceramics and composite materials.

Table 2.1 presents the results from various nanocomposite material investigations and the optimal weight percent (wt%) to increase fracture toughness. Included in the creation of compositions of nano-ceramics are a variety of processes used to produce specimens. Generally the procedure can be separated into the following categories: mixing, densification, and sintering. Mixing has been successfully performed using a ball mill with varying speeds, ball media, and additives, as well as by sonication and ultrasonic vibration. The mixing process is critical to homogenization of the compound for uniform fracturing, and can be aided by the addition of alcohols and emulsions [9]. Densification has been achieved through the application of die and isostatic pressure, freeze granulation, and spark plasma compaction performed simultaneously with oven sintering. The sintering process causes nano-ceramic powders to form into a strong crystalline phase typical of all ceramic materials. However, carbon nanotubes are temperature sensitive and care must be taken to not destroy the nanotubes through combustion or oxidation [21].

Table 2.1: Previous MWCNT-ceramic composite material, process, and fracture toughness comparison

Composite Material	Nanotube Details		Process Details			Improvement in Fracture Toughness Over Processed Material
	Type	Composition	Mixing	Densification	Sintering	
Silicon Carbide SiC [9]	SWCNTs	10 vol%	Ball milling	Hot isostatic pressing	Hot pressing at 1200°C	10.66%
Silicon Oxide SiO_2 [9]	MWCNTs	5 vol%	Powder mixing and ball milling	Hot pressing at 25 MPa	Sintering at 1300°C in nitrogen 30 minutes	280%
Aluminum Oxide Al_2O_3 [9]	SWCNTs	2.5 vol%	Powder mixing and ball milling	Hot pressing at 25 MPa	Sintering at 1450°C	13.70%
Aluminum Oxide Al_2O_3 [9]	SWCNTs	1wt%	Heterocoagulation[1]	Hot pressing at 30 MPa	Sintering at 1300°C to 1500°C in argon atmosphere	108%
Aluminum Oxide Al_2O_3 [17]	SWCNTs	10wt%	Ball milling with PVA[2] and ethanol	Spark plasma sintering at 63 MPa	Spark plasma vacuum sintering at 1050°C	200%
Hydroxyapatite $Ca_{10}(PO_4)_6(OH)_2$ [22]	MWCNTs	0.1wt%	Sonicate in water and ball milling	Freeze granulation technique	No sintering	200% increase in mechanical properties (i.e. hardness and Young's Modulus)
Hydroxyapatite $Ca_{10}(PO_4)_6(OH)_2$ [7]	MWCNTs	3wt%	Ultrasonic vibration	Cold press molding and isostatic compression	Pressureless sintering in vacuum at 1200°C	200%

Notes: [1] Addition of emulsion/dispersant with particles of opposite charge [2] Polyvinyl alcohol

As shown in Table 2.1, nanoceramic fracture toughness testing has been performed on a variety of bioceramic materials. These materials include silicon carbide, silicon dioxide, aluminum dioxide, and hydroxyapatite. Carbon nanotubes have been added to the ceramics in concentrations from 0.1wt% to 10wt% with an improvement in fracture toughness ranging from 10.7% to 280%.

There are several possible mechanisms responsible for toughening MWCNT-reinforced ceramics: crack deflection, crack bridging, and nanotube pull-out. These mechanisms are optimized in well-ordered, homogeneous composites. Effective load transfer from the ceramic matrix to the nanotubes results in increased fracture toughness [6]. Continued experimentation in nanocomposite fracture toughness and the associated development of bioceramics, which possess both optimal mechanical and biochemical properties, is critical to widespread medical use.

2.2. Impact of Continued Research

Over 2 million bone graft procedures are performed each year and 90% of these procedures use natural bone from the patient (autografts) or from a cadaver (allografts) [1]. Only 10% of bone graft procedures each year use synthetic materials. Natural bone is the optimal choice for such procedures, however there are drawbacks. Autografts require additional healing time and discomfort to the patient and allografts carry the risk of viral infection, immune system rejection and resorption and are not always available. Because of the limited natural bone material available a chemically synthesized material with reproducible structures and chemical composition is needed. The development of a bioceramic material that is able to form a stable interface with the surrounding natural tissue and meet the mechanical properties of the tissue being replaced will also significantly improve bone grafting methodologies and procedures as well as patient healing and response.

A carbon nanotube reinforced bioglass or bioceramic composite material has the potential to provide a biologically active material capable of repairing and restoring skeletal function throughout the body. This material could be utilized for major load

bearing applications, for which there is no current synthetic material. Advances in this field could also be used to develop new scaffold materials to aid in tissue regeneration providing structural skeletal support while aiding in the natural process of tissue regeneration.

Synthesis methodologies including mixing, compaction, and sintering must be investigated to obtain optimal composite mechanical properties. These investigations will require a review of the morphology, crystallography and chemical structure, and matrix interaction of MWCNTs in various bioceramic and bioglass composites to determine optimal mechanical performance.

CHAPTER 3: Raw Materials and Synthesis Procedure

The following raw materials and synthesis procedures were used during this investigation.

3.1. Materials

Characterized as a ceramic material, 45S5 Bioglass GL-0160 Bioactive Glass powder (Bioglass) has a low fracture toughness, hardness, and is susceptible to brittle fracture, but has been found to be an ideal biomaterial due to it's ability to incorporate and bind to tissues and bone in the body [22]. In an attempt to improve the fracture toughness of the material for use in load bearing biomedical applications, the development of a ceramic-matrix, MWCNT-fiber composite was investigated. The inclusion of fibers such as MWCNTs in the ceramic matrix has increased mechanical properties of the material significantly including quadrupling the fracture toughness in several materials [13]. During development of the biocomposite, varying weight percentages of MWCNTs were mixed with an amorphous Bioglass powder. MWCNTs and Bioglass are widely used materials in the field of biomaterial engineering and several investigations have been performed on the two materials independently and as a part of other composite materials [22]. A goal of this thesis is to develop a composite with the optimal wt% of uniformly distributed nanotubes fibers that effectively transmit stress from the bioglass matrix to improve the mechanical properties of the composite.

3.1.1. 42S5 Bioglass

Developed in 1969 by Larry Hench, bioglass powder has been used as a bone replacement material for over 20 years [1]. Bioglass was originally developed as a bioactive material to aid in the repair of bone and tissue by forming a direct bond with the affected tissue. In addition to biocompatibility, glass-ceramics are designed to have high mechanical strengths, low coefficients of thermal expansion, and good dielectric properties. The inorganic raw 45S5 Bioglass® GL-0160 Bioactive Glass powder used in

this investigation was produced commercially by MO-SCI Corporation in Rolla, Missouri and constitutes the matrix component of the composite material. Specifically the GL-0160 Bioactive Glass powder used in this thesis is composed of 24.5wt% Na_2O, 24.5wt% CaO, 45wt% SiO_2, and 6wt% P_2O_5 with a density of 2.70 g/cm^3. The material has a melting temperature of 1070°C [23]. The glass is manufactured by reacting and fusing batch raw materials in a platinum crucible, quenching the mixture, crushing the result, and then grinding and sieving the material to obtain appropriately sized particles. The powder material specification indicates that the particle size of the powder is less than 53 μm, however from SEM images of the raw powder a majority of the particles are significantly smaller than 53 μm. This material is commercially used to form glass fibers or glass microspheres for other research applications. The bioglass powder will constitute the matrix phase of the composite and act as the medium by which external loads and stresses are transmitted and distributed to the reinforcing MWCNT fibers.

Existing literature investigating the sintered crystallization of Bioglass identifies the formation of $Na_2Ca_2Si_3O_9$ as the main crystalline phase present in heat treatments over 600°C. The $Na_2Ca_2Si_3O_9$ phase has a hexagonal lattice structure with the following lattice parameters: a=b=105.61Å, c=13.199Å and $\alpha=\beta=90°$, $\gamma=120°$ [24]. In two different papers Lefebvre [23] and Bretcanu [24] proposed the following structural transformations of 45S5 Bioglass, a glass transition temperature 550°C, the nucleation of a major crystalline phase $Na_2CaSi_2O_9$ around 600°C and the crystallization of a secondary phase, $Na_2Ca_4(PO_4)2SiO_4$ around 850°C [25]. In Bretcanu's [24] study, maximum densification and crystallization of samples with an unsintered density around 0.50 were achieved using a sintering temperature of 1050°C for 140 minutes.

3.1.2. Multi-Wall Carbon Nanotubes (MWCNTs)

Carbon nanotubes were discovered by Iijima in 1991 and have since been incorporated into many different fields including energy storage, chemical engineering, devices such as probes, sensors, and other nanoelectric devices, and composites [2]. Carbon nanotubes are allotropes of carbon with cylindrical nanostructures. The

nanotubes used in this investigation are MWCNTs and consist of concentric rolled graphene sheets with an interlayer distance of ~0.34 nm [2, 26]. Nanotubes are composed of carbon fullerene structures with a cylindrical arrangement bonding all atoms in place by covalent sp^2 type chemical bonds. The mechanical properties of a composite material depend on the ability to transmit a load from the matrix to the fiber and the mechanical properties of the reinforcing fibers. Nanotubes have excellent tensile strength around 150 GPa and a Young's modulus at 1200 GPa far exceeding the strength and modulus of steel at 0.4 GPa and 208 GPa respectively [2]. The impressive mechanical properties of nanotubes make MWCNTs an attractive fiber choice for many ceramic composites and are attributed to their unique structure. The high strength properties of nanotubes are attributed to the high aspect or surface to volume ratio, length to width parameter, and the covalent sp^2 bonds formed between the individual carbon atoms. However, nanotubes are not as strong as steel under compression [27]. The hollow nature of the tubes and high aspect ratio allows the tubes to buckle when they experience compressive or bending stress [28]. MWCNTs successfully improved the mechanical properties of hydroxyapatite, a similar ceramic, in several studies with the optimal concentration ranging between 0.1wt% [22] to 3wt% [21] reporting an increase in fracture toughness of 8 times that of the material.

The MWCNTs used in this experiment were L. MWCNTs-1020 purchased from Shenzhen Nano-Technologies Port Co., Ltd. in Nanshan, Shenzhen, Guangdong China. According to the manufacturer, the MWCNTs have an external diameter of 10-20 nm, with an interlayer distance of 0.34 nm and a tube length of 5 to 15 μm. The purity of the material is greater than 95% with less than 2% amorphous carbon. XRD analysis on the pure MWCNTs shows signature carbon diffraction peaks visible at $2\theta = 26°$, 42°, 54°, and 77° [7, 29]. The MWCNTs constitute the fiber phase of the experimental composite under investigation. MWCNTs are an ideal reinforcement material because they have the potential to provide excellent mechanical strength to the ceramic composite without compromising the bioactivity of the Bioglass.

3.2. Synthesis Process and Sample Preparation

The synthesis process is critical to the development of composite material characteristics. As the literature presented in Chapter 2 shows, there are a variety of methods to mix, compact, and sinter ceramic-composites. These decisions affect the final composite and have the potential to improve or deteriorate mechanical properties. In an effort to improve the mechanical properties of Bioglass, the following procedures were used: ball mill mixing, cold die compaction and densification, and inert atmosphere sintering.

3.2.1. Mixing

The composite MWCNT-Bioglass composite was synthesized using dry mixing procedures to combine the Bioglass matrix and the MWCNTs fibers in a ball mill. Figure 3.1 shows MWCNTs and Bioglass powder placed in the ball mill prior to mixing. Additional photographs of the process can be found in Appendix D.

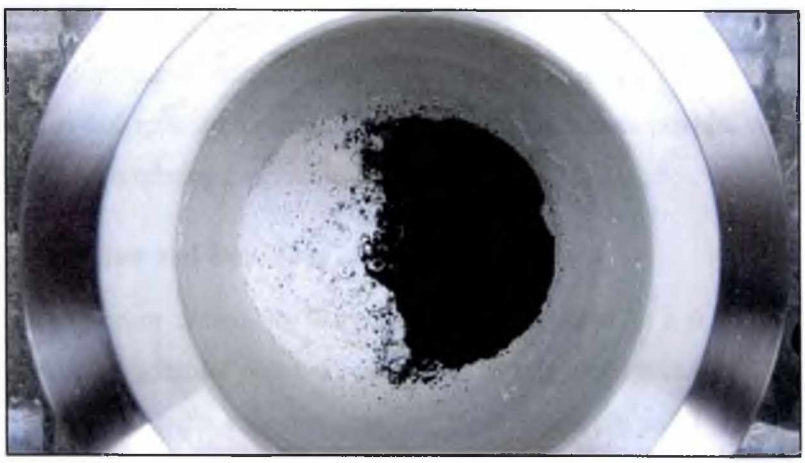

Figure 3.1: Raw MWCNT and Bioglass material in 3-inch inner diameter zirconium ball mill mixing bowl

There are several considerations when developing a nanocomposite material. The first and most important, according to previous studies [10, 15, 28], is to obtain a homogeneous distribution between the MWCNTs and the matrix material. A homogeneous distribution ensures uniform properties throughout the composite and will

promote interfacial bonding between the two materials. The distribution and interfacial bonding of the fibers within the matrix enables the effective transfer of applied stress from the Bioglass to the stronger MWCNT network improving the mechanical properties of the material. MWCNTs have the potential to agglomerate due to Van der Waals forces between the individual tubes decreasing the interaction with the Bioglass [22]. Studies presented by Esawi in 2007 identified agglomeration as a key concern for synthesis of composites with MWCNTs [28]. The agglomeration of the MWCNTs will reduce the interfacial interaction between the constituents resulting in composite heterogeneity which will weaken the overall strength of the composite [30].

A Retsch Ball Mill PM100 was used with a 250 ml zirconia oxide-grinding bowl and 1mm steatite balls to mix the composite. Low-density steatite balls were used to minimize damage to the MWCNTs during mixing. Polyvinyl alcohol (1 ml 10wt%) was added to the composite acting as a binder to improve the unsintered strength during compaction. In order to minimize milling of the 52μm particle Bioglass and to separate MWCNT clusters a high-energy mix at 300 rpm for 10 minutes was utilized to break apart the agglomerated nanotube clusters. Following the high-energy mix, the material was mixed at 100 rpm for a period of 50 minutes. A ball to powder weight ratio of 5:1 was used for both mixing processes.

3.2.2. Compaction and Densification

Each 3-gram composite sample was cold pressed in a 0.76-inch (in) diameter steel die using a hydraulic press. Photographs of this process can be found in Appendix D. Pressure on the die was increased to 10,000 pounds and held for a period of 5 minutes and then increased to 30,000 pounds for 55 minutes to compact the sample [31, 32]. Average compacted samples measured 0.2 in thick with a diameter of 0.76 in as shown in Figure 3.2. The average sample volume was approximately 0.11 in^3. Physical sample measurements and calculations are tabulated in Appendix C.2. Theoretical densities provided by the manufactures were used to calculate the relative density of the unsintered and sintered composites. Bioglass density was reported at 2.70 g/cm^3 and the

MWCNT density at 1.75 g/cm^3. Relative densities were calculated using the following equation:

$$RD = \rho_{composite} / \rho_{reference} \qquad \textbf{Equation 1}$$

$$\rho_{reference} = \frac{wt\%MWCNT \times 1.75\ g/cm^3}{wt\%Bioglass \times 2.70\ g/cm^3}$$

The post sintering measured composite weight is used to determine $\rho_{composite}$. The density of the unsintered composite samples was on average 60%.

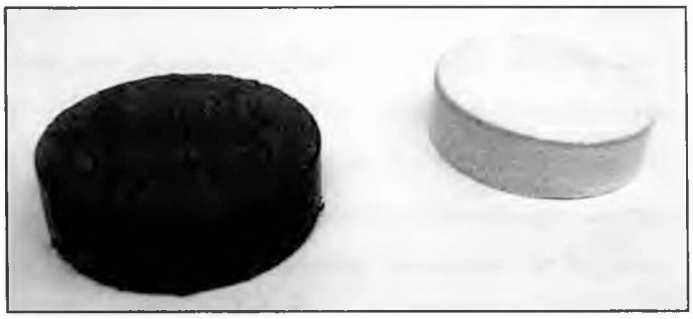

Figure 3.2: 10wt% MWCNT and 0wt% MWCNT samples after cold die compaction
The diameter of the samples is 0.76 in.

Cracking along the width of the 0wt% MWCNT sample was observed in many of the samples and is attributed to stress during die ejection.

3.2.3. Sintering

A Lucifer 82AM-F12 electrical heat treatment furnace with a 588 in^3 controlled atmosphere chamber was used to sinter the composites. Two sets of composites were sintered at 1000°C and 850°C. The samples were positioned onto a firebrick and into the furnace at room temperature. Upon initiation of the electrical heating element the chamber was purged with argon for 15 minutes. In order to ensure a 100% argon environment, a flow rate of 6.91 CFH equivalent to 20.3 chamber changes per hour was

directed through the furnace chamber during heating, sintering, and cooling of the samples. Once the argon environment was established, the samples were heated to 1000°C and 850°C and sintered for 20 minutes. This temperature and sinter time was developed to eliminate sample porosity, achieve bioglass crystallization, preserve MWCNTs, and to encourage interfacial bonding of the Bioglass matrix and MWCNTs fibers. Sintering temperatures ranging from 800°C to 1200°C were investigated in both an air and argon atmosphere. These investigations determined the optimal argon environment and sintering temperature at 1000°C and 850°C. To evaluate oxidation within the chamber, pure MWCNTs and a piece of steel were placed in the furnace. Following sintering the structure of the MWCNTs was verified using XRD. The steel was inspected to determine if oxidation was occurring. XRD analysis confirmed the presence of a smaller weight percent of MWCNTs after sintering and the steel showed small amounts of oxidized surface material. Samples from sintering events that did preserve the raw MWCNTs were not used in this experiment because the presence of MWCNTs could not be verified. The furnace chamber and sample arrangement are shown in Figure 3.3 before and after sintering. Additional photographs can be found in Appendix D.

Figure 3.3: Composite samples before and after sintering.

The images above show Bioglass and MWCNT samples before(left) and after(right) sintering. A steel cylinder and raw MWCNTs were placed on firebrick to

evaluate oxidation during sintering.

In order to achieve crystallization in the material the samples were heated at a rate of 9.00°C/min, held at temperature for 20 minutes, and cooled at a rate of 1.62°C/min. An argon environment was maintained until the furnace temperature dropped below 300°C to prevent oxidation of MWCNTs. The samples were cooled from 300°C to room temperature and then processed for testing.

3.2.4. Grinding and Polishing

Once the sintered disks cooled they were mounted into an epoxy mold made from a two-part chemical resin mixture composed of a styrene monomer (100-42-5), unsaturated polyester resin and bezoyl peroxide (94-36-0). A 1 ¼ in diameter by ¾ in high cylinder was poured into a cold quick release mold to secure the sintered composite for grinding, polishing, and XRD, SEM and hardness testing. Once secured in the mold, the samples were ground and polished to expose the composite structure below the oxidized surface. Approximately 0.07 in of the oxidized sample surface was removed during this process. Due to the varying hardness of the Bioglass matrix and MWCNT fiber components, only fixed abrasives were used during the polishing process to prevent loose abrasives from adhering to the composite. The sample was initially ground to a level surface using 100 grit SiC paper on with an EcoMet III Grinder and EcoMet 2 Powerhead. The EcoMet III automated grinder was programmed to distribute 10 pounds of force with a wheel rotation speed of 150 rpm. Once the oxidized surface was removed and the samples were level, the following polishing process was followed: 300 grit SiC paper for 1 hour: 400 grit SiC paper for 1 hour, 600 grit SiC paper for 1 hour. Water was used to cool the samples during SiC paper polishing and each sample was counter rotated for a total of 2 hours at each speed. Following the SiC grinding, a 9 μm polishing cloth and a 1 μm polishing cloth were used in succession to polish the sample for 20 minutes each with 3 pounds of force and rotation speed of 150 rpm. Due to the variation in hardness between the carbon MWCNTs and the Bioglass, a high wheel rotation speed was used with a lower sample pressure to prevent grain pullout, a

common problem of ceramic polishing [33]. Many of the 8wt% and 10wt% MWCNT samples required additional polishing with 400 and 600 grit SiC paper to achieve a polished surface to collect indentation measurements.

CHAPTER 4: Phase, Microstructure, and Mechanical Property Characterizations

Several testing methods were used to evaluate the composite material including XRD, SEM, and Vickers hardness indentation test. Each evaluation method is defined and described in the following sections. The standard operating procedures (SOPs) for the equipment and evaluation methods used are presented in Appendix B.

4.1. X-Ray Diffraction

In order to evaluate the individual constituents and the composite material through the various stages of synthesis, a PANalytical X'Pert PRO Materials Research Diffractometer (MRD) X-ray diffraction system was used to identify crystallographic components and phases [34]. The XRD, shown in Figure 4.1, was used to scan the material between each stage of development to track chemical and structural changes during the synthesis process. Scans were collected for the raw powder materials, after mixing to identify MWCNT concentration, and following sintering to determine crystallographic phases and to asses the oxidation of MWCNTs. The scans are presented and discussed in Section 5.1.2.

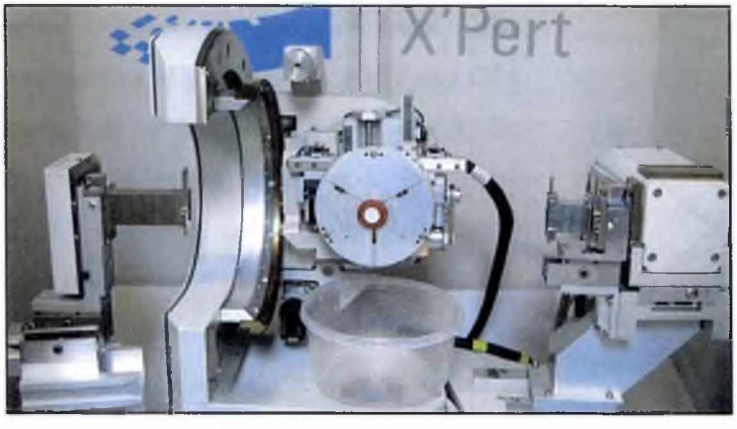

Figure 4.1: XRD Scanner with pure Bioglass sample mounted for XRD analysis

4.2. Scanning Electron Microscope / Environmental Scanning Electron Microscope

An ISI-SR-50-Scanning Electron Microscope (SEM) and an ElectroScan E2020 Environmental Scanning Electron Microscope (ESEM) were used to collect micrographs of the raw materials and composite evolution during synthesis. The SEM and ESEM were used to obtain high-resolution images of the topography and composition of a sample by scanning a focused beam of electrons over the surface of an electrically conductive specimen. Secondary electrons are collected and processed as a series of pixels on the viewing monitor. The ESEM used in this study was able to achieve a greater resolution on the samples. Due to the conductive nature of the specimens, samples were viewed with and without gold coating.

4.3. Vickers Hardness Test

A Buehler Micromet 5101 was used to perform the Vickers indentation hardness test on the composite ceramic. The Vickers indentation hardness test applies a load on the sample using a 136° square based diamond pyramid indenter as shown in Figure 4.2 [35]. Hardness is determined by optical measurement of the resulting indentation surface diagonals using a microscope. The Vickers hardness number is presented in HVN and GPa units and is determined by dividing the load applied by the indenter by the indenter surface area in square millimeters [10, 36]. For these experiments, loads of 500 and 200-gram force were used and the time for the test load application was set at 15 seconds. For each sample 10 indentation acceptable indentations were recorded as recommended by the ASTM C 1327-08 standard [36]. The indentations were collected over the polished surface of the composite with an average area of 0.40 in^2.

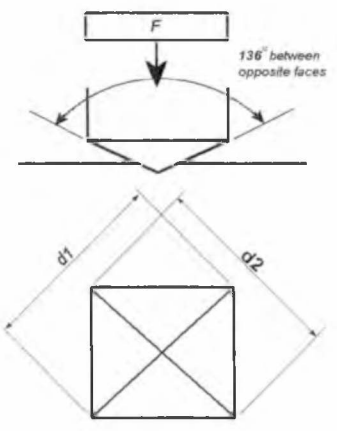

Figure 4.2: Diagram of Vickers hardness indentation test [35]

The Vickers hardness indentation test is used to determine hardness of the

ceramic because the sharp indenter produces well defined cracks which are to calculate fracture toughness and hardness values [37]. Hardness is a measure of the strength of a material and its resistance to deformation. Hardness tests are performed more frequently than any other mechanical test because they are simple, nondestructive, and can be used to derive other mechanical properties such as fracture toughness [12, 13]. Fracture toughness represents a material's resistance to fracture when a crack or deformation is present and corresponds to the maximum energy a material can absorb before fracture occurs. Toughness can be estimated using cracks produced by hardness indents and is represented by K_{IC}, the critical value of the stress intensity factor at a crack tip necessary to produce tensile mode catastrophic failure under simple uniaxial loading [13, 38]. The following equations were used to calculate hardness and fracture toughness of the specimen.

$$HVN = 1.8544(\frac{P}{d^2}) \text{ Vickers hardness number} \qquad \textbf{Equation 2}$$

$$HV = 0.0018544(\frac{F}{d^2}) \text{ GPa} \qquad \textbf{Equation 3}$$

where HVN is the hardness value in Vickers hardness number units, HV is the hardness value in GPa, P represents the load in newtons, F represents the load in kgf, and d the average indentation diagonal in millimeters [36]. Fracture toughness was evaluated using the following formula presented by Evans and Charles in 1976. The for which does not require the use of Young's Modulus (E) to determine fracture toughness [33, 39].

$$K_{IC} \approx 0.15(H\sqrt{a})(\frac{c}{a})^{-1.5} \qquad \textbf{Equation 4}$$

where H is the hardness value in Pascals obtained from the Vickers hardness indentation tests and Equations 2 and 3. The a and c are parameters measured from the indentation. The a is half the diagonal length d and the c parameter is the measure of the liner crack length as shown in Figures 4.3 and 4.4. The following dimensions were recorded during the Vickers hardness test to calculate the hardness and fracture toughness values of the

composite.

d_1 = vertical indentation diagonal length

d_2 = horizontal indentation diagonal length

c = crack distance from the tip of the diamond to the termination of the crack

a_1 = ½ vertical length of indentation

All data collected to support this thesis was recorded to three significant digits. The raw data for each sample measurement are tabulated in Appendix C.2.

Figure 4.3: Vickers hardness indentation on a 1wt% MWCNT composite sintered at 1000°C

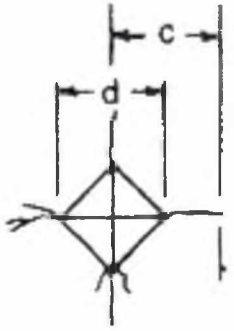

Figure 4.4: ASTM diagram of recorded hardness measurements [36]

Standard deviation for the samples was calculated and is represented by error bars on the figures in Chapter 5 [40]. Due to the variability of the composite samples these values indicate a wide range in sample values and substantial variation in the mechanical properties of the material [40]. The above equation calculations including the standard deviation can be found in the table in Appendix C.1.

CHAPTER 5: Results

The composite samples were evaluated throughout the synthesis process using XRD and SEM technology to confirm the presence of material components, verify crystallography of the sintered material, and assess mixing effectiveness and interfacial bonding of the nanotubes and Bioglass. Following synthesis, the mechanical properties of the composite were evaluated using the Vickers indentation hardness test to quantify the hardness and fracture toughness of the material. The results from these analysis methods and experiments are presented in this chapter.

5.1. XRD Phase Analysis

XRD scans were performed on the raw materials, composite mixtures, and on sintered composites. Raw MWCNTs were placed in the furnace chamber adjacent to the composites during each sintering event and analyzed using XRD to determine the MWCNTs were oxidizing. The following XRD scans displayed as Figure 5.1 and 5.2 show MWCNT scans corresponding to different sintering temperatures. Raw Bioglass and composite mixtures were also evaluated using the XRD before and after sintering. The composite scans after sintering are consolidated in two stacked plots based on the sintering temperature.

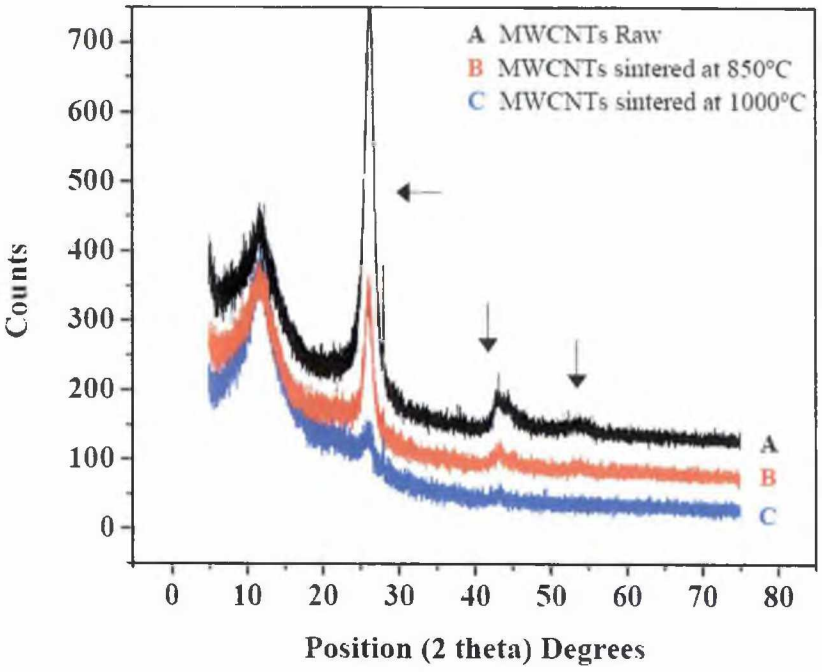

Figure 5.1: XRD scan of MWCNTs before and after sintering

Signature MWCNT peaks are identified in the above XRD scan by arrows.

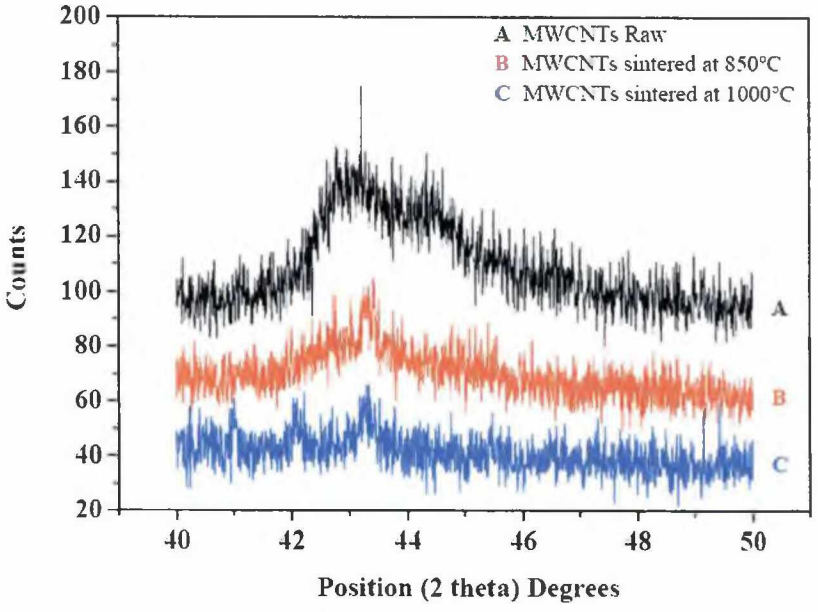

Figure 5.2: Focused XRD scan of MWCNTs before and after sintering

Arrows on Figure 5.1 at 2θ = 26.5°, 42.7°, and 53° identify the MWCNT signature peaks. These peaks correspond to previous research performed on MWCNTs [29, 41, 42]. The peak at 53° is visible on the unsintered MWCNT sample but is not visible on the sintered material.

XRD scans were also performed on raw Bioglass material, the composite mixtures, and the sintered samples. The following scan, Figure 5.3, shows the original amorphous phase of the unsintered Bioglass powder.

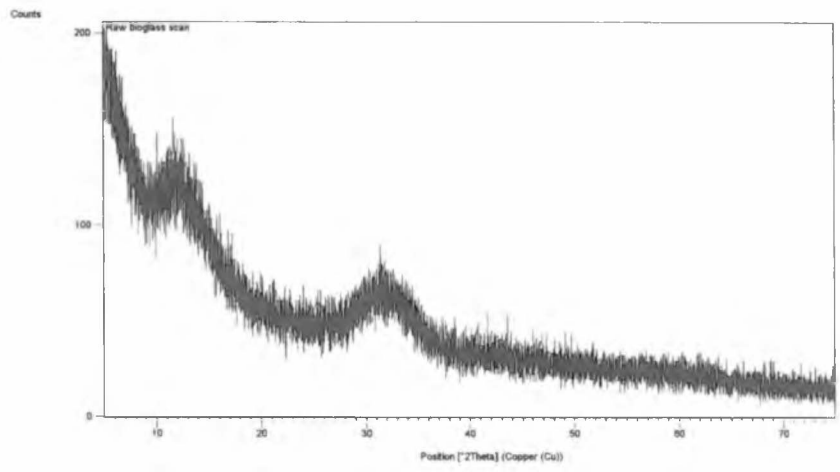

Figure 5.3: XRD scan of Bioglass powder

Figures 5.4 – 5.6 compare XRD scans showing crystallization of pure Bioglass samples sintered at 1000°C and 85θ°C. The crystallization peaks of the bioglass structure confirmed the presence of the main crystalline phase $Na_2Ca_2Si_3O_9$, (2θ = 23°, 34°, 49°) and the secondary phase $Na_2Ca_4(PO_4)_2SiO_4$ (2θ = 32°) identified in previous studies [31].

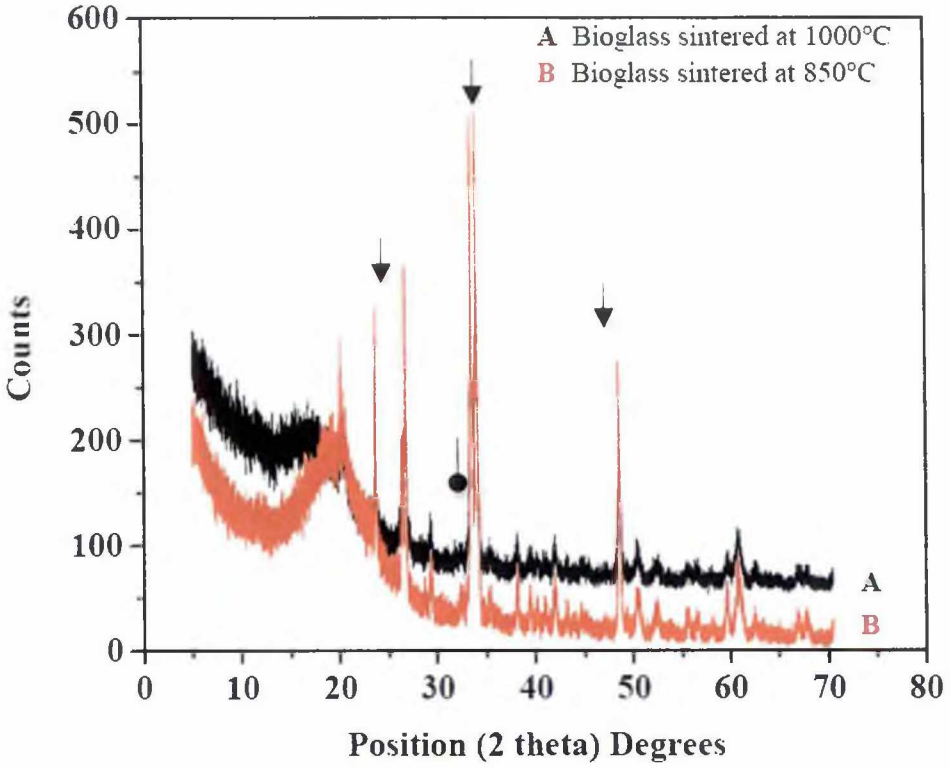

Figure 5.4: XRD scan of Bioglass sintered at 1000°C and 850°C

The main crystalline phase is identified on the figure below with arrows ↓ and the secondary phase is identified with a point● . The secondary phase is more obvious on the red scan. Figure 5.4 shows identical XRD patters for both the samples despite the different sintering temperatures.

The following XRD figures display stacked scans of the composite samples sintered at 1000°C and 850°C respectively.

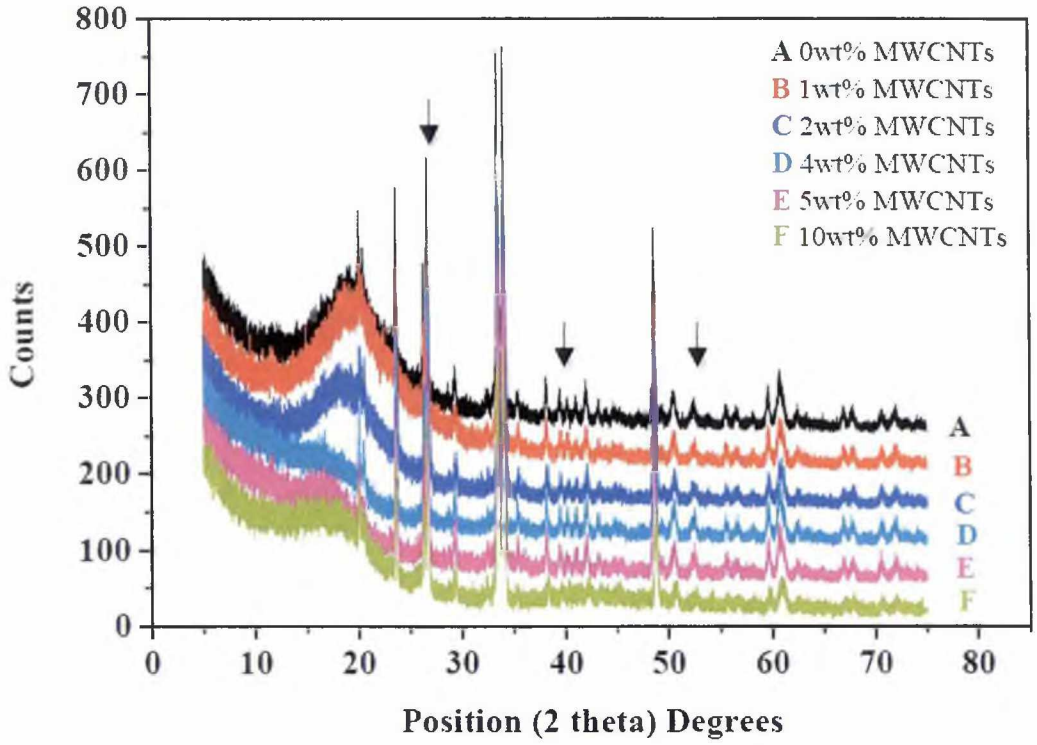

Figure 5.5: Consolidated XRD scans of composites sintered at 1000°C

The arrows ↓ indicate the location of the MWCNT peaks which are not visible on the sintered samples.

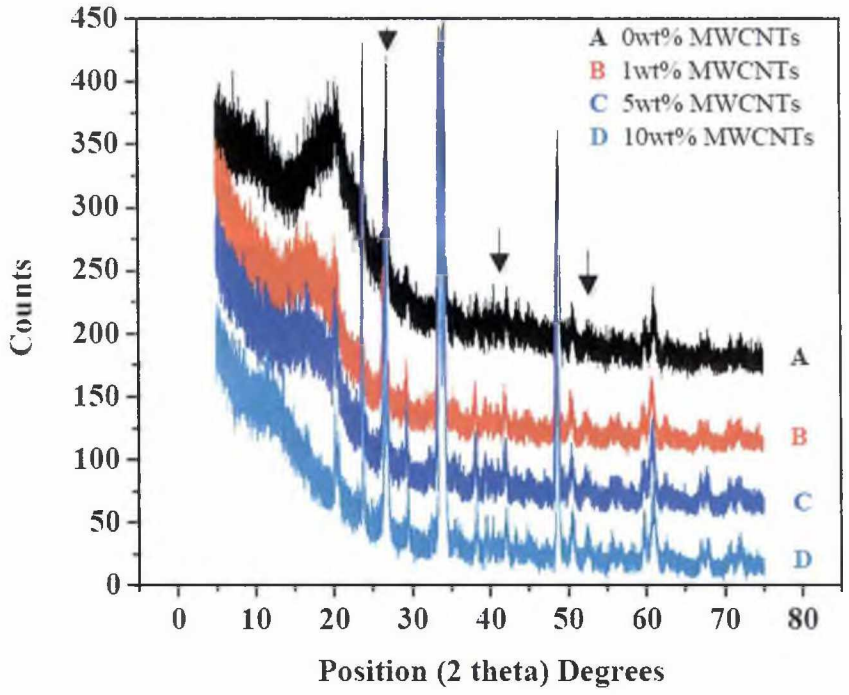

Figure 5.6: XRD scans of MWCNT composites sintered at 850°C

The arrows ↓ indicate the location of the MWCNT peaks. These peaks are not visible in the sintered composite samples.

5.2. SEM Images

SEM images were collected during the synthesis process and during hardness testing. Images of the raw materials, sintered samples, fracture surfaces, and Vickers indentations are shown in Figures 5.7 – 5.10.

Figure 5.7: Bioglass 53 μm sized particles

The SEM image is viewed at approximately 680x with a horizontal field of view of 140 μm.

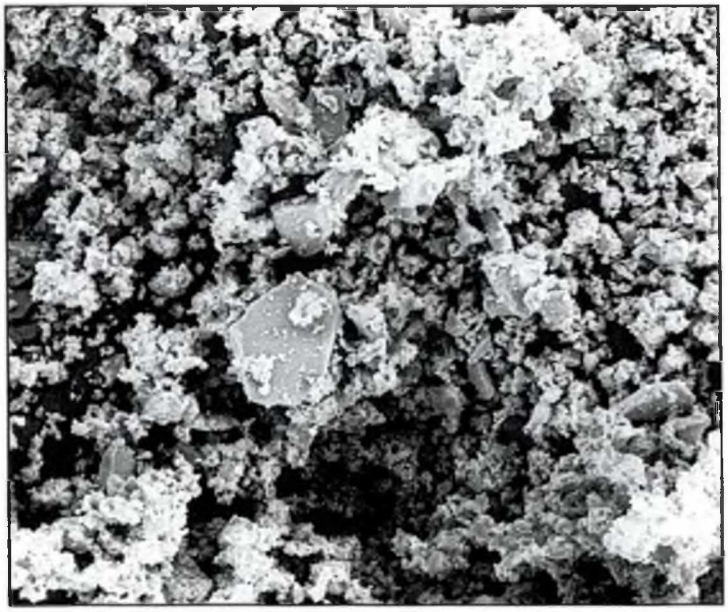

Figure 5.8: Bioglass mixed in the ball mill

The SEM image is viewed at approximately 80x with a horizontal field of view of 235 μm.

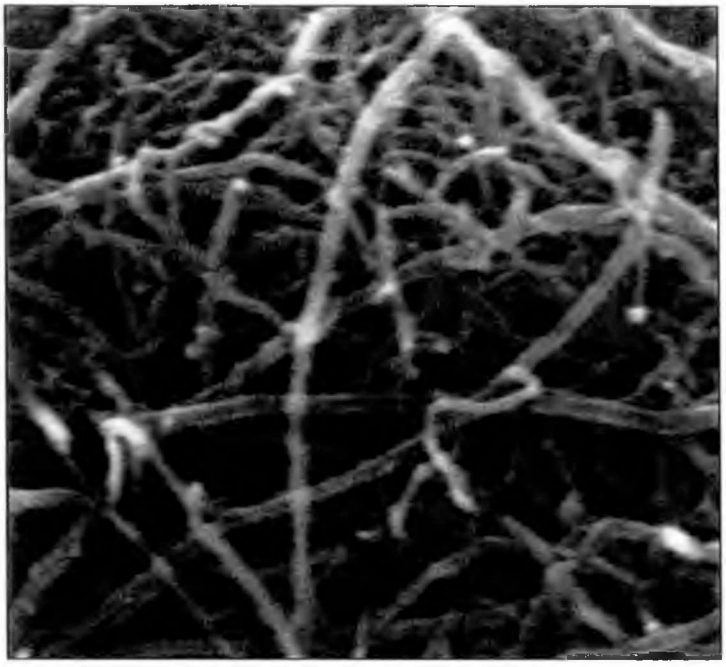

Figure 5.9: Raw MWCNTs

The SEM image is viewed at approximately 20,000x with a horizontal field of view of 5 μm.

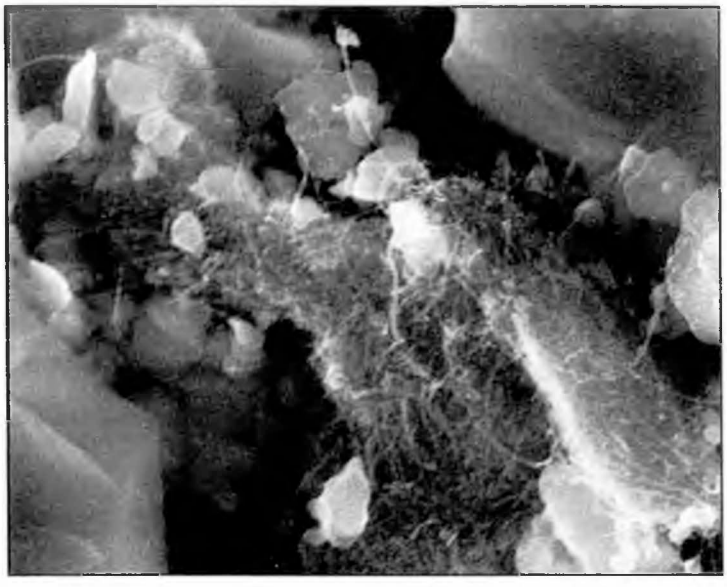

Figure 5.10: Agglomeration of the MWCNTs in an 8wt% composite

The SEM image is viewed at approximately 5,000x with a horizontal field of view of 17 μm.

Figures 5.11 and 5.12 show the even distribution of the MWCNTs following the high-energy mixing process detailed in Section 3.2.1.

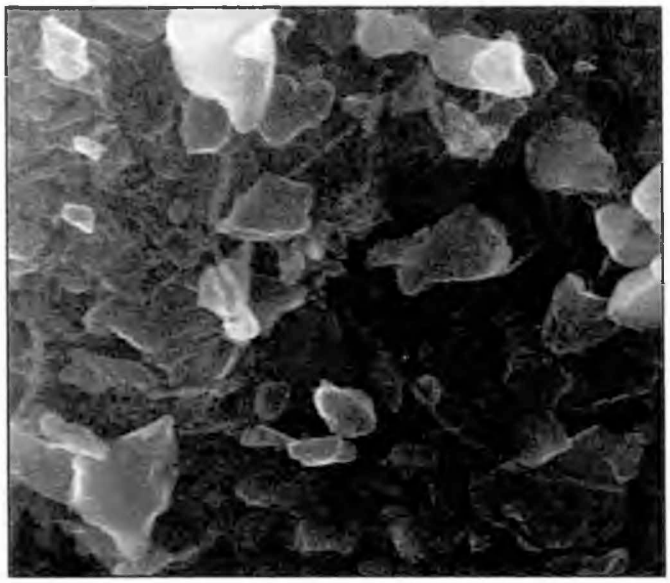

Figure 5.11: Well mixed 10wt% MWCNT composite

The SEM image is viewed at approximately 10,000x with a horizontal field of view of 10 μm.

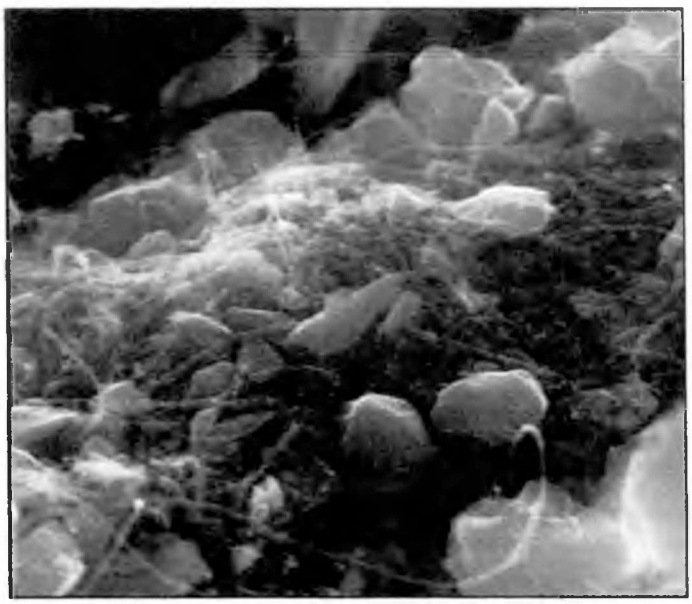

Figure 5.12: Well distributed MWCNTs in a 10wt% composite mixture

The SEM image is viewed at approximately 10,000x with a horizontal field of view of 10 μm.

To evaluate the sintered composite several samples were fractured to view the composition and interaction of the MWCNTs and bioglass along a fracture surface. Figures 5.13 – 5.14 show interfacial bonding between the MWCNT fibers and the Bioglass matrix. Several MWCNTs are shown bridging gaps in the composite in Figure 5.14.

Figure 5.13: Fracture surface of 8wt% MWCNT sintered at 850°C

The SEM image is viewed at approximately 10,000x with a horizontal field of view of 5 μm.

Figure 5.14: MWCNTs bridging fracture surface of a 8wt% composite sample sintered at 850°C

The SEM image is viewed at approximately 10,000x with a horizontal field of view of 8 μm.

The resolution of the SEM did not allow the ability to capture images showing the pullout of MWCNTs and residual holes along the fracture surface.

To evaluate the hardness and fracture toughness of the material, microhardness indentation tests were performed on the composite samples. The following images, Figures 5.15 – 5.17, show Vickers diamond shaped indentations for the pure Bioglass and composite material. The following figures are arranged in order of highest fracture toughness to lowest fracture toughness and show indentation and radial cracking as a result of the applied force.

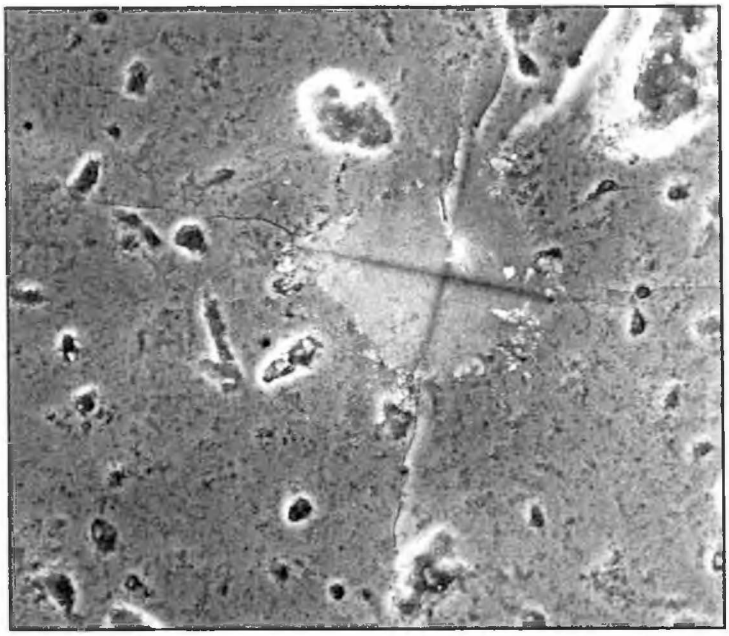

Figure 5.15: Indentation test of a 500g load on pure Bioglass sintered at 1000°C

The SEM image is viewed at approximately 860x with a horizontal field of view of 140 μm.

Figure 5.16: Indentation test of a 500g load on 1wt% MWCNT composite sintered at 1000°C

The SEM image is viewed at approximately 1,000x with a horizontal field of view of 80 μm.

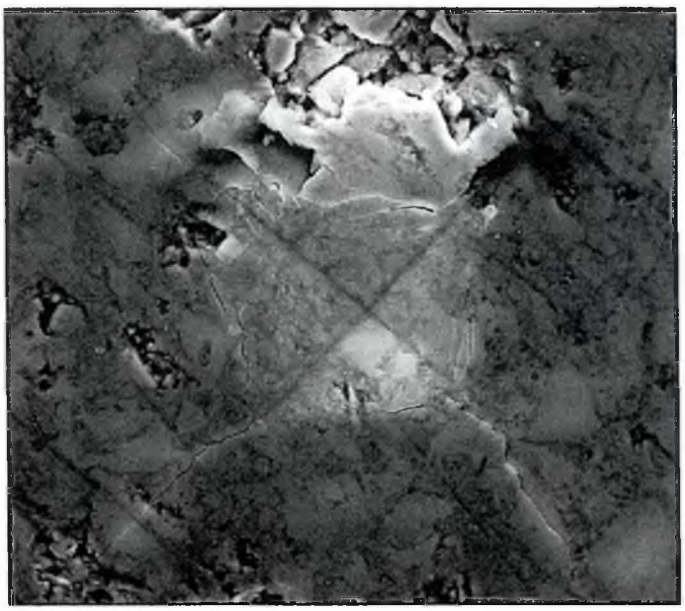

Figure 5.17: Indentation test of a 500g load on 2wt% MWCNT composite sintered at 1000°C

The SEM image is viewed at approximately 500x with a horizontal field of view of 150 μm.

5.3. Hardness and Fracture Toughness Data

Hardness and fracture toughness values were computed from Vickers hardness indentation tests. The complete raw data set from these tests are in Appendix B. Hardness values were calculated using the following formulas presented in the ASTM C 1327-08 and as Equations 2 and 3 in Chapter 4 of this document.

Photographs were taken along with parameter measurements of the indentation surfaces to determine hardness and fracture toughness of the material. Figures 5.18 – 5.20 show representative images of indentation and crack propagation (identified by arrows) in the composite samples sintered at 1000°C and 850°C. Images for indentations at each MWCNT wt% and sintering temperature can be found in the Photographic Log in Appendix E of this document.

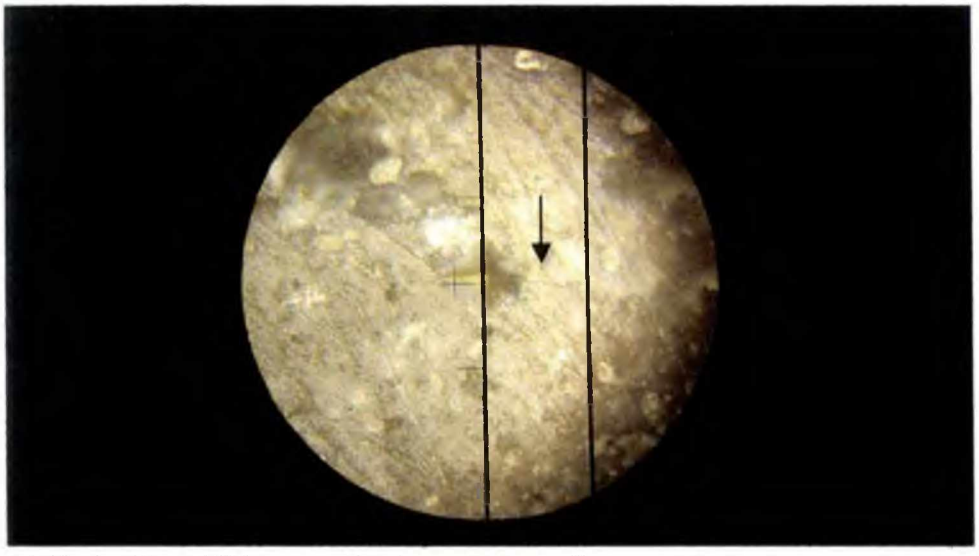

Figure 5.18: 1wt% MWCNTs composite sintered at 1000°C

This image shows the indentation resulting from a 500g force at 50x magnification. Field of view diameter is 0.29 mm.

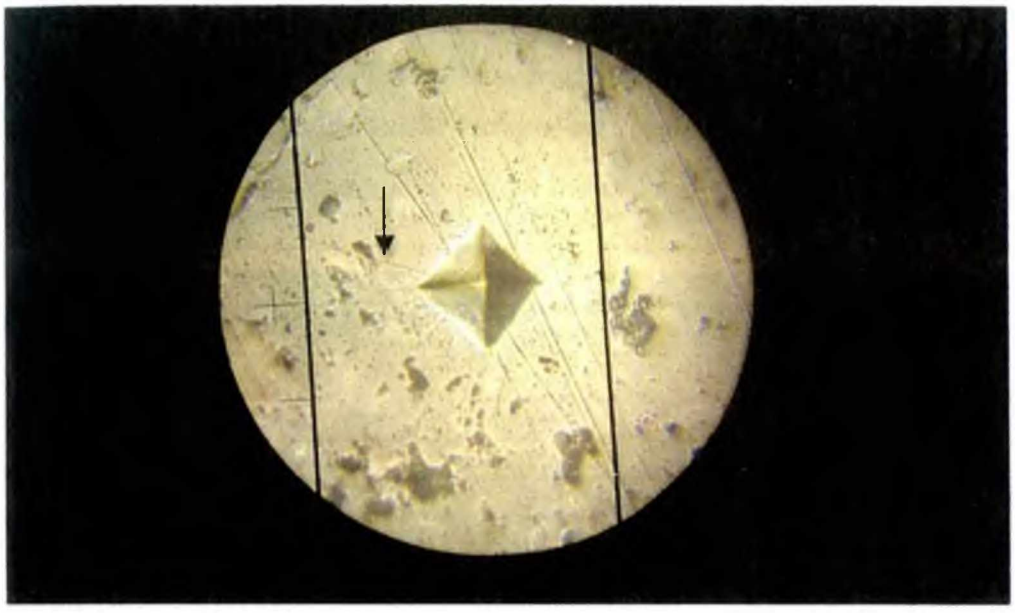

Figure 5.19: 2wt% MWCNT composite sintered at 1000°C

This image shows the indentation resulting from a 500g force at 50x magnification. Field of view diameter is 0.29 mm.

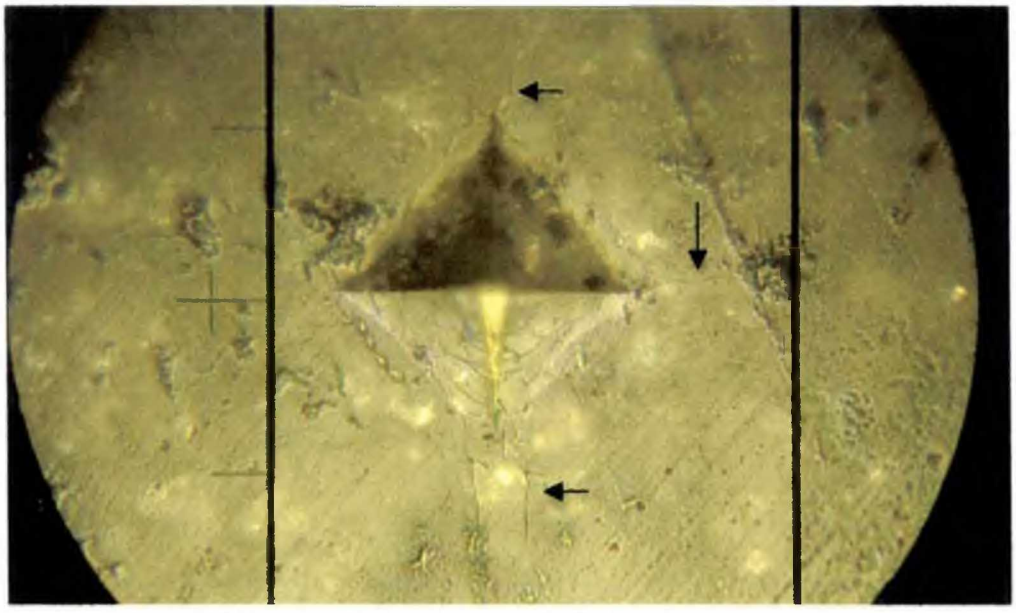

Figure 5.20: 4wt% MWCNT composition sintered at 850°C

This 500g force indentation is shown at 50x magnification. The field of view diameter is 0.29 mm.

Relative density of the composite samples was recorded during the synthesis process. The following table shows the average sintered relative density of the samples. Density values were not obtained for fractured samples.

Table 5.1: Average relative density of the samples after sintering at 1000°C and 850°C

Composition	Average Relative Density of Sintered Samples at 1000°C and 850°C	
0wt% MWCNT	84%	84%
1wt% MWCNT	81%	82%
2wt% MWCNT	82%	80%
4wt% MWCNT	-	84%
5wt% MWCNT	71%	83%
8wt% MWCNT	-	72%
10wt% MWCNT	64%	-

Following the indentation tests, measurement data was processed to obtain the following hardness and fracture toughness values for each composite. Figures 5.21 through 5.24 illustrate a decrease in hardness with an increase in the concentration of carbon MWCNTs.

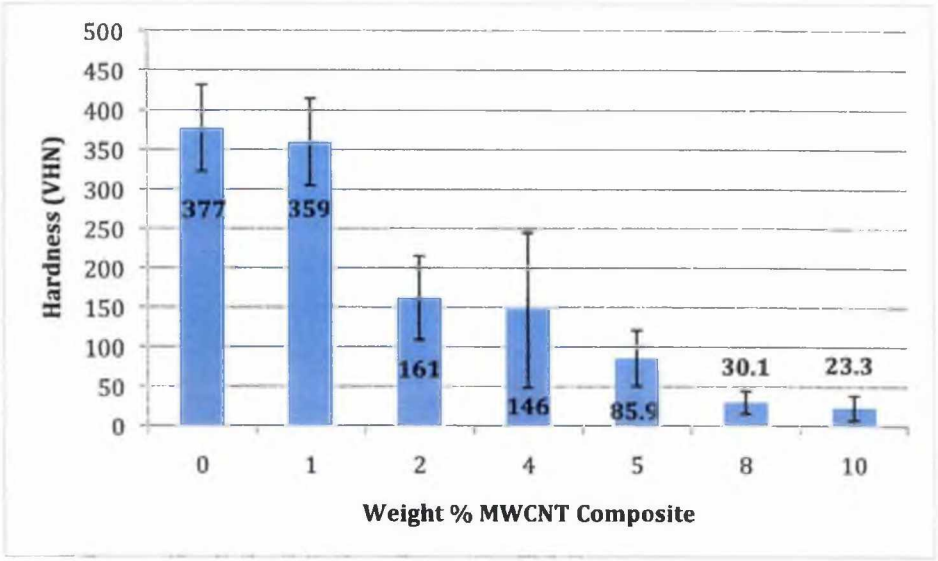

Figure 5.21: Hardness in HVN for composite samples sintered at 1000°C

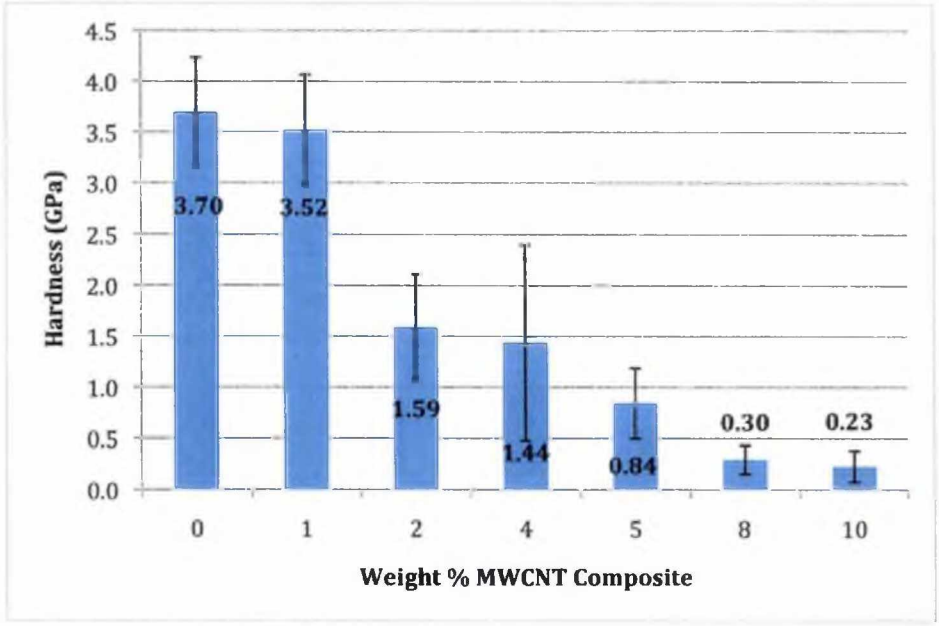

Figure 5.22: Hardness in GPa for composites sintered at 1000°C

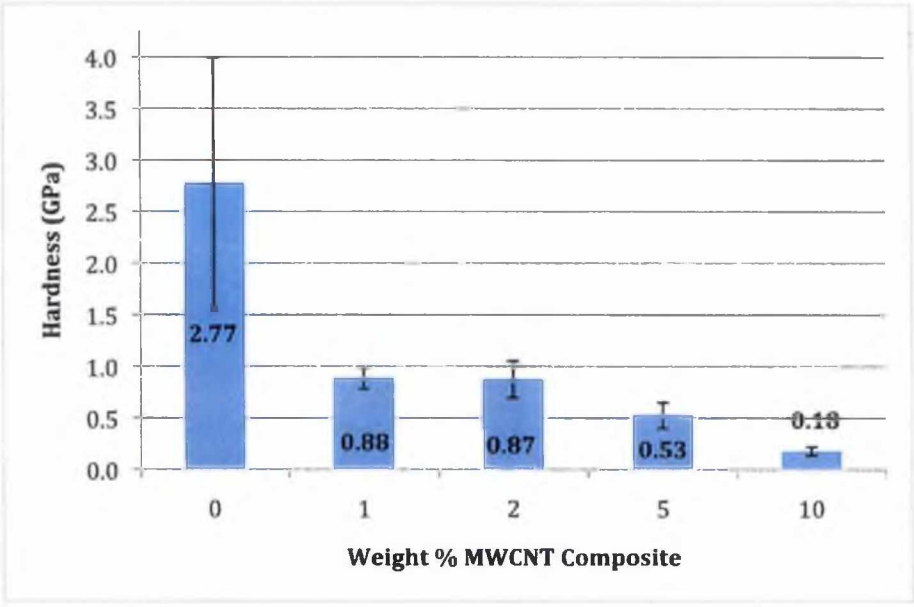

Figure 5.23: Hardness in GPa for composites sintered at 850°C

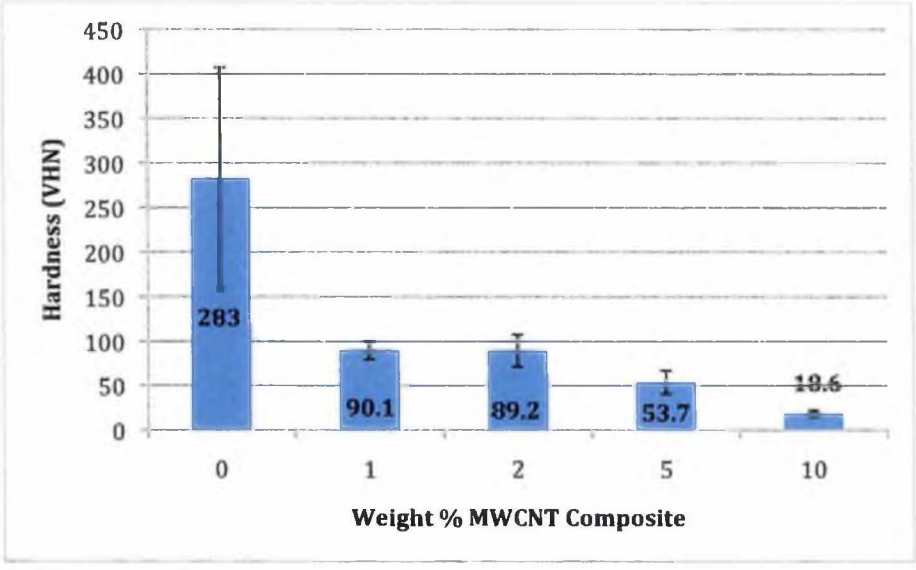

Figure 5.24: Hardness HVN for composites sintered at 850°C

The following graphs, Figures 5.25 – 5.26, show the fracture toughness of the composites sintered at 1000°C and 850°C.

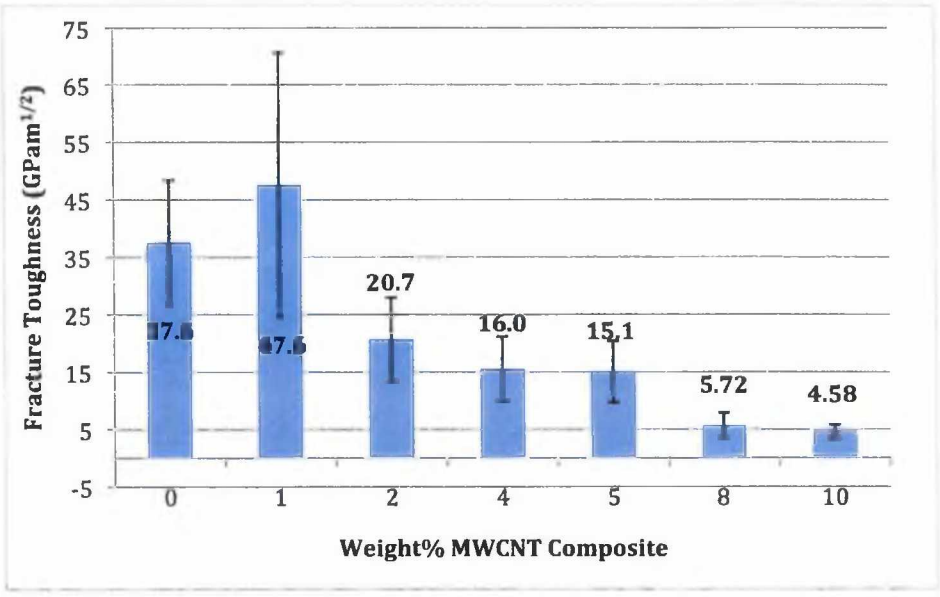

Figure 5.25: Fracture toughness of composite samples sintered at 1000°C

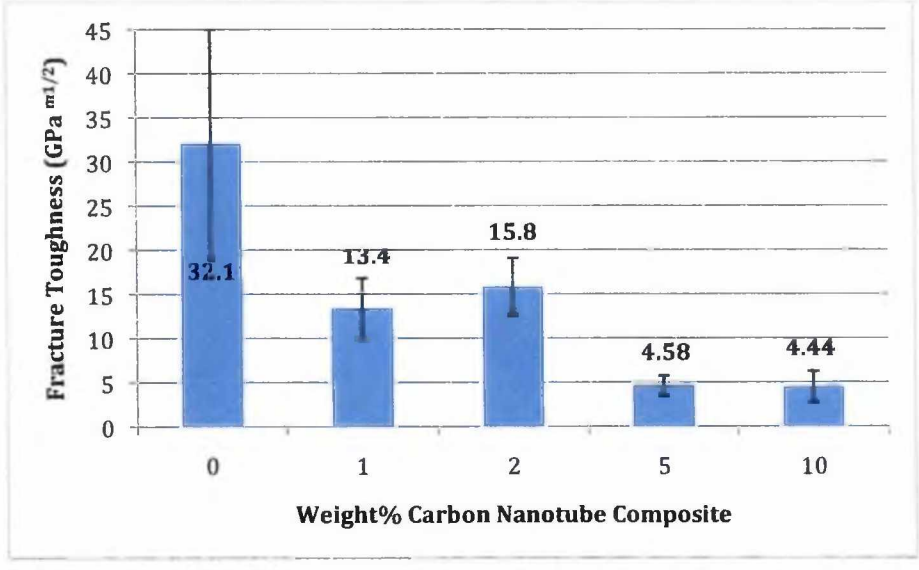

Figure 5.26: Fracture toughness of composite samples sintered at 850°

Figure 5.26 shows an increase in fracture toughness at 1wt% MWCNTs in the samples sintered at 1000°C. As concentrations continue to increase above 1wt%

MWCNTs the fracture toughness decreases. The toughness results of the samples sintered at 850°C show than none of the composite samples exceed the fracture toughness of the pure Bioglass sample.

The following tables summarize the hardness and fracture toughness data for each wt% MWCNTs.

Table 5.2: Hardness and fracture toughness summary for composite samples sintered at 1000°C.

Percent MWCNT Composition	Reiative Density	Hardness						Fracture Toughness		
		GPa			HVN			$GPa \cdot m^{1/2}$		
0	0.84	3.70	±	0.54	377	±	54.6	37.5	±	10.8
1	0.82	3.52	±	0.54	359	±	55.0	47.6	±	23.0
2	0.80	1.59	±	0.52	161	±	53.2	20.7	±	7.25
4	0.84	1.44	±	0.96	146	±	97.9	15.5	±	5.60
5	0.82	0.84	±	0.35	85.9	±	35.2	15.1	±	5.30
8	0.72	0.30	±	0.14	30.1	±	14.3	5.72	±	2.15
10	0.64[1]	0.23	±	0.15	23.3	±	15.5	4.58	±	1.17

Notes: [1]Specimen fractured, density estimated

Table 5.3: Hardness and fracture toughness summary for composite samples sintered at 850°C.

Percent MWCNT Composition	Relative Density	Hardness						Fracture Toughness		
		GPa			HVN			$GPa \cdot m^{1/2}$		
0	0.84	2.78	±	1.22	283	±	124	32.0	±	12.9
1	0.82	0.88	±	0.10	90.1	±	10.2	13.3	±	3.43
2	0.81	0.88	±	1.33	89.2	±	18.3	15.8	±	3.28
5	0.79	0.53	±	0.13	53.6	±	12.9	11.4	±	3.97
10	0.64	0.18	±	0.04	18.5	±	4.14	4.44	±	1.80

Notes: 4wt% and 8wt% samples were not evaluated for hardness and fracture toughness

CHAPTER 6: Discussion

The composite samples were evaluated throughout the synthesis process using XRD and SEM technology to confirm the presence of material components during processing, verify crystallography of the sintered material, and to assess mixing effectiveness and interfacial bonding of the materials. Synthesis procedures significantly affect and alter the properties of a ceramic composite and are discussed in the data evaluation. Following synthesis, a Vickers indentation hardness test was performed to quantify the hardness and fracture toughness of the composite. The results and findings from these analysis methods and experiments are presented below.

6.1. XRD Data Analysis

XRD scans were performed to verify composite phases and crystallization of the bioglass material. Oxidation of the MWCNTs at the selected sintering temperature was a concern during the investigation. The optimal sintering temperature for Bioglass was identified in Bretcanu's [24] paper, at 1040°C. However, recent studies [15] found the oxidation of MWCNTs to occur between 760°C and 810°C [15]. During initial sintering attempts, obvious oxidation of the surface MWCNTs was identified visually by the change in color from black, unsintered samples, to white after sintering. This finding corresponded with similar findings presented by Kealley et al. where over 99% of the MWCNTs were oxidized between 760°C and 810°C in an air environment [15]. Controlled sintering environments in argon were found to partially preserve the MWCNTs [22]. Approximately 23% of the MWCNTs were preserved during heating in an argon environment in previous studies [22]. Raw MWCNTs were placed in the furnace chamber adjacent to the composites during each sintering event to confirm complete oxidation was not occurring and to quantify sample oxidation. Following sintering, the MWCNT material was removed from the furnace and scanned using the XRD. Figure 5.1 shows the XRD scans for the sintered MWCNTs. This graph clearly shows a decrease in signature MWCNT peaks, corresponding to a decrease in the

number of MWCNTs present; however, the scans do confirm the presence of a portion of the MWCNTs. Several methods were proposed to evaluate the amount of a material using XRD scans including the peak height and the area under the peak. An evaluation of the 26.5° peak height on Figure 5.1 and oxidized MWCNT mass following sintering produced the following MWCNT wt% percentages after sintering. The peak height for the three scans shown in Figure 5.1 are 627 counts for unsintered MWCNTs, 217 counts for MWCNTs sintered at 850°C, and 125 counts for MWCNTs sintered at 1000°C. These values correspond to the oxidation of 75.4% for the samples sintered at 850°C and 80% for the samples sintered at 1000°C. These values assumed uniform oxidation throughout the sample resulting in unusually high oxidation percentages. Weight loss calculations were performed to approximate the complete oxidation of an outer shell in order to obtain an accurate post sintering MWCNT wt%. Calculations to support the post sintering MWCNT wt% can be found in Appendix C.3. All composites will be referred to by their original wt% throughout this document.

Table 6.1: Post sintering MWCNT estimated wt%

Mixed MWCNT wt%	Sintering Temp. °C	Post Sintering MWCNT wt%
0	1000	0
	850	0
1	1000	0.74
	850	0.80
2	1000	1.57
	850	1.78
4	1000	3.26
	850	3.77
5	1000	4.09
	850	4.39
8	1000	6.51
	850	7.77
10	1000	8.44
	850	-

Note: 10wt% at 850°C fractured after sintering

Table 6.1 shows a clear decrease in the amount of MWCNTs in the composites

after sintering. Following sintering, the surface MWCNTs clearly oxidized as is shown in Figure 3.3. However, during sintering the interior portion of the samples retained the MWCNTs, as is evidenced by the oxidized ring around the 4wt% MWCNT composite in Figure 6.1. The sample was ground to obtain values for the hardness and fracture toughness equation from the middle of the sample, which experienced minimal oxidation. The oxidation concentrations presented in Table 6.1 account for the complete oxidation of the surface of the sample with an 0.08 mm thick shell. The calculation assumed approximate oxidation of the interior portion of the sample based on a MWCNT wt% correction for additional weight loss after sintering. The interior portion of the sample is assumed to experience uniform MWCNT oxidation. The MWCNT wt% loss for samples sintered at 1000°C and 850°C is approximately 20% and 12% respectively.

Figure 6.1: 4wt% MWCNT composite sample 1¼ inch diameter section with clear surface oxidation

The signature peaks of the MWCNTs can be identified in Figure 5.1 at 26.5°, 42.7°, and 53°. However, due the oxidation during sintering and the peak at 53° is visible only on the unsintered MWCNT sample but is not visible after sintering due to the deterioration of the nanotubes. In the detailed scan presented in Figure 5.2 the deterioration of the MWCNT peak at 42.7° is apparent. The MWCNTs sintered at 1000°C deteriorated more than the nanotubes sintered at 850°C corresponding to the post sintering MWCNT% calculations.

The XRD was also used to confirm crystallization of the bioglass sample matrix. Sintering of a 0wt% composite showed the crystallization characteristic of a glass-

ceramic structure and confirmed the presence of the main crystalline phase $Na_2Ca_2Si_3O_9$, and the secondary phase $Na_2Ca_4(PO_4)_2SiO_4$ was also identified [31] in Figure 5.4. Crystallization of the Bioglass occurs between 600°C and 750°C depending on the heating rate of the samples, however Bretcanu's [24] paper shows that the material is highly crystalline before it reaches the second crystallization step between 850°C and 1000°C, indicating that a lower temperature to accommodate retention of the carbon MWCNTs may result is a slightly less dense, but still highly crystallized Bioglass matrix. The secondary phase is apparent in the samples sintered at 1000°C and at 850°C. Lefebvre [23] indicated that this peak appears at ($2\theta \approx 32°$) representing the formation of a secondary crystalline phosphate phase after sintering in the 800°C to 950°C range.

In ceramics secondary recrystallization is used to identify discontinuous or exaggerated grain growth where a small fraction of the grains grow unusually large and consume surrounding grains [12]. Secondary growth is likely to occur when grain growth is inhibited by pores and can be detrimental to the material properties [12]. Bretcanu identified both phases at 800°C indicating the development of the minor phase is dependent on sintering parameters such as heating rates [24]. Several studies have investigated the crystallization of Bioglass and have agreed that crystallization of the material is dominated by surface crystallization mechanisms (Avrami parameter $n = 1$) [23, 24].

In order to achieve crystallization in the material, the samples were heated at a rate of 9.00°C/min, held at temperature for 20 minutes, and cooled at a rate of 1.62°C/min. Temperature profiles for the furnace are show in Figure 6.2.

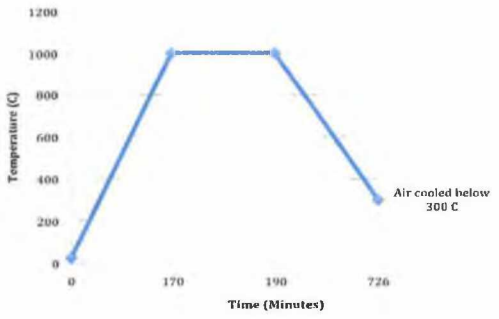

Figure 6.2: Lucifer furnace argon chamber temperature profile

As a result of the slow heating and cooling times, the samples were kept in the furnace for over 9 hours. This long period in the furnace easily could have extended crystallization of the bioglass, increased oxidation of the MWCNTs, and affected the interfacial bonding between the two components. Sintering times, temperatures, and heating profiles are an important factor in the final properties of a material and should be thoroughly investigated in future studies.

The MWCNT peaks are completely obscured by the crystallization of the Bioglass material as is shown in Figure 5.6. The absence of definable MWCNT peaks in the sintered composite can be explained by the dilution of the MWCNTs within the Bioglass matrix, the deterioration of the MWCNTs during sintering, and the overlap with the crystallization pattern of bioglass.

6.2. SEM Image Analysis

Mixing and milling synthesis procedures were evaluated for effectiveness with the SEM. Figure 5.7 shows the raw Bioglass powder with a particle size of less than 53 μm. Figure 5.8 shows that milling of the material occurred during mixing reducing the particle size. The average Bioglass particle size following this mixing procedure is ~10μm based on SEM visual observation indicating milling of the Bioglass occurred. The reduction in particle size allows for better mixing and bonding between the Bioglass

matrix and the MWCNT fibers. Ball milling and mixing procedures are outlined in Section 3.2.1.

Raw MWCNTs are shown in Figure 5.9. Agglomeration of MWCNTs is a common problem due to Van der Waals forces between the MWCNTs. The sides of the tubes are very smooth allowing the carbon bonds and electrons in one nanotube to lie very close to adjacent nanotubes electrons allowing Van der Waals short-range attractive force to bind the tubes. The binding energy between adjacent tubes due to this force is approximately 0.5eV per nanometer of contact length [26]. The agglomeration of MWCNTs prevents the Bioglass matrix from penetrating into the bundles resulting in matrix bonding with the outside of an agglomerated bundle [22, 43]. Agglomerated MWCNTs are shown in Figure 5.10. The mechanical behavior of MWCNTs and the ultimate strength of the composite depends on the magnitude of interfacial bonding between the MWCNT fibers and the bioglass composite [5]. Inadequate bonding between the components reduces the transfer of stress from the brittle matrix to the high strength fibers resulting in premature failure of the composite [12].

In order to separate the MWCNTs, a high-energy ball mill mixing process was used for a period of 10 minutes, followed by a low energy mixing process for 50 minutes to distribute the MWCNTs throughout the Bioglass powder. Figure 5.11 and 5.12 show the even distribution of the MWCNTs following the mixing process detailed above.

To evaluate the sintered composites several samples were fractured to view the composition and interaction of the MWCNTs and bioglass along a fracture surface in Figure 5.15 and Figure 5.14. The resolution of the SEM restricted the ability to capture images showing the pullout of MWCNTs and residual holes along the fracture surface. These images could have confirmed that the interfacial structure was well mixed and bonded to facilitate effective stress transfer from the matrix to the MWCNT fibers. The MWCNTs do not appear uniformly distributed in the composite sample.

Agglomeration of the MWCNTs is apparent in the samples as shown in Figure 5.14. The MWCNTs are shown clustered in the center of the micrograph. The

agglomeration of the tubes will result in weak areas of the sample; however, the distribution of some of the MWCNTs throughout the sample will still improve the mechanical properties of the composite.

6.3. Hardness and Fracture Toughness Analysis

The Vickers indentation hardness tests resulted in a variety of indentation sizes and crack lengths. For homogeneous materials the cracks propagating from the indentation tips should be equal, indicating the load is evenly distributed across the surface [13].

To evaluate the hardness and fracture toughness of the material, microhardness indentation tests were conducted. Representative photographs of these indentations from are shown in Chapter 5: Results. As the wt% of the MWCNTs increases shorter cracks and larger indentations in the material are evident, indicating less of an ability to absorb energy before failure. For indentations of similar sizes, a longer crack length indicates the material is able to absorb less energy and is characterized by a lower fracture toughness value. Under the same test load, a larger indentation diameter results in a lower fracture toughness value. In Figure 5.18 the indentation size on the 1wt% MWCNT sample is much smaller than the indentations in Figure 5.19, 2wt% MWCNT, and Figure 5.20, 4wt% MWCNT. The smaller indentation in the 1wt% sample corresponds to the highest fracture toughness value of the samples sintered at 1000°C.

Several samples, including the 2wt% MWCNT composite shown in Figure 5.19, displayed indentations with similarly sized cracks indicating homogeneity of the composite. However, the majority of the samples produced varied cracks indicating the composites were not homogeneous. Pores on the surface and within the material are a likely contributor to inconsistent failure of the composite at the indentation point. The low relative density of the samples, as presented in Table 5.1, is likely a contributor to variations in the composite hardness and fracture toughness data. Fully compact samples with 100% relative density would allow for less pore and void spaces within the sample. A smaller material particle size and high-pressure compaction techniques would

increase compaction of the sample and decrease variability in the data.

In the high wt% MWCNT samples (8wt% and 10wt%) the agglomeration of MWCNTs is visible in the indentation images and is likely causing premature and inconsistent failure of the material during loading. Agglomeration of the MWCNTs also affected sample processing techniques. Due to the large difference in hardness between the sintered Bioglass and the agglomerated MWCNTs, grinding and polishing were varied to obtain samples with a smooth surface to conduct the hardness experiments. In order to obtain a smooth surface, additional grinding time was required for the higher wt% MWCNT samples to conduct indentation testing. This machining may have affected the microstructure and indentation measurements by inducing cracking in the material prior to testing. Future research should include a thorough analysis of homogeneous mixing procedures.

Hardness and fracture toughness values were computed from Vickers hardness indentation tests. The complete raw data set from these tests can be found in Appendix B. Hardness values were calculated using the following formulas presented in the ASTM C 1327-08. Hardness is a measure of the strength of the material and this decrease is attributed to the addition of the relatively soft carbon MWCNTs into the hard bioglass matrix. Hardness results ranged from 3.70 GPa to 0.23 GPa (377 to 18.6 HVN) for the composite samples at 0wt% to 10wt% respectively. The results trend corresponds to the hardness data of carbon nanotube composites published by Tjong [9]. These values exceeded the measured hardness of bone at 0.396 GPa and 40.4 HVN [19]. Hydroxyapatite, a similar bioceramic measures hardness values slightly above raw Bioglass at 5.3 GPa and 537.5 HVN.

Figure 5.25 shows the maximum fracture toughness for the 1wt% MWCNTs in the samples sintered at 1000°C. As concentrations continue to increase above 1wt% the fracture toughness decreases; this is likely due to the agglomeration of MWCNTs, which weaken the material strength. The agglomeration of MWCNTs is documented in many previous studies when the wt% approaches 10 [9, 28]. The fracture toughness results

from the samples sintered at 850°C show than none of the composite samples exceed the fracture toughness of the pure Bioglass sample indicating that the sintering temperature is important to establish interfacial bonding between the matrix and the fiber reinforcements and to achieve optimal crystallization of the material. The optimal fracture toughness result at 47.6 $GPa \cdot m^{1/2}$ was obtained at 1wt% MWCNT concentration after sintering at a temperature of 1000°C. This value exceeds the fracture toughness of bone which is measured between 2 and 12 $GPa \cdot m^{1/2}$ and the fracture toughness of hydroxyapatite at 1 $GPa \cdot m^{1/2}$ [5]. These results indicate that a MWCNT-Bioglass composite can meet or exceed some of the mechanical properties of bone and has potential for use as a load bearing synthetic bone material.

CHAPTER 7: Conclusion

Through this investigation a novel carbon nanotube-bioglass composite was successfully synthesized using mixing, compaction, and sintering techniques. The mechanical properties of the composite were evaluated using Vickers indentation technique to determine hardness and fracture toughness. The results showed that hardness for both the composites sintered at 1000°C and 850°C generally decreased with increasing MWCNT concentration, and is attributed to the addition of the soft MWCNT fibers with poor compressive strength into the Bioglass. The toughness of the samples increases in the 1000°C samples from pure Bioglass to 1wt% MWCNT concentration which reported a fracture toughness of 47.6 $GPa \cdot m^{1/2}$. This value far exceeds the fracture toughness value for load bearing bone at 12 $GPa \cdot m^{1/2}$ and appears to be an excellent candidate material for biomedical load bearing applications [5]. This initial increase in fracture toughness is due to the reinforcement of the matrix through interfacial bonding with MWCNT fibers. The decrease in fracture toughness with increasing MWCNT concentration above 1wt% is likely due to the agglomeration of MWCNTs. The agglomeration prevents distribution and bonding of MWCNT fibers in the matrix and decreases the composite's ability to resist fracture. Images collected on a SEM confirmed the agglomeration of MWCNTs at higher weight percents.

In the composites sintered at 850°C the samples did not exceed the fracture toughness of the pure Bioglass material. The mechanical properties decreased substantially with the addition of MWCNTs indicating the lower temperature did not promote interfacial bonding between the components. All fracture toughness values from the composites sintered at 850°C were lower than those sintered at 1000°C. XRD analysis confirmed the crystallization of the main crystalline phase $Na_2Ca_2Si_3O_9$ in the Bioglass material at both 1000°C and 850°C. Bioglass experiences a recrystallization, densification, and grain growth stage which was experienced by composites sintered at 1000°C and likely resulted in an increase in fracture toughness over the samples sintered at 850°C. These results confirm the promising potential of MWCNT-Bioglass

composites for use as a synthetic bone material to restore function in load bearing human bone structures.

The increase in fracture toughness of this material is encouraging for the future of this composite in the field of biomedical engineering. In order to further improve the mechanical properties of this composite, the synthesis procedure should be evaluated for effectiveness specifically in regard to; the use of a vacuum furnace to prevent oxidation of the MWCNTs, a mixing method developed to prevent agglomeration of the MWCNTs at all concentrations, and the use of hot pressing techniques to obtain fully dense samples.

Literature Cited

1. Best, S.M., et al., *Bioceramics: Past, present and for the future.* Journal of the European Ceramic Society, 2008. 28(7): p. 1319-1327.

2. Meyyappan, M., *Carbon Nanotubes: Science and Application.* NASA Ames Research Center, Moffett Field, California, 2005.

3. Ratner, et al., *Biomaterials Science*. 2nd ed. 2004, New York: Elsevier Academic Press.

4. Vallet-Regì, M., *Evolution of bioceramics within the field of biomaterials.* Comptes Rendus Chimie, 2009.

5. White, et al., *Hydroxyapatite-Carbon Nanotube Conposites for Biomedical Applications: A Review*. Applied Ceramic Technology, 2007. 4(1): p. 1-13.

6. Goller, G., et al., *Processing and characterization of bioglass reinforced hydroxyapatite composites.* Ceramics International, 2003. 29(6): p. 721-724.

7. Li, A., et al., *Mechanical properties, microstructure and histocompatibility of MWCNTs/HAp biocomposites.* Materials Letters, 2007. 61(8-9): p. 1839-1844.

8. Zhang, F., et al., *Bioinspired structure of bioceramics for bone regeneration in load-bearing sites.* Acta Biomaterialia, 2007. 3(6): p. 896-904.

9. Tjong, S.C., *Carbon Nanotube Reinforced Composites: Metals and Ceramic Materials*. 2009, Weinheim: Wiley-VCH.

10. Nagendra, N. and S. Bandopadhyay, *Strength and fracture toughness of LSFCO membranes exposed to reducing conditions*. Scripta Materialia, 2003. 48(1): p. 37-42.

11. Boch, P.N., Jean-Claude, *Ceramics Materials: Processes, Properties and Applications*. 2006, London: ISTE.

12. Carter, et al., M. Grant, *Ceramic Materials: Science and Engineering*. 2007, New York: Springer.

13. Callister, W.D., *Materials Science and Engineering: An Introduction*. 7th ed.

2007, New York: John Wiley & Sons, Inc.

14. Dorozhkin, S.V., *Bioceramics of calcium orthophosphates.* Biomaterials. 31(7): p. 1465-1485.

15. Kealley, C., et al., *Development of carbon nanotube-reinforced hydroxyapatite bioceramics.* Physica B: Condensed Matter, 2006. 385-386(Part 1): p. 496-498.

16. Zhan, G., et al., *Processing and Characterization of Nanoceramic Composites With Interesting Structural and Functional Properties. Review of Advanced Materials Science*, 2005(10): p. 185-196.

17. Jiang, D., et al., *Effect of sintering temperature on a single-wall carbon nanotube-toughened alumina-based nanocomposite.* Scripta Materialia, 2007. 56(11): p. 959-962.

18. Benzaid, R., et al., *Fracture toughness, strength and slow crack growth in a ceria stabilized zirconia-alumina nanocomposite for medical applications.* Biomaterials, 2008. 29(27): p. 3636-3641.

19. Pramenik, S.et al., *Development of High Strength Hydroxyapatite for Hard Tissue Replacement.* Biomaterial Trends, 2005. 19(1): p. 46-51.

20. Tancret, F., et al., *Modelling the mechanical properties of microporous and macroporous biphasic calcium phosphate bioceramics.* Journal of the European Ceramic Society, 2006. 26(16): p. 3647-3656.

21. Li, W., et al., *Preparation and Characterization of Multiwalled Carbon Nanotube-Supported Platinum for Cathode Catalysts of Direct Methanol Fuel Cells.* Journal of Physical Chemistry, 2003(107): p. 6292 - 6299.

22. Singh, et al., *Hydroxyapatite Modified with Carbon-Nanotube-Reinforced Poly(methyl methacrylate): A Nanocomposite Material for Biomedical Applications.* Advanced Functional Materials, 2008(18): p. 694-700.

23. Lefebvre, L., et al., *Structural transformations of bioactive glass 45S5 with thermal treatments.* Acta Materialia, 2007. 55(10): p. 3305-3313.

24. Bretcanu, O., et al., *Sintering and crystallisation of 45S5 BioglassÆ powder.* Journal of the European Ceramic Society, 2009.

25. Amaral, M., et al., *Densification route and mechanical properties of Si3N4-*

bioglass biocomposites. Biomaterials, 2002. 23(3): p. 857-862.

26. Popov, et al., ed. *Carbon Nanotubes*. 2006, Springer: Netherlands.

27. Yusa, H. and T. Watanuki, *X-ray diffraction of multiwalled carbon nanotube under high pressure: Structural durability on static compression.* Carbon, 2005. 43(3): p. 519-523.

28. Esawi, A. and K. Morsi, *Dispersion of carbon nanotubes (CNTs) in aluminum powder.* Composites Part A: Applied Science and Manufacturing, 2007. 38(2): p. 646-650.

29. Andrews, R., et al., *Purification and structural annealing of multiwalled carbon nanotubes at graphitization temperatures.* Carbon, 2001. 39(11): p. 1681-1687.

30. Bal·zsi, C., et al., *Application of carbon nanotubes to silicon nitride matrix reinforcements.* Current Applied Physics, 2006. 6(2): p. 124-130.

31. Lin, K., et al., *Fabrication and characterization of 45S5 bioglass reinforced macroporous calcium silicate bioceramics.* Journal of the European Ceramic Society, 2009. 29(14): p. 2937-2943.

32. Ramesh, S., et al., *Rapid densification of nanocrystalline hydroxyapatite for biomedical applications.* Ceramics International, 2007. 33(7): p. 1363-1367.

33. Agarwal, S. and P.V. Rao, *Experimental investigation of surface/subsurface damage formation and material removal mechanisms in SiC grinding.* International Journal of Machine Tools and Manufacture, 2008. 48(6): p. 698-710.

34. PANalytical, X-Ray Diffraction User's Guide. 2007.

35. Black, J.T., and Ronald A. Kohser., *Degarmo's Materials and Processes in Manufacturing.* 2008. 10th Edition: p. 39.

36. ASTM, *Standard Test Method for Vickers Indentation Hardness of Advanced Ceramics*. 2009. ASTM C 1327-08.

37. Denry, I.L. and J.A. Holloway, *Elastic constants, Vickers hardness, and fracture toughness of fluorrichterite-based glass-ceramics.* Dental Materials, 2004. 20(3): p. 213-219.

38. Gong, J., J. Wu, and Z. Guan, *Examination of the indentation size effect in low-*

load vickers hardness testing of ceramics. Journal of the European Ceramic Society, 1999. 19(15): p. 2625-2631.

39. Barsoum, M.W., *Fundementals of Ceramics*. 2003, New York: Taylor & Francis.

40. Montgomery, et al., *Applies Statistics and Probability for Engineers*. 3rd ed. 2003, New York: John Wiley & Sons, Inc.

41. Mahanandia, P., et al., *Multiwall carbon nanotubes from pyrolysis of tetrahydrofuran.* Materials Research Bulletin, 2006. 41(12): p. 2311-2317.

42. Emmanuel, B., et al., *Simulated XRD profiles of carbon nanotubes (CNTs): An efficient algorithm and a recurrence relation for characterising CNTs. Journal of Alloys and Compounds,* 2009. 479(1-2): p. 484-488.

43. Shi, D., et al., Yonggang Y. Huang; Keh-Chih Hwang; Huajian Gao, *The Effect of Nanotube Waviness and Agglomeration on the Elastic Property of Carbon Nanotube-Reinforced Composites.* Jornal of Engineering Materials and Technology, 2004. 126: p. 250 - 257.

APPENDIX A: Material Data Sheets

A.1. 45S5 Bioglass

A.2. Multi-Wall Carbon Nanotubes

MO-SCI Corporation

MO-SCI Health Care, L.L.C. and MO-SCI Specialty Products, L.L.C.
4040 HyPoint North
Rolla, MO 65401 USA
Telephone: 573-364-2338 Fax: 573-364-9589

Material Safety Data Sheet

Section 1 - Product And Company Identification

1.1 Product Identity: GL-0160 Bioactive Glass

1.2 Product Name and/or Product Code: 45S5 Bioactive Glass Spheres, Beads, Balls, Frit, Fiber, Ribbons, Discs and/or Rods

1.3 Manufacturer Name and Address: MO-SCI Corporation
4040 HyPoint North
Rolla, Missouri, USA 65401

1.4 Emergency Telephone Number: 573-364-2338 (USA)
Hours of Operation are Monday through Friday; 8am to 5pm CST

Section 2 - Hazards Information

2.1 Emergency Overview: None

2.2 OSHA Regulatory Status: None

2.3 Potential Health Effects:
Glass and nuisance dust may cause temporary respiratory and/or eye irritation.
Possible contact dermatitis.
Slipping hazard can be present when spilled on floor.

2.4 Potential Environmental Effects: None

Section 3 - Composition / Information on Ingredients

Chemical Name	CAS #	EINECS(ELINCS)	WT%
Glass, oxide & Chemicals	65997-17-3	266-046-0	≤100%

Section 4 - First Aid Measures

4.1 Flush irritated eye with water or commercial eyewash. If unable to remove dust or beads by this method, seek medical care.
For respiratory irritation, remove victim to well-vented area. Seek medical care if this does not alleviate the condition.
Thorough cleansing reduces contact dermatitis.

Section 5 - Fire-Fighting Measures

5.1 Not applicable; Not a fire hazard.

Section 6 - Accidental Release Measures

6.1 Vacuum or sweep up spilled material to prevent slipping hazards.

Section 7 - Handling And Storage

7.1 No special precautions are needed, but gloves reduce the chance of contact dermatitis, glasses reduce possibility of eye irritation, and a dust mask reduces the effects of nuisance dust.

7.2 Store in ambient conditions.

MO-SCI Corporation

MO-SCI Health Care, L.L.C. and MO-SCI Specialty Products, L.L.C.
4040 HyPoint North
Rolla, MO 65401 USA
Telephone: 573-364-2338 Fax: 573-364-9589

Section 8 - Exposure Controls/Personal Protection

8.1 Exposure Guidelines:

Component	OSHA PEL	ACGIH TLV	Unit
Nuisance dust (>5µm)	15	10	mg/m^3
Nuisance dust-respirable (<5µm)	5	5	mg/m^3

8.2 Engineering Controls: Adequate ventilation

8.3 Personal Protective Equipment: Dust mask and Safety glasses

Section 9 – Physical and Chemical Properties

9.1 Glass appears to be white in color, tasteless, odorless.

9.2 No important health, safety or environmental information is available.

9.3 Physical Properties

Specific Gravity	2.7 g/cm^3	Boiling Point	Not Measurable
Softening Point	550°C	Vapor Pressure	Not Applicable
Soluble in water			

Section 10 - Stability and Reactivity

10.1 Conditions to Avoid: Not Applicable

10.2 Materials to Avoid: Breakdown occurs in strong acids and bases, such as Hydrofluoric Acid and Sodium Hydroxide. Material is soluble in water.

10.3 Hazardous Decomposition Products: Not Applicable

Section 11 - Toxicological Information

11.1 Possible Routes of Exposure:

Inhalation is not likely for materials >5µm in diameter
Ingestion is possible if good hygiene practices are not followed
Eye Irritation is possible if safety glasses/goggles are not worn.
Skin contact may result in contact dermatitis

Section 12 - Ecological Information

12.1 Not Applicable

Section 13 - Disposal Considerations

13.1 Glass can be disposed of in a solid waste landfill.

Section 14 - Transport Information

14.1 Class 55; Item Number 87660

14.2 Proper Shipping Name: Glass

Section 15 - Regulatory Information

15.1 Not Applicable

Section 16 - Other Information

16.1 Disclaimer: The information and recommendations herein are based upon data believed to be correct for material as shipped. However, no guarantee or warranty of any kind, expressed or implied, is made with respect to this information.

MATERIAL SAFET DATA SHEET

1. Chemical Identification

Name: Carbon Nanotubes,

2. Composition/Information on Ingredients

Cas #	None
Purity	90-95%
Diameter	1-100 Nanometer
Amorphous Carbon particles	< 3-5%
Ash	< 0.2-2wt%

3. Hazards Identification

- Irritant
- Irritating to eyes and respiratory system.
- In case of contact with eyes, rinse immediately with plenty of water and seek medical advice.
- Wear suitable protective clothing.

4. First-Aid Measures

- If swallowed, wash out mouth with water, provided person is conscious, please call a physician.
- If inhaled, remove to fresh air.
- If not breathing, give artificial respiration.
- If breathing is difficult, give oxygen.
- In case of contact, immediately wash skin with soap and copious amounts of water.
- In case of contact, immediately flush eyes with copious amounts of water for at least 15 minutes.

5. Fire Fighting Measures

- Extinguishing Media

  Water spray. Carbon dioxide. Dry chemical powder or appropriate foam.
- Special Firefighting Procedures

  Wear self-contained breathing apparatus and protective clothing to prevent contact with skin and eyes.
- Unusual Fire And Explosions Hazards

  Emits toxic fumes (CO_2, CO, etc…) under fire conditions.

6. Accidental Release Measures

- Wear respirator, safety goggles, rubber boots and rubber gloves.
- Sweep up, place in a bag and hold for waste disposal.
- Avoid raising dust.
- Ventilate area and wash spill site after material pickup is complete.

7. Handling and Storage

- Store in a cool dry place.
- Safety shower and eye bath.

- Mechanical exhaust required.
- Wash thoroughly after handling.
- Do not breathe dust.
- Avoid contact with eyes, skin and clothing.
- Compatible chemical-resistant gloves.
- Safety goggles.
- Keep tightly closed.

8. Physical and Chemical Properties
   - Solubility in water: Insoluble
   - Appearance: Black
   - Odor: odorless
   - PH value（5%aqueous solution）: 6-7
9. Stability and Reactivity
   - Stability Stable.
   - Incompatibilities Strong oxidizing agents
   - Hazardous Combustion or Decomposition Products
     Carbon monoxide, carbon dioxide
   - Hazardous Polymerization Will not occur.
10. Toxicological Information
    - May be harmful if absorbed through the skin.
    - May be harmful if swallowed.
    - To the best of our knowledge, the chemical, physical and toxicological properties have not been thoroughly investigated.
    - May cause skin irritation.
    - Causes eye irritation.
    - Material is irritating to mucous membranes and upper respiratory tract.
11. Ecological Information
    - Data not yet available.
12. Disposal Considerations
    - Observe local environmental regulations. Incineration recommended as ultimate disposal method.
13. Other Information
    - The above information is believed to be correct but does not purport to be all inclusive and shall be used only as a guide. Juwei shall not be held liable for any damage resulting from handling or from contact with the above product.
    -
    - License granted to make unlimited paper copies for internal use only.
14. Contact Information

Shenzhen Nanotech Port Co., Ltd.
Phone: 86-137-9840-8160
Nanshan, Shenzhen, Guangdong
China 518000

SEARCH PEAK RESULTS:

VOLTAGE : 35 kV
FILTER :
DETECTOR : PC
SLITS : DS= 1 deg
SS= 1 deg
RS= .2 mm

CURREN : 30 mA
MONOCHRO :
WAVE LENGTH: 1.54184

SCAN MODE : Continuous
START ANGLE: 10 deg
SCAN SPEED : 0.1 deg/sec

DRIVE AXIS : Theta-2Theta
STOP ANGLE : 90 deg
SAMPLING TIME: 1 sec

No.	ANGLE	D-VALUE	INTEN	FWHM	I/I0	No.	ANGLE	D-VALUE	INTEN	FWHM	I/I0
1	25.610	3.4783	897	2.250	100.0	3	43.150	2.0965	158	0.450	17.6
2	42.742	2.1156	156	0.750	17.4						

ANGLE RANGE: 10.000deg --- 90.000deg

CONDITIONS : PEAK HEIGHT(min.)= 0 PEAK WIDTH(min.)= 0.000 WAVE LENGTH= 1.54184

FILE NAME: C:KCNTC 10-30 nm SAMPLE NAME: KCNTC

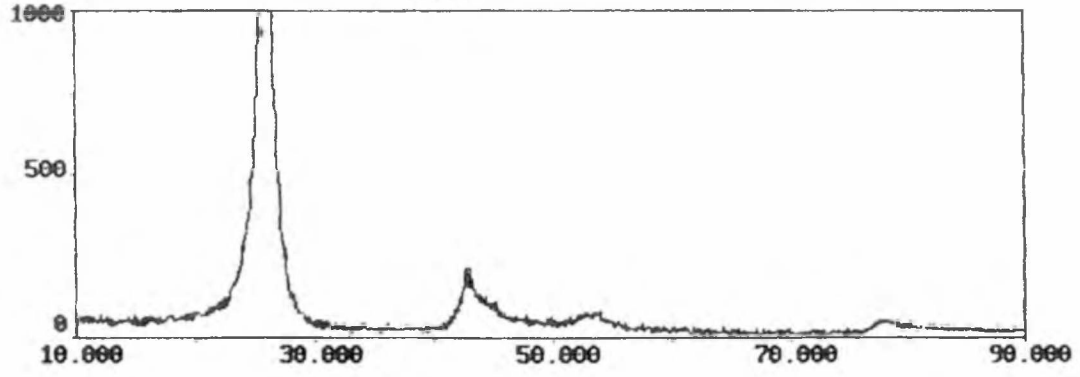

APPENDIX B: Equipment Standard Operating Procedures

B.1. XRD

B.2. SEM

B.3. Vickers Hardness Tester

B.4. Retsch Ball Mill

B.5. Lucifer Furnace

APPENDIX B: Equipment Standard Operating Procedures

B.1. XRD

Equipment

The PANalytical X'Pert PRO MRD utilizes a horizontally positioned PW3050/6x Goniometer upon which the X-ray tube, incident beam optics, sample stage, and diffracted beam optics including the detector are mounted at specific positions to control the omega and 2 theta basic XRD axes.

A ceramic diffraction X-ray tube housing a tungsten cathode filament is mounted onto the goniometer and focuses electrons from the high-tension generator toward a copper anode where they are converted into X-rays. A copper anode is used primarily for phase identification, quantitative analysis, and high resolution diffraction [26].

Incident beam optics are used to prepare and focus the X-ray beam in line focus applications such as phase analysis. A 5 mm incident beam mask was used during the bioglass scans. The optimal anti-scatter slit size is twice that of the divergence slit, therefore 1° (opening 1.5 mm) anti-scatter slit was used in conjunction with a 1/2° (opening 0.75 mm) fixed divergence slit in order to scatter [26].

Test/Analysis Performed

The XRD was used to confirm crystallization phases of the Bioglass and to identify the presence of MWCNTs after sintering.

Parameters Used

Scan Axis	Gonio
Start Position [°2Th.]	5.0203
End Position [°2Th.]	75.557
Step Size [°2Th.]	0.0376
Scan Step Time [s]	5.0800
Scan Type	Continuous
PSD Mode	Scanning
PSD Length [°2Th.]	1.59
Offset [°2Th.]	0.0000
Divergence Slit Type	Fixed

Divergence Slit Size [°]	0.4354
Specimen Length [mm]	10.00
Measurement Temperature [°C]	25.00
Anode Material	Cu
K-Alpha1 [Å]	1.54060
K-Alpha2 [Å]	1.54443
K-Beta [Å]	1.39225
K-A2 / K-A1 Ratio	0.50000
Generator Settings	40 mA, 45 kV
Diffractometer Type	00000000011040813
Diffractometer Number	0
Goniometer Radius [mm]	320.00
Dist. Focus-Diverg. Slit [mm]	100.00
Incident Beam Monochromator	No
Spinning	No

Notes

Three scans were obtained and averaged for each sample analyzed by the XRD.

B.2. SEM

Equipment

An ISI-SR-50-Scanning Electron Microscope and an ElectroScan E2020 Environmental Scanning Electron Microscope (ESEM) was also used to view the raw materials and composite samples.

Test/Analysis Performed

The SEM was utilized for the purpose of creating micrographs to evaluate mixing effectiveness and to evaluate of microscopic characteristics of the composite.

Parameters Used

Images ranging in magnification from 80x to 10,000x were collected and analyzed. Images were collected at 25 KeV.

Notes

Some of the specimens used in this thesis were not coated prior to use in the SEM.

B.3. Vickers Hardness Tester

Equipment

A Buehler Micromet 5101 was used to perform the Vickers indentation hardness test on the composite ceramic. The instrument is capable of applying an indentation force ranging from 50g to 1000g. The manual turret carries two objectives (10x and 50x) and one indenter position with the Vickers indenter mounted.

Test/Analysis Performed

The Vickers indentation hardness test was performed with this tester and applies a load on the sample using a 136° square based diamond pyramid indenter [25]. Hardness is determined by optical measurement of the resulting indentation surface diagonals using a microscope. The Vickers hardness number is determined by dividing the load applied by the indenter by the indenter surface area in square millimeters [26, 27].

Parameters Used

Desirable indentation results were obtained using 200g and 500g indentation forces. Higher wt% composite disks were observed to be generally softer and responded well to a 200g indentation force. Lower wt% composite disks responded favorably to a 500g force. All viewing and measuring was performed using the 50x objective, and indentation photographs were taken through the eyepiece at 50x.

Notes

Quality control checks were performed using calibration standards and materials of known hardness.

B.4. Retsch Planetary Ball Mill PM 200

Equipment

The Planetary Ball Mill used for the milling process pulverizes and mixes soft, medium-hard to extremely hard, brittle and fibrous materials. The grinding jars are arranged eccentrically on the sun wheel of the planetary ball mill. The direction of movement of the sun wheel is opposite to that of the grinding jars in the ratio 1:-2. The grinding balls in the grinding jars are subjected to superimposed rotational movements, the so-called Coriolis forces. The difference in speeds between the balls and grinding jars produces an interaction between frictional and impact forces, which releases high dynamic energies. The interplay between these forces produces the high and very effective degree of size reduction of the planetary ball mill.

Test/Analysis Performed

The ball mill was used to mix the composite materials.

Parameters Used

Balls: 1mm Steatite

Ball to powder ratio: 5:1 (weight)

Bowl: zirconia

RPM: 10 minutes at 300 rpm followed by 50 minutes at 100 rpm.

Notes

The jar was counter rotated every 20 minutes during the mixing procedure.

B.5. Lucifer Furnace

Equipment

A Lucifer 82Am-F12 electric heat treatment furnace was used to sinter samples for this thesis.

Test/Analysis Performed

Samples were sintered at 850°C and 1000°C in an argon atmosphere.

Parameters Used

Samples were positioned on firebrick and inserted into the chamber. Argon gas was purged through the chamber at a rate of 6.91 CFH for 15 minutes before heating. Once the chamber was purged the samples were heated to temperature and cooled to 300°C in an argon environment. A stopcock outflow valve was kept partially open to pull argon consistently through the muffle chamber. This resulted in the additional consumption of argon, but maintained an argon environment in the chamber.

Notes

Chamber temperature was controlled by the controller and was maintained manually at temperature for 20 minutes. The furnace was shut down and allowed to cool following the high temperature period. Argon was maintained in the chamber until the samples reached 300°C.

APPENDIX C: Experimental Data and Calculations

C.1. Composite Synthesis Data

C.2. Hardness Testing and Fracture Toughness Data and Calculations For Samples Sintered at 1000°C

C.3. Hardness Testing and Fracture Toughness Data and Calculations For Samples Sintered at 850°C

C.4. MWCNT Oxidation Calculations

Appendix C.1 Composite Synthesis Data

Sample ID	Mixing			Ball Mill Process				Ball Mill Specs	Cold Die Compression				
	MWCNT(gr)	[illegible] Weight(gr)	Weight Percent MWCNT(wt.%)	Pre-mixing RPM	Pre-mixing Duration (Minutes)	Main mixing RPM	Main mixing Duration (Minutes)		Weight of material compressed (gr)	Force (Pounds)	Diameter (in)	Height (in)	Total Volume (in^3)
00CNT1000C01	0.00	15.00	0	300	10	100	50	Zirconia bowl, 65 steatite 1mm balls Polyvinyl alcohol (1ml) added as a binder for compaction with the raw materials Material was checked and mixed with spoon every 25 minutes	3.0	10,000 for 5 minutes, then to 30,000 for 55 minutes	0.76	0.245	0.111
00CNT1000C02	0.00	15.00	0	300	10	100	50	Zirconia bowl, 65 steatite 1mm balls Polyvinyl alcohol (1ml) added as a binder for compaction with the raw materials Material was checked and mixed with spoon every 25 minutes	3.0	10,000 for 5 minutes, then to 30,000 for 55 minutes	0.76	0.21	0.95
01CNT1000C01	0.15	14.85	1	300	10	100	50	Zirconia bowl, 65 steatite 1mm balls Polyvinyl alcohol (1ml) added as a binder for compaction with the raw materials Material was checked and mixed with spoon every 25 minutes	3.0	10,000 for 5 minutes, then to 30,000 for 55 minutes	0.76	0.240	0.11
01CNT1000C02	0.15	14.85	1	300	10	100	50	Zirconia bowl, 65 steatite 1mm balls Polyvinyl alcohol (1ml) added as a binder for compaction with the raw materials Material was checked and mixed with spoon every 25 minutes	3.0	10,000 for 5 minutes, then to 30,000 for 55 minutes	0.76	0.23	0.10
02CNT1000C01	0.30	14.70	2	300	10	100	50	Zirconia bowl, 65 steatite 1mm balls Polyvinyl alcohol (1ml) added as a binder for compaction with the raw materials Material was checked and mixed with spoon every 25 minutes	3.0	10,000 for 5 minutes, then to 30,000 for 55 minutes	0.76	0.241	0.11
02CNT1000C02	0.30	14.70	2	300	10	100	50	Zirconia bowl, 65 steatite 1mm balls Polyvinyl alcohol (1ml) added as a binder for compaction with the raw materials Material was checked and mixed with spoon every 25 minutes	3.0	10,000 for 5 minutes, then to 30,000 for 55 minutes	0.76	0.24	0.11
04CNT1000C01	0.60	14.40	4	300	10	100	50	Zirconia bowl, 65 steatite 1mm balls Polyvinyl alcohol (1ml) added as a binder for compaction with the raw materials Material was checked and mixed with spoon every 25 minutes	3.0	10,000 for 5 minutes, then to 30,000 for 55 minutes	0.76	0.233	0.11
04CNT1000C02	0.60	14.40	4	300	10	100	50	Zirconia bowl, 65 steatite 1mm balls Polyvinyl alcohol (1ml) added as a binder for compaction with the raw materials Material was checked and mixed with spoon every 25 minutes	3.0	10,000 for 5 minutes, then to 30,000 for 55 minutes	0.76	0.22	0.10
05CNT1000C01	0.75	14.25	5	300	10	100	50	Zirconia bowl, 65 steatite 1mm balls Polyvinyl alcohol (1ml) added as a binder for compaction with the raw materials Material was checked and mixed with spoon every 25 minutes	3.0	10,000 for 5 minutes, then to 30,000 for 55 minutes	0.76	0.24	0.11
05CNT1000C02	0.75	14.25	5	300	10	100	50	Zirconia bowl, 65 steatite 1mm balls Polyvinyl alcohol (1ml) added as a binder for compaction with the raw materials Material was checked and mixed with spoon every 25 minutes	3.0	10,000 for 5 minutes, then to 30,000 for 55 minutes	0.76	0.24	0.11
08CNT1000C01	1.20	13.80	8	300	10	100	50	Zirconia bowl, 65 steatite 1mm balls Polyvinyl alcohol (1ml) added as a binder for compaction with the raw materials Material was checked and mixed with spoon every 25 minutes	3.0	10,000 for 5 minutes, then to 30,000 for 55 minutes	0.76	0.24	0.11
10CNT1000C01	1.50	13.50	10	300	10	100	50	Zirconia bowl, 65 steatite 1mm balls Polyvinyl alcohol (1ml) added as a binder for compaction with the raw materials Material was checked and mixed with spoon every 25 minutes	3.0	10,000 for 5 minutes, then to 30,000 for 55 minutes	0.76	0.24	0.11
10CNT1000C02	1.50	13.50	10	300	10	100	50	Zirconia bowl, 65 steatite 1mm balls Polyvinyl alcohol (1ml) added as a binder for compaction with the raw materials Material was checked and mixed with spoon every 25 minutes	3.0	10,000 for 5 minutes, then to 30,000 for 55 minutes	0.76	0.24	0.11

Appendix C.1 Composite Synthesis Data

Sample ID		Sintering Set Up			Post Sintering					Sample Testing Preparation			Additional Comments
	Weight (g)	Temp (°C)	Time (min)	Environment	Weight (g)	Diameter (in)	Height (in)	Volume (in^3)	Relative Density	Mount Material	Grinding Process	Comments	
00CNT1000C01	3.00	1000	20	Air 100%@6.91 CFH	2.9	0.696	0.205	0.078	0.840	Fiberglass epoxy	30|400/600/9µm/1µm cloth	30 minutes at low pressure and moderate speed on laping wheel with water for each stage	
00CNT1000C02	3.03	1000	20	Air 100%@6.91 CFH	-	-	-	-	-	Fiberglass epoxy	300/400/600/9µm/1µm cloth	30 minutes at low pressure and moderate speed on laping wheel with water for each stage	Sample fractured during ejection from mold
01CNT1000C01	3.02	1000	20	Air 100%@6.91 CFH	3.02	0.69	0.223	0.083	0.821	Fiberglass epoxy	300 400/600/9um/1µm cloth	30 minutes at low pressure and moderate speed on laping wheel with water for each stage	
01CNT1000C02	3.00	1000	20	Air 100%@6.91 CFH	-	-	-	-	-	Fiberglass epoxy	300/400/600/9µm/1µm cloth	30 minutes at low pressure and moderate speed on laping wheel with water for each stage	Sample fractured during ejection from mold
02CNT1000C01	2.98	1000	20	AR 100%@6.91 CFH	2.87	0.702	0.21	0.081	0.804	Fiberglass epoxy	300/400/600/9µm/1µm cloth	30 minutes at low pressure and moderate speed on laping wheel with water for each stage	
02CNT1000C02	3.12	1000	20	Air 100%@6.91 CFH	-	-	-	-	-	Fiberglass epoxy	300/400/600/9µm/1µm cloth	30 minutes at low pressure and moderate speed on laping wheel with water for each stage	Sample fractured during ejection from mold
04CNT1000C01	2.99	1000	20	Air 100%@6.91 CFH	2.83	0.7	0.2	0.077	0.843	Fiberglass epoxy	300/400/600/9µm/1µm cloth	30 minutes at low pressure and moderate speed on laping wheel with water for each stage	
04CNT1000C02	3.10	1000	20	Air 100%@6.91 CFH	2.8	-	-	-	-	Fiberglass epoxy	300/400/600/9µm/1µm cloth	30 minutes at low pressure and moderate speed on laping wheel with water for each stage	Sample fractured during ejection from mold
05CNT1000C01	3.00	1000	20	AR 100%@6.91 CFH	2.7	0.71	0.19	0.075	0.826	Fiberglass epoxy	300/400/600/9µm/1µm cloth	30 minutes at low pressure and moderate speed on laping wheel with water for each stage	
05CNT1000C02	3.07	1000	20	AR 100%@6.91 CFH	2.73	-	-	-	-	Fiberglass epoxy	300/400/600/9µm/1µm cloth	30 minutes at low pressure and moderate speed on laping wheel with water for each stage	Sample fractured during ejection from mold
08CNT1000C01	3.00	-	-	AR 100%@6.91 CFH	2.71	0.71	0.22	0.087	0.724	Fiberglass epoxy	300/400/600/9µm/1µm cloth	30 minutes at low pressure and moderate speed on laping wheel with water for each stage	
10CNT1000C01	2.97	1000	20	Air 100%@6.91 CFH	N/A	0.745	0.29	0.126	-	Fiberglass epoxy	300/400/600/9µm/1µm cloth	30 minutes at low pressure and moderate speed on laping wheel with water for each stage	Cracking and fracture of the top section occurred most frequently on the 10% CNT samples
10CNT1000C02	2.98	1000	20	AR 100%@6.91 CFH	2.62	-	-	-	-	Fiberglass epoxy	300/400/600/9µm/1µm cloth	30 minutes at low pressure and moderate speed on laping wheel with water for each stage	Sample fractured during ejection from mold

Appendix C.1 Composite Synthesis Data

Sample ID	Ball Mill Process								Cold Die Compression				
	Mixture			De-clumping		Homogenizing		Ball Mill Specs	Weight of material compressed (g)	Force (pounds)	Diameter (in)	Height (in)	Total Volume (in^3)
	MWCNTs (g)	[illegible] Binding (g)	Weight Percent MWCNTS %	RPM	Duration (Minutes)	RPM	Duration (Minutes)						
00CNT850C02	0.00	15.00	0	300	10	100	50	Zirconia bowl, 65 steatite 1mm balls. Polyvinyl alcohol (1ml) added as a binder for compaction with the raw materials. Material was checked and mixed with spoon every 25 minutes.	3.0	10,000 for 5 minutes, then to 30,000 for 55 minutes	0.76	0.21	0.10
01CNT850C02	0.15	14.85	1	300	10	100	50	Zirconia bowl, 65 steatite 1mm balls. Polyvinyl alcohol (1ml) added as a binder for compaction with the raw materials. Material was checked and mixed with spoon every 25 minutes.	3.0	10,000 for 5 minutes, then to 30,000 for 55 minutes	0.76	0.215	0.10
02CNT850C02	0.30	14.70	2	300	10	100	50	Zirconia bowl, 65 steatite 1mm balls. Polyvinyl alcohol (1ml) added as a binder for compaction with the raw materials. Material was checked and mixed with spoon every 25 minutes.	3.0	10,000 for 5 minutes, then to 30,000 for 55 minutes	0.76	0.22	0.10
04CNT850C01	0.60	14.40	4	300	10	100	50	Zirconia bowl, 65 steatite 1mm balls. Polyvinyl alcohol (1ml) added as a binder for compaction with the raw materials. Material was checked and mixed with spoon every 25 minutes.	3.0	10,000 for 5 minutes, then to 30,000 for 55 minutes	0.76	0.235	0.11
05CNT850C02	0.75	14.25	5	300	10	100	50	Zirconia bowl, 65 steatite 1mm balls. Polyvinyl alcohol (1ml) added as a binder for compaction with the raw materials. Material was checked and mixed with spoon every 25 minutes.	3.0	10,000 for 5 minutes, then to 30,000 for 55 minutes	0.76	0.24	0.11
08CNT850C02	1.20	13.80	8	300	10	100	50	Zirconia bowl, 65 steatite 1mm balls. Polyvinyl alcohol (1ml) added as a binder for compaction with the raw materials. Material was checked and mixed with spoon every 25 minutes.	3.0	10,000 for 5 minutes, then to 30,000 for 55 minutes	0.76	0.219	0.10
10CNT850C02	1.50	13.50	10	300	10	100	50	Zirconia bowl, 65 steatite 1mm balls. Polyvinyl alcohol (1ml) added as a binder for compaction with the raw materials. Material was checked and mixed with spoon every 25 minutes.	3.0	10,000 for 5 minutes, then to 30,000 for 55 minutes	0.76	0.23	0.10

Appendix C.1 Composite Synthesis Data

Sample ID		Sintering Set Up			Post Sintering					Sample Testing Preparation			Additional Comments
	Weight (g)	Temp °C	Time (min)	Environment	Weight (g)	Diameter (in)	Height (in)	Volume (in^3)	Relative Density	Mount Material	Grinding Process	Comments	
00CNT850C02	3.03	850	20	AR 100% 6.91 CFH	2.89	0.72	0.19	0.077	0.844	Fiberglass epoxy	300/400/600/9μm/ 1μm cloth	30 minutes at low pressure and moderate speed on laping wheel with water for each stage	
01CNT850C02	3.00	850	20	AR 100% 6.91 CFH	2.9	0.704	0.205	0.080	0.824	Fiberglass epoxy	300/400/600/9μm/ 1μm cloth	30 minutes at low pressure and moderate speed on laping wheel with water for each stage	
02CNT850C02	3.12	850	20	AR 100% 6.91 CFH	2.82	0.7	0.205	0.079	0.814	Fiberglass epoxy	300/400/600/9μm/ 1μm cloth	30 minutes at low pressure and moderate speed on laping wheel with water for each stage	
04CNT850C01	3.10	850	20	AR 100% 6.91 CFH	2.76	0.703	0.2	0.078	0.815	Fiberglass epoxy	300/400/600/9μm/ 1μm cloth	30 minutes at low pressure and moderate speed on laping wheel with water for each stage	Cleaved
05CNT850C02	2.97	850	20	AR 100% 6.91 CFH	2.79	0.715	0.2	0.080	0.799	Fiberglass epoxy	300/400/600/9μm/ 1μm cloth	30 minutes at low pressure and moderate speed on laping wheel with water for each stage	CNTS burned up in sinter
08CNT850C02	3.02	850	20	AR 100% 6.91 CFH	2.72	0.725	0.21	0.087	0.709	Fiberglass epoxy	300/400/600/9μm/ 1μm cloth	30 minutes at low pressure and moderate speed on laping wheel with water for each stage	CNTS burned up in sinter
10CNT850C02	3.02	850	20	AR 100% 6.91 CFH	2.55	0.732	0.22	0.093	0.645	Fiberglass epoxy	300/400/600/9μm/ 1μm cloth	30 minutes at low pressure and moderate speed on laping wheel with water for each stage	Cleaved

Appendix C.2 Vickers Indentation Test Data

Sample ID			Equipment Parameters			Measurement Data									
% MWCNT	Sinter Temp	Number	Magnification	Force (g)	Indentor	Offset Distance	d1'	d1 (mm)	d2'	d2 (mm)	D average	c1'	c1 (mm)	c2'	c2 (mm)
0MWCNT	1000C	1	50	500	Diamond	0.04	244.5	0.05	237.0	0.05	0.05	157.0	0.03	203.0	0.04
0MWCNT	1000C	1	50	500	Diamond	0.04	275.0	0.05	254.0	0.05	0.05	210.0	0.04	206.0	0.04
0MWCNT	1000C	1	50	500	Diamond	0.04	295.0	0.06	288.0	0.06	0.06	217.0	0.04	205.0	0.04
0MWCNT	1000C	1	50	500	Diamond	0.04	225.0	0.04	222.0	0.04	0.04	299.0	0.06	166.0	0.03
0MWCNT	1000C	1	50	500	Diamond	0.04	274.0	0.05	277.0	0.06	0.06	190.0	0.04	165.0	0.03
0MWCNT	1000C	1	50	500	Diamond	0.04	242.0	0.05	254.0	0.05	0.05	196.0	0.04	153.0	0.03
0MWCNT	1000C	1	50	500	Diamond	0.04	260.0	0.05	253.0	0.05	0.05	220.0	0.04	157.0	0.03
0MWCNT	1000C	1	50	500	Diamond	0.04	280.0	0.06	275.0	0.05	0.06	311.0	0.06	167.0	0.03
0MWCNT	1000C	1	50	500	Diamond	0.04	267.0	0.05	253.0	0.05	0.05	175.0	0.03	205.0	0.04
0MWCNT	1000C	1	50	500	Diamond	0.04	243.5	0.05	236.5	0.05	0.05	174.5	0.03	168.3	0.03
0MWCNT	1000C	2	50	500	Diamond	0.02	241.8	0.05	239.0	0.05	0.05	245.5	0.05	278.5	0.05
0MWCNT	1000C	2	50	500	Diamond	0.02	237.5	0.05	241.0	0.05	0.05	261.5	0.05	243.3	0.05
0MWCNT	1000C	2	50	500	Diamond	0.02	239.5	0.05	239.0	0.05	0.05	166.5	0.03	237.3	0.05
0MWCNT	1000C	2	50	500	Diamond	0.02	233.5	0.05	233.0	0.05	0.05	301.5	0.06	333.3	0.07
0MWCNT	1000C	2	50	500	Diamond	0.02	242.0	0.05	244.8	0.05	0.05	299.0	0.06	182.0	0.04
0MWCNT	1000C	2	50	500	Diamond	0.02	284.5	0.06	283.5	0.06	0.06	185.0	0.04	234.5	0.05
0MWCNT	1000C	2	50	500	Diamond	0.02	241.0	0.05	235.0	0.05	0.05	142.8	0.03	328.5	0.07
0MWCNT	1000C	2	50	500	Diamond	0.02	248.0	0.05	242.5	0.05	0.05	220.0	0.04	234.5	0.05
0MWCNT	1000C	2	50	500	Diamond	0.02	217.5	0.04	233.3	0.05	0.05	317.5	0.06	267.0	0.05
0MWCNT	1000C	2	50	500	Diamond	0.02	238.0	0.05	229.0	0.05	0.05	197.5	0.04	362.3	0.07
0%MWCNT															
1MWCNT	1000C	1	50	500	Diamond	0.04	263.5	0.05	270.0	0.05	0.05	115.0	0.02	129.0	0.03
1MWCNT	1000C	1	50	500	Diamond	0.04	276.0	0.05	275.5	0.05	0.05	133.0	0.03	145.0	0.03
1MWCNT	1000C	1	50	500	Diamond	0.04	283.0	0.06	277.0	0.05	0.06	229.0	0.05	305.0	0.06
1MWCNT	1000C	1	50	500	Diamond	0.04	257.0	0.05	245.0	0.05	0.05	248.5	0.05	248.5	0.05
1MWCNT	1000C	1	50	500	Diamond	0.04	219.5	0.04	223.0	0.04	0.04	184.0	0.04	202.0	0.04
1MWCNT	1000C	1	50	500	Diamond	0.04	233.5	0.05	221.0	0.04	0.05	224.0	0.04	174.5	0.03
1MWCNT	1000C	1	50	500	Diamond	0.04	287.0	0.06	219.0	0.04	0.05	187.0	0.04	216.0	0.04
1MWCNT	1000C	1	50	500	Diamond	0.04	265.0	0.05	212.0	0.04	0.05	176.0	0.04	205.0	0.04
1MWCNT	1000C	1	50	500	Diamond	0.04	289.0	0.06	272.0	0.06	0.06	215.0	0.05	213.0	0.04
1MWCNT	1000C	1	50	500	Diamond	0.04	251.0	0.05	262.0	0.05	0.05	166.0	0.03	164.0	0.03
1MWCNT	1000C	2	50	500	Diamond	0.04	263.5	0.05	259.5	0.05	0.05	390.8	0.08	299.5	0.06
1MWCNT	1000C	2	50	500	Diamond	0.04	265.5	0.05	256.4	0.05	0.05	199.5	0.04	210.0	0.04
1MWCNT	1000C	2	50	500	Diamond	0.04	255.5	0.05	257.5	0.05	0.05	269.0	0.05	163.0	0.03
1MWCNT	1000C	2	50	500	Diamond	0.04	227.8	0.05	248.0	0.05	0.05	292.5	0.06	261.0	0.05
1MWCNT	1000C	2	50	500	Diamond	0.04	280.0	0.06	273.5	0.05	0.06	217.3	0.04	216.3	0.04
1MWCNT	1000C	2	50	500	Diamond	0.04	297.5	0.06	286.0	0.06	0.06	242.0	0.05	246.8	0.05
1MWCNT	1000C	2	50	500	Diamond	0.04	273.0	0.05	260.5	0.05	0.05	194.3	0.04	250.8	0.05
1MWCNT	1000C	2	50	500	Diamond	0.04	264.3	0.05	263.0	0.05	0.05	130.5	0.03	344.5	0.07
1MWCNT	1000C	2	50	500	Diamond	0.04	254.0	0.05	250.0	0.05	0.05	186.0	0.04	204.5	0.04
1MWCNT	1000C	2	50	500	Diamond	0.04	257.5	0.05	260.0	0.05	0.05	144.0	0.03	214.0	0.04
1%MWCNT															

Appendix C.2 Vickers Indentation Test Data

Sample ID			Equipment Parameters			Measurement Data									
% MWCNT	Sinter Temp	Number	Magnification	Force (g)	Indentor	Offset Distance	d1'	d1 (mm)	d2'	d2 (mm)	D average	c1'	c1 (mm)	c2'	c2 (mm)
2MWCNT	1000C	1	50	500	Diamond	0.03	358.3	0.07	344.0	0.07	0.07	234.8	0.05	306.3	0.06
2MWCNT	1000C	1	50	500	Diamond	0.03	353.5	0.07	362.0	0.07	0.07	334.3	0.07	291.0	0.06
2MWCNT	1000C	1	50	500	Diamond	0.03	367.5	0.07	367.0	0.07	0.07	326.5	0.07	177.3	0.04
2MWCNT	1000C	1	50	500	Diamond	0.03	420.0	0.08	415.5	0.08	0.08	401.5	0.08	275.3	0.06
2MWCNT	1000C	1	50	500	Diamond	0.03	447.5	0.09	439.0	0.09	0.09	377.5	0.08	307.0	0.06
2MWCNT	1000C	1	50	500	Diamond	0.03	541.8	0.11	530.5	0.11	0.11	333.5	0.07	173.3	0.07
2MWCNT	1000C	1	50	500	Diamond	0.03	391.3	0.08	391.5	0.08	0.08	271.0	0.05	226.3	0.05
2MWCNT	1000C	1	50	500	Diamond	0.03	417.5	0.08	422.5	0.08	0.08	310.5	0.06	391.3	0.08
2MWCNT	1000C	1	50	500	Diamond	0.03	289.5	0.06	290.0	0.06	0.06	150.0	0.03	368.0	0.06
2MWCNT	1000C	1	50	500	Diamond	0.03	347.0	0.07	339.5	0.07	0.07	309.5	0.06	398.0	0.10
2%MWCNT															
4MWCNT	1000C	1	50	200	Diamond	0.02	363.3	0.07	366.5	0.07	0.07	285.0	0.08	367.0	0.07
4MWCNT	1000C	1	50	200	Diamond	0.02	289.0	0.06	278.0	0.06	0.06	284.5	0.06	219.8	0.04
4MWCNT	1000C	1	50	200	Diamond	0.02	295.8	0.06	279.8	0.05	0.05	219.0	0.04	215.5	0.04
4MWCNT	1000C	1	50	200	Diamond	0.02	363.3	0.07	351.0	0.07	0.07	237.8	0.05	255.0	0.05
4MWCNT	1000C	1	50	200	Diamond	0.02	365.3	0.07	367.0	0.07	0.07	302.5	0.06	140.0	0.07
4MWCNT	1000C	1	50	200	Diamond	0.02	192.5	0.04	187.8	0.04	0.04	118.5	0.02	114.0	0.03
4MWCNT	1000C	1	50	200	Diamond	0.02	287.0	0.06	260.0	0.05	0.05	150.0	0.00	248.8	0.05
4MWCNT	1000C	1	50	200	Diamond	0.02	211.3	0.04	219.0	0.04	0.04	173.3	0.03	154.5	0.03
4MWCNT	1000C	1	50	200	Diamond	0.02	159.5	0.03	161.0	0.03	0.03	154.5	0.03	121.5	0.02
4MWCNT	1000C	1	50	200	Diamond	0.02	362.0	0.07	377.8	0.08	0.07	309.0	0.06	298.3	0.06
4%MWCNT															
5MWCNT	1000C	1	50	200	Diamond	0.02	242.3	0.05	245.5	0.05	0.05	171.0	0.03	213.5	0.04
5MWCNT	1000C	1	50	200	Diamond	0.02	289.0	0.06	286.5	0.06	0.06	239.5	0.05	173.3	0.03
5MWCNT	1000C	1	50	200	Diamond	0.02	320.5	0.06	314.8	0.06	0.06	187.3	0.04	198.0	0.04
5MWCNT	1000C	1	50	200	Diamond	0.02	381.0	0.08	373.3	0.07	0.08	267.5	0.05	251.8	0.05
5MWCNT	1000C	1	50	200	Diamond	0.02	298.8	0.06	296.8	0.06	0.06	214.5	0.04	209.3	0.04
5MWCNT	1000C	1	50	200	Diamond	0.02	321.5	0.06	322.0	0.06	0.06	160.8	0.03	184.5	0.04
5MWCNT	1000C	1	50	200	Diamond	0.02	318.8	0.06	307.5	0.06	0.06	162.0	0.04	172.3	0.04
5MWCNT	1000C	1	50	200	Diamond	0.02	453.0	0.09	422.8	0.08	0.09	220.3	0.04	214.8	0.04
5MWCNT	1000C	1	50	200	Diamond	0.02	426.8	0.09	417.0	0.08	0.08	248.0	0.05	259.0	0.05
5MWCNT	1000C	1	50	200	Diamond	0.02	485.5	0.10	461.8	0.09	0.09	259.5	0.05	275.0	0.05
5%MWCNT															
8MWCNT	1000C	1	50	200	Diamond	0.02	439.5	0.09	463.0	0.09	0.09	474.5	0.09	258.8	0.05
8MWCNT	1000C	1	50	200	Diamond	0.02	590.0	0.12	597.3	0.12	0.12	405.0	0.08	441.5	0.09
8MWCNT	1000C	1	50	200	Diamond	0.02	414.8	0.09	418.0	0.08	0.09	289.5	0.06	264.3	0.05
8MWCNT	1000C	1	50	200	Diamond	0.02	690.5	0.14	673.8	0.13	0.14	601.8	0.12	512.3	0.10
8MWCNT	1000C	1	50	200	Diamond	0.02	732.0	0.15	741.5	0.15	0.15	497.0	0.10	476.8	0.10
8MWCNT	1000C	1	50	200	Diamond	0.02	578.8	0.11	544.0	0.11	0.11	304.3	0.06	295.0	0.06
8MWCNT	1000C	1	50	200	Diamond	0.02	617.3	0.13	645.3	0.13	0.13	422.8	0.08	398.5	0.08
8MWCNT	1000C	1	50	200	Diamond	0.02	703.8	0.14	718.5	0.14	0.14	416.5	0.08	427.8	0.09
8MWCNT	1000C	1	50	200	Diamond	0.02	425.8	0.09	415.8	0.08	0.08	296.0	0.06	278.5	0.06
8MWCNT	1000C	1	50	200	Diamond	0.02	759.0	0.15	748.5	0.15	0.15	561.3	0.11	393.3	0.08
8%MWCNT															

Appendix C.2 Vickers Indentation Test Data

Sample ID			Equipment Parameters			Measurement Data									
% MWCNT	Sinter Temp	Number	Magnification	Force (g)	Indentor	Offset Distance	d1[1]	d1 (mm)	d2[1]	d2 (mm)	D average	c1[1]	c1 (mm)	c2[1]	c2 (mm)
10MWCNT	1000C	1	50	200	Diamond	0.02	593.5	0.12	557.3	0.11	0.12	492.0	0.10	499.5	0.10
10MWCNT	1000C	1	50	200	Diamond	0.02	563.0	0.11	571.5	0.11	0.11	579.0	0.11	572.0	0.11
10MWCNT	1000C	1	50	200	Diamond	0.02	599.0	0.12	550.8	0.11	0.11	392.0	0.08	470.0	0.09
10MWCNT	1000C	1	50	200	Diamond	0.02	875.3	0.18	844.0	0.17	0.17	416.0	0.08	453.0	0.09
10MWCNT	1000C	1	50	200	Diamond	0.02	693.0	0.14	715.0	0.14	0.14	392.0	0.08	318.5	0.06
10MWCNT	1000C	1	50	200	Diamond	0.02	707.0	0.14	705.5	0.14	0.14	580.3	0.12	545.5	0.11
10MWCNT	1000C	1	50	200	Diamond	0.02	621.5	0.12	649.5	0.13	0.13	403.5	0.08	441.0	0.09
10MWCNT	1000C	1	50	200	Diamond	0.02	794.0	0.16	820.5	0.16	0.16	552.3	0.11	550.0	0.11
10MWCNT	1000C	1	50	200	Diamond	0.02	850.5	0.17	826.8	0.17	0.17	657.3	0.13	604.5	0.12
10MWCNT	1000C	1	50	200	Diamond	0.02	614.0	0.12	560.5	0.11	0.12	398.5	0.08	386.5	0.08
10MWCNT	1000C	2	50	200	Diamond	0.02	328.5	0.07	335.3	0.07	0.07	357.0	0.07	294.5	0.06
10MWCNT	1000C	2	50	200	Diamond	0.02	587.5	0.12	569.8	0.11	0.12	398.0	0.08	350.3	0.07
10MWCNT	1000C	2	50	200	Diamond	0.02	673.5	0.13	594.5	0.12	0.13	500.0	0.10	462.3	0.09
10MWCNT	1000C	2	50	200	Diamond	0.02	722.8	0.14	738.3	0.15	0.15	562.5	0.11	560.0	0.11
10MWCNT	1000C	2	50	200	Diamond	0.02	583.3	0.12	572.5	0.11	0.12	486.0	0.10	433.5	0.09
10MWCNT	1000C	2	50	200	Diamond	0.02	825.0	0.16	862.0	0.17	0.17	401.5	0.08	422.0	0.08
10MWCNT	1000C	2	50	200	Diamond	0.02	775.0	0.15	734.8	0.15	0.15	576.3	0.12	523.0	0.10
10MWCNT	1000C	2	50	200	Diamond	0.02	801.0	0.16	779.5	0.16	0.16	562.5	0.11	503.8	0.10
10MWCNT	1000C	2	50	200	Diamond	0.02	822.5	0.16	815.3	0.16	0.16	496.8	0.10	462.3	0.09
10MWCNT	1000C	2	50	200	Diamond	0.02	719.0	0.15	762.0	0.15	0.15	404.5	0.08	385.0	0.08
10%MWCNT															

Notes:
[1]Micromet 5101 instrument measurement units

Appendix C.2 Vickers Indentation Test Data

Sample ID			Equipment Parameters			Measurement Data				Average C	Average a	Hardness		Standard Hardness Deviation		Fracture Toughness
% MWCNT	Sinter Temp	Number	Magnification	Force (g)	Indentor	a1'	a1 (mm)	a2'	a2 (mm)	mm	mm	GPa	VHN	GPa	VHN	GPa m^1/2
0MWCNT	1000C	1	50	500	Diamond	98.0	0.02	112.0	0.02	0.04	0.02	3.92	400.1			37.98
0MWCNT	1000C	1	50	500	Diamond	119.0	0.02	111.0	0.02	0.04	0.02	3.25	331.5			30.39
0MWCNT	1000C	1	50	500	Diamond	126.0	0.03	126.0	0.03	0.04	0.03	2.68	272.9			29.40
0MWCNT	1000C	1	50	500	Diamond	105.0	0.02	120.0	0.02	0.05	0.02	4.55	464.2			34.46
0MWCNT	1000C	1	50	500	Diamond	115.0	0.02	118.0	0.02	0.04	0.02	3.00	305.5			36.46
0MWCNT	1000C	1	50	500	Diamond	101.0	0.02	130.0	0.03	0.03	0.02	3.70	377.0			45.37
0MWCNT	1000C	1	50	500	Diamond	137.0	0.03	134.0	0.03	0.04	0.03	3.46	352.4			37.00
0MWCNT	1000C	1	50	500	Diamond	132.0	0.03	210.0	0.04	0.05	0.03	2.95	301.1			49.56
0MWCNT	1000C	1	50	500	Diamond	112.0	0.02	134.0	0.03	0.04	0.02	3.36	343.0			41.21
0MWCNT	1000C	1	50	500	Diamond	104.5	0.02	106.5	0.02	0.03	0.02	3.95	403.0			41.58
0MWCNT	1000C	2	50	500	Diamond	124.5	0.02	194.0	0.02	0.05	0.02	3.94	401.3			28.94
0MWCNT	1000C	2	50	500	Diamond	128.5	0.03	117.0	0.02	0.05	0.02	3.97	405.1			31.66
0MWCNT	1000C	2	50	500	Diamond	123.0	0.02	115.0	0.02	0.04	0.02	3.97	405.1			41.60
0MWCNT	1000C	2	50	500	Diamond	120.5	0.02	117.0	0.02	0.06	0.02	4.18	426.2			22.11
0MWCNT	1000C	2	50	500	Diamond	120.8	0.02	124.5	0.02	0.05	0.02	3.84	391.5			32.83
0MWCNT	1000C	2	50	500	Diamond	197.3	0.04	177.0	0.04	0.04	0.04	2.82	287.5			68.93
0MWCNT	1000C	2	50	500	Diamond	127.3	0.03	110.5	0.02	0.05	0.02	3.98	405.9			32.99
0MWCNT	1000C	2	50	500	Diamond	115.5	0.02	120.5	0.02	0.05	0.02	3.78	385.5			32.59
0MWCNT	1000C	2	50	500	Diamond	109.8	0.02	107.5	0.02	0.06	0.02	4.48	456.5			22.42
0MWCNT	1000C	2	50	500	Diamond	127.0	0.03	108.5	0.02	0.04	0.02	4.17	425.3			39.31
0%MWCNT						Summary						3.70	377.0	0.54	54.64	37.59
1MWCNT	1000C	1	50	500	Diamond	114.0	0.02	121.0	0.02	0.02	0.02	3.20	325.9			69.44
1MWCNT	1000C	1	50	500	Diamond	119.0	0.02	133.0	0.03	0.03	0.03	4.09	417.2			84.07
1MWCNT	1000C	1	50	500	Diamond	210.0	0.04	175.0	0.03	0.05	0.04	2.94	300.0			53.00
1MWCNT	1000C	1	50	500	Diamond	112.0	0.02	113.0	0.02	0.05	0.02	3.61	368.1			24.73
1MWCNT	1000C	1	50	500	Diamond	112.0	0.02	112.0	0.02	0.04	0.02	4.65	473.7			46.09
1MWCNT	1000C	1	50	500	Diamond	160.0	0.03	156.0	0.03	0.04	0.03	4.42	451.0			83.76
1MWCNT	1000C	1	50	500	Diamond	190.0	0.04	177.0	0.04	0.04	0.04	3.55	362.3			88.71
1MWCNT	1000C	1	50	500	Diamond	168.0	0.03	166.0	0.03	0.04	0.03	4.00	407.7			89.94
1MWCNT	1000C	1	50	500	Diamond	147.0	0.03	143.0	0.03	0.04	0.03	2.72	278.6			36.21
1MWCNT	1000C	1	50	500	Diamond	111.0	0.02	121.0	0.02	0.03	0.02	3.46	352.4			46.53
1MWCNT	1000C	2	50	500	Diamond	128.8	0.03	133.0	0.03	0.07	0.03	3.33	339.1			18.84
1MWCNT	1000C	2	50	500	Diamond	127.5	0.03	127.0	0.03	0.04	0.03	3.34	340.5			39.14
1MWCNT	1000C	2	50	500	Diamond	115.8	0.02	116.0	0.02	0.04	0.02	4.07	414.6			36.46
1MWCNT	1000C	2	50	500	Diamond	134.5	0.03	119.0	0.02	0.06	0.03	4.02	409.8			29.74
1MWCNT	1000C	2	50	500	Diamond	148.0	0.03	137.5	0.03	0.04	0.03	2.97	302.7			40.21
1MWCNT	1000C	2	50	500	Diamond	117.0	0.02	113.0	0.02	0.05	0.02	2.67	272.4			19.27
1MWCNT	1000C	2	50	500	Diamond	125.5	0.03	119.0	0.02	0.04	0.02	3.20	325.9			30.52
1MWCNT	1000C	2	50	500	Diamond	117.0	0.02	135.0	0.03	0.05	0.03	3.27	333.6			30.10
1MWCNT	1000C	2	50	500	Diamond	123.0	0.02	117.5	0.02	0.04	0.02	3.58	365.1			40.25
1MWCNT	1000C	2	50	500	Diamond	120.0	0.02	127.5	0.03	0.04	0.02	3.40	346.7			46.10
1%MWCNT						Summary						3.52	359.4	0.54	55.04	47.63

Appendix C.2 Vickers Indentation Test Data

Sample ID			Equipment Parameters			Measurement Data				Average C	Average a	Hardness		Standard Hardness Deviation		Fracture Toughness
% MWCNT	Sinter Temp	Number	Magnification	Force (g)	Indentor	a1'	a1 (mm)	a2'	a2 (mm)	mm	mm	GPa	VHN	GPa	VHN	GPa m^1/2
2MWCNT	1000C	1	50	500	Diamond	165.5	0.03	160.0	0.03	0.05	0.03	1.84	188.1			23.29
2MWCNT	1000C	1	50	500	Diamond	193.5	0.04	184.0	0.04	0.06	0.04	1.68	171.4			22.98
2MWCNT	1000C	1	50	500	Diamond	155.0	0.03	174.5	0.03	0.05	0.03	1.69	171.9			24.28
2MWCNT	1000C	1	50	500	Diamond	185.0	0.04	182.3	0.04	0.07	0.04	1.30	132.9			14.92
2MWCNT	1000C	1	50	500	Diamond	196.0	0.04	210.0	0.04	0.07	0.04	1.16	118.0			15.98
2MWCNT	1000C	1	50	500	Diamond	244.0	0.05	218.5	0.04	0.07	0.05	0.79	80.7			13.51
2MWCNT	1000C	1	50	500	Diamond	190.0	0.04	182.5	0.04	0.05	0.04	1.49	151.5			27.88
2MWCNT	1000C	1	50	500	Diamond	186.0	0.04	181.5	0.04	0.07	0.04	1.29	131.4			14.04
2MWCNT	1000C	1	50	500	Diamond	128.5	0.03	163.3	0.03	0.05	0.03	2.71	276.2			35.27
2MWCNT	1000C	1	50	500	Diamond	166.0	0.03	177.5	0.04	0.08	0.03	1.93	196.8			14.88
2%MWCNT						**Summary**						**1.50**	**161.9**	**0.52**	**53.29**	**20.71**
4MWCNT	1000C	1	50	200	Diamond	203.5	0.04	196.8	0.04	0.07	0.04	0.68	69.7			8.02
4MWCNT	1000C	1	50	200	Diamond	173.5	0.03	175.5	0.04	0.05	0.03	1.13	115.4			18.26
4MWCNT	1000C	1	50	200	Diamond	137.8	0.03	116.0	0.02	0.04	0.03	1.27	129.4			13.53
4MWCNT	1000C	1	50	200	Diamond	169.0	0.03	186.3	0.04	0.05	0.04	0.71	72.7			12.34
4MWCNT	1000C	1	50	200	Diamond	214.5	0.04	189.5	0.04	0.06	0.04	0.66	69.2			10.20
4MWCNT	1000C	1	50	200	Diamond	72.5	0.01	77.8	0.02	0.03	0.02	2.52	256.6			21.23
4MWCNT	1000C	1	50	200	Diamond	118.0	0.02	115.0	0.02	0.03	0.02	1.23	124.0			23.11
4MWCNT	1000C	1	50	200	Diamond	97.0	0.02	96.8	0.02	0.03	0.02	1.97	200.4			18.65
4MWCNT	1000C	1	50	200	Diamond	55.5	0.01	80.8	0.02	0.03	0.01	3.54	361.2			21.27
4MWCNT	1000C	1	50	200	Diamond	177.5	0.04	189.0	0.04	0.06	0.04	0.66	67.8			8.95
4%MWCNT						**Summary**						**1.44**	**146.6**	**0.96**	**97.97**	**15.56**
5MWCNT	1000C	1	50	200	Diamond	100.0	0.02	115.8	0.02	0.04	0.02	1.53	155.9			14.05
5MWCNT	1000C	1	50	200	Diamond	130.8	0.03	116.8	0.02	0.04	0.02	1.10	112.0			12.02
5MWCNT	1000C	1	50	200	Diamond	159.5	0.03	174.0	0.03	0.04	0.03	0.90	91.9			20.20
5MWCNT	1000C	1	50	200	Diamond	168.8	0.03	177.5	0.04	0.05	0.03	0.64	65.2			9.72
5MWCNT	1000C	1	50	200	Diamond	162.0	0.03	153.0	0.03	0.04	0.03	1.06	108.2			15.88
5MWCNT	1000C	1	50	200	Diamond	172.5	0.03	158.8	0.03	0.03	0.03	0.88	89.6			22.54
5MWCNT	1000C	1	50	200	Diamond	186.3	0.04	161.5	0.03	0.04	0.03	0.93	94.6			23.74
5MWCNT	1000C	1	50	200	Diamond	208.0	0.04	197.0	0.04	0.04	0.04	0.47	48.4			12.86
5MWCNT	1000C	1	50	200	Diamond	175.0	0.03	164.8	0.03	0.05	0.03	0.51	52.1			7.75
5MWCNT	1000C	1	50	200	Diamond	248.5	0.05	260.0	0.05	0.05	0.05	0.41	41.7			12.73
5%MWCNT						**Summary**						**0.84**	**85.9**	**0.35**	**35.24**	**15.10**
8MWCNT	1000C	1	50	200	Diamond	213.0	0.04	197.5	0.04	0.07	0.04	0.45	45.5			5.69
8MWCNT	1000C	1	50	200	Diamond	266.8	0.05	291.0	0.06	0.08	0.06	0.26	26.3			4.87
8MWCNT	1000C	1	50	200	Diamond	180.5	0.04	180.5	0.04	0.06	0.04	0.50	51.0			7.50
8MWCNT	1000C	1	50	200	Diamond	367.0	0.07	340.8	0.07	0.11	0.07	0.20	19.9			3.95
8MWCNT	1000C	1	50	200	Diamond	391.5	0.08	382.3	0.08	0.10	0.08	0.17	17.1			4.95
8MWCNT	1000C	1	50	200	Diamond	271.8	0.05	258.0	0.05	0.06	0.05	0.32	32.2			9.07
8MWCNT	1000C	1	50	200	Diamond	311.0	0.06	287.5	0.06	0.08	0.06	0.22	22.6			5.08
8MWCNT	1000C	1	50	200	Diamond	359.3	0.07	390.0	0.08	0.08	0.07	0.18	18.4			6.18
8MWCNT	1000C	1	50	200	Diamond	187.8	0.04	195.0	0.04	0.06	0.04	0.51	52.4			8.20
8MWCNT	1000C	1	50	200	Diamond	231.0	0.05	228.0	0.05	0.10	0.05	0.16	16.3			1.72
8%MWCNT						**Summary**						**0.30**	**30.2**	**0.14**	**14.31**	**5.72**

Appendix C.2 Vickers Indentation Test Data

Sample ID			Equipment Parameters			Measurement Data				Average C	Average a	Hardness		Standard Hardness Deviation		Fracture Toughness
% MWCNT	Sinter Temp	Number	Magnification	Force (g)	Indentor	a1[1]	a1 (mm)	a2[1]	a2 (mm)	mm	mm	GPa	VHN	GPa	VHN	GPa m^1/2
10MWCNT	1000C	1	50	500	Diamond	250.0	0.05	285.0	0.06	0.10	0.05	0.27	28.0			3.78
10MWCNT	1000C	1	50	200	Diamond	254.0	0.05	267.5	0.05	0.11	0.05	0.28	28.8			2.98
10MWCNT	1000C	1	50	200	Diamond	233.0	0.05	252.0	0.07	0.09	0.06	0.28	28.1			5.68
10MWCNT	1000C	1	50	200	Diamond	400.0	0.08	415.0	0.08	0.09	0.08	0.12	12.6			4.79
10MWCNT	1000C	1	50	200	Diamond	295.3	0.06	314.3	0.06	0.07	0.06	0.18	18.7			5.40
10MWCNT	1000C	1	50	200	Diamond	475.3	0.10	451.3	0.09	0.11	0.09	0.18	18.7			0.26
10MWCNT	1000C	1	50	200	Diamond	331.5	0.07	305.0	0.06	0.08	0.06	0.23	23.0			5.58
10MWCNT	1000C	1	50	200	Diamond	307.3	0.06	355.5	0.07	0.11	0.07	0.14	14.2			2.51
10MWCNT	1000C	1	50	200	Diamond	470.8	0.09	376.0	0.08	0.13	0.08	0.13	13.1			3.08
10MWCNT	1000C	1	50	200	Diamond	281.0	0.06	259.5	0.06	0.08	0.06	0.26	26.9			5.65
10MWCNT	1000C	2	50	200	Diamond	153.5	0.03	147.3	0.03	0.07	0.03	0.83	84.2			6.74
10MWCNT	1000C	2	50	200	Diamond	235.8	0.05	280.0	0.06	0.07	0.05	0.27	27.7			5.30
10MWCNT	1000C	2	50	200	Diamond	310.5	0.06	285.5	0.06	0.10	0.06	0.23	23.1			4.04
10MWCNT	1000C	2	50	200	Diamond	375.0	0.07	390.5	0.08	0.11	0.08	0.17	17.5			4.00
10MWCNT	1000C	2	50	200	Diamond	283.3	0.06	265.8	0.05	0.09	0.05	0.27	27.8			4.41
10MWCNT	1000C	2	50	200	Diamond	385.0	0.08	406.5	0.08	0.08	0.08	0.13	13.0			5.08
10MWCNT	1000C	2	50	200	Diamond	387.0	0.08	397.5	0.08	0.11	0.08	0.16	16.3			4.04
10MWCNT	1000C	2	50	200	Diamond	345.0	0.07	377.3	0.08	0.11	0.07	0.15	14.9			3.27
10MWCNT	1000C	2	50	200	Diamond	333.5	0.07	391.8	0.08	0.09	0.07	0.14	13.8			1.72
10MWCNT	1000C	2	50	200	Diamond	369.8	0.07	327.0	0.07	0.08	0.07	0.16	16.6			5.33
10%MWCNT						Summary						0.23	23.3	0.15	15.52	4.58

Notes:
[1]Micromet 5101 instrument measurement units

Appendix C.2 Vickers Indentation Test Data

Sample ID			Equipment Parameters			Standard Fracture Toughness Deviation
% MWCNT	Sinter Temp	Number	Magnification	Force (g)	Indentor	
0MWCNT	1000C	1	50	500	Diamond	
0MWCNT	1000C	1	50	500	Diamond	
0MWCNT	1000C	1	50	500	Diamond	
0MWCNT	1000C	1	50	500	Diamond	
0MWCNT	1000C	1	50	500	Diamond	
0MWCNT	1000C	1	50	500	Diamond	
0MWCNT	1000C	1	50	500	Diamond	
0MWCNT	1000C	1	50	500	Diamond	
0MWCNT	1000C	1	50	500	Diamond	
0MWCNT	1000C	1	50	500	Diamond	
0MWCNT	1000C	2	50	500	Diamond	
0MWCNT	1000C	2	50	500	Diamond	
0MWCNT	1000C	2	50	500	Diamond	
0MWCNT	1000C	2	50	500	Diamond	
0MWCNT	1000C	2	50	500	Diamond	
0MWCNT	1000C	2	50	500	Diamond	
0MWCNT	1000C	2	50	500	Diamond	
0MWCNT	1000C	2	50	500	Diamond	
0MWCNT	1000C	2	50	500	Diamond	
0MWCNT	1000C	2	50	500	Diamond	
0%MWCNT						10.81
1MWCNT	1000C	1	50	500	Diamond	
1MWCNT	1000C	1	50	500	Diamond	
1MWCNT	1000C	1	50	500	Diamond	
1MWCNT	1000C	1	50	500	Diamond	
1MWCNT	1000C	1	50	500	Diamond	
1MWCNT	1000C	1	50	500	Diamond	
1MWCNT	1000C	1	50	500	Diamond	
1MWCNT	1000C	1	50	500	Diamond	
1MWCNT	1000C	1	50	500	Diamond	
1MWCNT	1000C	1	50	500	Diamond	
1MWCNT	1000C	2	50	500	Diamond	
1MWCNT	1000C	2	50	500	Diamond	
1MWCNT	1000C	2	50	500	Diamond	
1MWCNT	1000C	2	50	500	Diamond	
1MWCNT	1000C	2	50	500	Diamond	
1MWCNT	1000C	2	50	500	Diamond	
1MWCNT	1000C	2	50	500	Diamond	
1MWCNT	1000C	2	50	500	Diamond	
1MWCNT	1000C	2	50	500	Diamond	
1MWCNT	1000C	2	50	500	Diamond	
1%MWCNT						23.06

Appendix C.2 Vickers Indentation Test Data

Sample ID			Equipment Parameters			Standard Fracture Toughness Deviation
% MWCNT	Sinter Temp	Number	Magnification	Force (g)	Indentor	
2MWCNT	1000C	1	50	500	Diamond	
2MWCNT	1000C	1	50	500	Diamond	
2MWCNT	1000C	1	50	500	Diamond	
2MWCNT	1000C	1	50	500	Diamond	
2MWCNT	1000C	1	50	500	Diamond	
2MWCNT	1000C	1	50	500	Diamond	
2MWCNT	1000C	1	50	500	Diamond	
2MWCNT	1000C	1	50	500	Diamond	
2MWCNT	1000C	1	50	500	Diamond	
2MWCNT	1000C	1	50	500	Diamond	
2%MWCNT						7.25
4MWCNT	1000C	1	50	200	Diamond	
4MWCNT	1000C	1	50	200	Diamond	
4MWCNT	1000C	1	50	200	Diamond	
4MWCNT	1000C	1	50	200	Diamond	
4MWCNT	1000C	1	50	200	Diamond	
4MWCNT	1000C	1	50	200	Diamond	
4MWCNT	1000C	1	50	200	Diamond	
4MWCNT	1000C	1	50	200	Diamond	
4MWCNT	1000C	1	50	200	Diamond	
4MWCNT	1000C	1	50	200	Diamond	
4%MWCNT						5.60
5MWCNT	1000C	1	50	200	Diamond	
5MWCNT	1000C	1	50	200	Diamond	
5MWCNT	1000C	1	50	200	Diamond	
5MWCNT	1000C	1	50	200	Diamond	
5MWCNT	1000C	1	50	200	Diamond	
5MWCNT	1000C	1	50	200	Diamond	
5MWCNT	1000C	1	50	200	Diamond	
5MWCNT	1000C	1	50	200	Diamond	
5MWCNT	1000C	1	50	200	Diamond	
5MWCNT	1000C	1	50	200	Diamond	
5%MWCNT						5.30
8MWCNT	1000C	1	50	200	Diamond	
8MWCNT	1000C	1	50	200	Diamond	
8MWCNT	1000C	1	50	200	Diamond	
8MWCNT	1000C	1	50	200	Diamond	
8MWCNT	1000C	1	50	200	Diamond	
8MWCNT	1000C	1	50	200	Diamond	
8MWCNT	1000C	1	50	200	Diamond	
8MWCNT	1000C	1	50	200	Diamond	
8MWCNT	1000C	1	50	200	Diamond	
8MWCNT	1000C	1	50	200	Diamond	
8%MWCNT						2.15

Appendix C.2 Vickers Indentation Test Data

Sample ID			Equipment Parameters			Standard Fracture Toughness Deviation
% MWCNT	Sinter Temp	Number	Magnification	Force (g)	Indentor	
10MWCNT	1000C	1	50	200	Diamond	
10MWCNT	1000C	1	50	200	Diamond	
10MWCNT	1000C	1	50	200	Diamond	
10MWCNT	1000C	1	50	200	Diamond	
10MWCNT	1000C	1	50	200	Diamond	
10MWCNT	1000C	1	50	200	Diamond	
10MWCNT	1000C	1	50	200	Diamond	
10MWCNT	1000C	1	50	200	Diamond	
10MWCNT	1000C	1	50	200	Diamond	
10MWCNT	1000C	1	50	200	Diamond	
10MWCNT	1000C	2	50	200	Diamond	
10MWCNT	1000C	2	50	200	Diamond	
10MWCNT	1000C	2	50	200	Diamond	
10MWCNT	1000C	2	50	200	Diamond	
10MWCNT	1000C	2	50	200	Diamond	
10MWCNT	1000C	2	50	200	Diamond	
10MWCNT	1000C	2	50	200	Diamond	
10MWCNT	1000C	2	50	200	Diamond	
10MWCNT	1000C	2	50	200	Diamond	
10%MWCNT						1.17

Notes:
*Micromet 5101 instrument measurement units

Appendix C.3 Vickers Indentation Test Data

Sample ID			Equipment Parameters			Measurement Data									
% MWCNTs	Sinter Temp	Number	Magnification	Force (g)	Indenter	Offset Distance	d1[1]	d1 (mm)	d3[1]	d2 (mm)	D average	c1[1]	c1 (mm)	c3[1]	c2 (mm)
0 MWCNTs	850C	1	50	500	Diamond	0.02	273.5	0.05	266.0	0.05	0.05	230.5	0.05	194.5	0.04
0MWCNT	850C	1	50	500	Diamond	0.02	256.0	0.05	250.0	0.05	0.05	279.3	0.06	266.8	0.05
0MWCNT	850C	1	50	500	Diamond	0.02	214.8	0.04	197.5	0.04	0.04	187.0	0.04	202.5	0.04
0MWCNT	850C	1	50	500	Diamond	0.02	294.8	0.06	282.0	0.06	0.06	246.5	0.05	257.3	0.05
0MWCNT	850C	1	50	500	Diamond	0.02	398.5	0.08	394.0	0.08	0.08	311.0	0.06	313.0	0.06
0MWCNT	850C	1	50	500	Diamond	0.02	373.5	0.07	361.8	0.07	0.07	428.0	0.09	295.5	0.06
0MWCNT	850C	1	50	500	Diamond	0.02	243.3	0.05	257.8	0.05	0.05	344.5	0.07	301.8	0.06
0MWCNT	850C	1	50	500	Diamond	0.02	383.5	0.08	372.5	0.07	0.08	255.5	0.05	252.8	0.05
0MWCNT	850C	1	50	500	Diamond	0.02	363.0	0.07	339.5	0.07	0.07	396.3	0.07	323.5	0.06
0MWCNT	850C	1	50	500	Diamond	0.02	290.5	0.06	279.0	0.06	0.06	259.5	0.05	200.0	0.04
0% MWCNTs															
1MWCNT	850C	2	50	500	Diamond	0.03	477.0	0.10	494.5	0.10	0.10	396.8	0.08	469.0	0.09
1MWCNT	850C	2	50	500	Diamond	0.03	536.0	0.11	550.5	0.11	0.11	422.5	0.08	397.0	0.08
1MWCNT	850C	2	50	500	Diamond	0.03	480.0	0.10	497.5	0.10	0.10	580.5	0.12	499.5	0.10
1MWCNT	850C	2	50	500	Diamond	0.03	502.5	0.10	480.0	0.10	0.10	332.5	0.07	352.3	0.07
1MWCNT	850C	2	50	500	Diamond	0.03	546.0	0.11	547.5	0.11	0.11	500.0	0.10	535.5	0.11
1MWCNT	850C	2	50	500	Diamond	0.03	510.8	0.10	507.0	0.10	0.10	300.0	0.06	272.0	0.05
1MWCNT	850C	2	50	500	Diamond	0.03	462.5	0.09	504.0	0.10	0.10	399.5	0.08	381.3	0.08
1MWCNT	850C	2	50	500	Diamond	0.03	477.0	0.10	463.5	0.09	0.09	537.3	0.11	335.0	0.07
1MWCNT	850C	2	50	500	Diamond	0.03	539.0	0.11	534.3	0.11	0.11	424.0	0.08	438.5	0.09
1MWCNT	850C	2	50	500	Diamond	0.03	499.5	0.10	577.0	0.12	0.11	344.0	0.07	290.5	0.06
1% MWCNTs															
2MWCNT	850C	2	50	500	Diamond	0.02	508.0	0.10	476.5	0.10	0.10	517.3	0.10	333.0	0.07
2MWCNT	850C	2	50	500	Diamond	0.02	555.3	0.11	567.5	0.11	0.11	510.5	0.10	458.0	0.09
2MWCNT	850C	2	50	500	Diamond	0.02	593.5	0.12	566.0	0.11	0.12	510.8	0.10	534.5	0.11
2MWCNT	850C	2	50	500	Diamond	0.02	501.3	0.10	432.5	0.09	0.09	379.0	0.08	363.5	0.07
2MWCNT	850C	2	50	500	Diamond	0.02	495.0	0.10	470.0	0.09	0.10	396.3	0.08	298.0	0.06
2MWCNT	850C	2	50	500	Diamond	0.02	560.5	0.11	504.8	0.10	0.11	392.0	0.08	494.5	0.10
2MWCNT	850C	2	50	500	Diamond	0.02	592.0	0.12	615.0	0.12	0.12	511.0	0.10	429.0	0.09
2MWCNT	850C	2	50	500	Diamond	0.02	555.0	0.11	535.0	0.11	0.11	313.0	0.06	435.5	0.09
2MWCNT	850C	2	50	500	Diamond	0.02	442.0	0.09	453.5	0.09	0.09	330.5	0.07	280.5	0.06
2MWCNT	850C	2	50	500	Diamond	0.02	472.0	0.09	450.0	0.09	0.09	452.0	0.09	452.0	0.09
3% MWCNTs															
5MWCNT	850C	2	50	500	Diamond	0.02	595.0	0.12	606.5	0.12	0.12	492.8	0.10	485.0	0.10
5MWCNT	850C	2	50	500	Diamond	0.02	573.5	0.11	595.0	0.12	0.12	377.3	0.08	374.8	0.06
5MWCNT	850C	2	50	500	Diamond	0.02	610.0	0.12	562.5	0.11	0.12	457.5	0.09	448.5	0.09
5MWCNT	850C	2	50	500	Diamond	0.02	608.5	0.12	596.8	0.12	0.12	520.0	0.10	474.5	0.09
5MWCNT	850C	2	50	500	Diamond	0.02	735.5	0.15	687.0	0.14	0.14	514.0	0.10	564.8	0.11
5MWCNT	850C	2	50	500	Diamond	0.02	634.0	0.13	582.5	0.12	0.12	547.5	0.11	436.0	0.09
5MWCNT	850C	2	50	500	Diamond	0.02	675.5	0.14	713.0	0.14	0.14	515.8	0.10	480.5	0.10
5MWCNT	850C	2	50	500	Diamond	0.02	732.5	0.15	698.8	0.14	0.14	520.5	0.10	506.0	0.10
5MWCNT	850C	2	50	500	Diamond	0.02	782.5	0.16	795.5	0.16	0.16	571.8	0.11	565.0	0.11
5MWCNT	850C	2	50	500	Diamond	0.02	809.0	0.16	875.3	0.17	0.16	580.0	0.12	488.5	0.10
5% MWCNTs															
10MWCNT	850C	2	50	200	Diamond	0.02	612.5	0.12	558.8	0.11	0.12	517.5	0.10	595.0	0.12
10MWCNT	850C	2	50	200	Diamond	0.02	764.0	0.15	747.3	0.15	0.15	500.5	0.10	371.0	0.07
10MWCNT	850C	2	50	200	Diamond	0.02	681.0	0.14	720.0	0.14	0.14	320.0	0.06	407.8	0.08
10MWCNT	850C	2	50	200	Diamond	0.02	845.3	0.17	827.5	0.17	0.17	422.5	0.08	419.5	0.08
10MWCNT	850C	2	50	200	Diamond	0.02	615.8	0.12	662.3	0.13	0.13	377.8	0.08	392.0	0.08
10MWCNT	850C	2	50	200	Diamond	0.02	688.0	0.14	644.5	0.13	0.13	427.0	0.09	440.5	0.09
10MWCNT	850C	2	50	200	Diamond	0.02	798.8	0.16	803.0	0.16	0.16	553.3	0.11	540.0	0.11
10MWCNT	850C	2	50	200	Diamond	0.02	703.8	0.14	681.5	0.14	0.14	482.0	0.10	526.0	0.11
10 MWCNT	850C	2	50	200	Diamond	0.02	771.0	0.15	730.3	0.15	0.15	528.5	0.11	500.5	0.10
10 MWCNT	850C	2	50	200	Diamond	0.02	768.3	0.15	734.5	0.15	0.15	561.3	0.11	393.3	0.08
10% MWCNTs															

Notes:

[1]Micromet 5101 instrument measurement units

Appendix C.3 Vickers Indentation Test Data

Sample ID			Equipment Parameters			Measurement Data				Average C	Average a	Hardness		Standard Hardness Deviation	
% MWCNTs	Sinter Temp	Number	Magnification	Force (g)	Indenter	a1[1]	a1 (mm)	a2[1]	a2 (mm)	mm	mm	GPa	VHN	GPa	VHN
0 MWCNTs	850C	1	50	500	Diamond	132.5	0.03	135.1	0.03	0.04	0.03	3.12	318.6		
0MWCNT	850C	1	50	500	Diamond	161.5	0.03	146.5	0.03	0.05	0.03	3.55	362.2		
0MWCNT	850C	1	50	500	Diamond	120.0	0.02	97.0	0.02	0.04	0.02	5.35	545.7		
0MWCNT	850C	1	50	500	Diamond	138.3	0.03	122.5	0.02	0.05	0.03	2.73	278.8		
0MWCNT	850C	1	50	500	Diamond	174.3	0.05	189.8	0.04	0.06	0.04	1.45	147.7		
0MWCNT	850C	1	50	500	Diamond	175.0	0.03	187.0	0.04	0.07	0.04	1.68	171.6		
0MWCNT	850C	1	50	500	Diamond	145.5	0.03	148.5	0.03	0.06	0.03	3.62	369.5		
0MWCNT	850C	1	50	500	Diamond	178.0	0.04	194.3	0.04	0.05	0.04	1.59	162.3		
0MWCNT	850C	1	50	500	Diamond	188.3	0.04	178.0	0.04	0.07	0.04	1.84	187.9		
0MWCNT	850C	1	50	500	Diamond	183.3	0.04	173.5	0.03	0.05	0.04	2.80	286.0		
0% MWCNTs						**SUMMARY**						**2.76**	**283.0**	**1.22**	**124.02**
1MWCNT	850C	2	50	500	Diamond	220.5	0.04	214.0	0.04	0.09	0.04	0.96	98.3		
1MWCNT	850C	2	50	500	Diamond	271.5	0.05	271.5	0.05	0.08	0.05	0.77	78.6		
1MWCNT	850C	2	50	500	Diamond	225.3	0.05	232.0	0.05	0.11	0.05	0.95	97.1		
1MWCNT	850C	2	50	500	Diamond	264.5	0.05	247.8	0.05	0.07	0.05	0.94	96.1		
1MWCNT	850C	2	50	500	Diamond	280.0	0.06	274.0	0.05	0.10	0.06	0.76	77.6		
1MWCNT	850C	2	50	500	Diamond	210.3	0.04	195.8	0.04	0.06	0.04	0.88	89.5		
1MWCNT	850C	2	50	500	Diamond	220.5	0.04	254.0	0.05	0.08	0.05	0.97	99.3		
1MWCNT	850C	2	50	500	Diamond	232.0	0.05	225.5	0.05	0.09	0.05	1.03	104.8		
1MWCNT	850C	2	50	500	Diamond	257.8	0.05	261.5	0.05	0.09	0.05	0.79	80.5		
1MWCNT	850C	2	50	500	Diamond	202.0	0.04	214.8	0.04	0.06	0.04	0.78	80.0		
1% MWCNTs						**SUMMARY**						**0.88**	**90.2**	**0.10**	**10.20**
2MWCNT	850C	2	50	500	Diamond	235.5	0.05	313.8	0.06	0.09	0.05	0.94	95.7		
2MWCNT	850C	2	50	500	Diamond	305.8	0.06	271.5	0.05	0.10	0.06	0.72	73.6		
2MWCNT	850C	2	50	500	Diamond	427.0	0.09	410.0	0.08	0.10	0.08	0.68	69.0		
2MWCNT	850C	2	50	500	Diamond	344.0	0.05	217.5	0.04	0.07	0.05	1.04	106.4		
2MWCNT	850C	2	50	500	Diamond	220.5	0.04	197.5	0.04	0.07	0.04	0.98	99.6		
2MWCNT	850C	2	50	500	Diamond	266.5	0.03	274.0	0.05	0.09	0.05	0.80	81.7		
2MWCNT	850C	2	50	500	Diamond	319.5	0.06	307.3	0.06	0.09	0.06	0.62	63.7		
2MWCNT	850C	2	50	500	Diamond	253.0	0.05	268.5	0.05	0.07	0.05	0.77	78.1		
2MWCNT	850C	2	50	500	Diamond	201.5	0.04	235.3	0.05	0.06	0.04	1.13	115.7		
2MWCNT	850C	2	50	500	Diamond	252.0	0.05	247.5	0.05	0.09	0.05	1.07	109.1		
2% MWCNTs						**SUMMARY**						**0.88**	**89.2**	**0.18**	**18.34**
5MWCNT	850C	2	50	500	Diamond	340.5	0.07	398.5	0.08	0.10	0.07	0.63	64.2		
5MWCNT	850C	2	50	500	Diamond	278.0	0.06	266.5	0.05	0.07	0.05	0.67	67.9		
5MWCNT	850C	2	50	500	Diamond	229.5	0.05	317.3	0.06	0.09	0.05	0.66	67.5		
5MWCNT	850C	2	50	500	Diamond	232.0	0.05	312.0	0.06	0.10	0.05	0.63	63.8		
5MWCNT	850C	2	50	500	Diamond	391.5	0.08	378.5	0.08	0.11	0.08	0.45	45.8		
5MWCNT	850C	2	50	500	Diamond	243.8	0.05	290.0	0.06	0.10	0.05	0.61	62.7		
5MWCNT	850C	2	50	500	Diamond	480.8	0.10	409.0	0.08	0.10	0.09	0.47	48.1		
5MWCNT	850C	2	50	500	Diamond	304.3	0.06	322.8	0.06	0.10	0.06	0.44	45.3		
5MWCNT	850C	2	50	500	Diamond	358.8	0.07	394.0	0.08	0.11	0.08	0.37	37.2		
5MWCNT	850C	2	50	500	Diamond	385.0	0.08	356.5	0.07	0.11	0.07	0.34	34.2		
5% MWCNTs						**SUMMARY**						**0.53**	**53.7**	**0.13**	**12.91**
10MWCNT	850C	2	50	200	Diamond	391.5	0.08	413.0	0.08	0.11	0.08	0.27	27.0		
10MWCNT	850C	2	50	200	Diamond	271.8	0.05	243.5	0.05	0.09	0.05	0.16	16.2		
10MWCNT	850C	2	50	200	Diamond	294.0	0.06	339.0	0.07	0.07	0.06	0.19	18.9		
10MWCNT	850C	2	50	200	Diamond	398.8	0.08	375.0	0.07	0.08	0.08	0.13	13.3		
10MWCNT	850C	2	50	200	Diamond	319.3	0.06	348.5	0.07	0.08	0.07	0.22	22.7		
10MWCNT	850C	2	50	200	Diamond	340.5	0.07	306.5	0.06	0.09	0.06	0.20	20.9		
10MWCNT	850C	2	50	200	Diamond	374.0	0.07	360.5	0.07	0.11	0.07	0.14	14.5		
10MWCNT	850C	2	50	200	Diamond	350.3	0.07	362.0	0.07	0.10	0.07	0.19	19.3		
10 MWCNT	850C	2	50	200	Diamond	313.3	0.06	342.3	0.07	0.10	0.07	0.16	16.5		
10 MWCNT	850C	2	50	200	Diamond	235.0	0.05	221.0	0.04	0.10	0.05	0.16	16.4		
10% MWCNTs						**SUMMARY**						**0.18**	**18.6**	**0.04**	**4.14**

Notes:
[1]Micromet 5101 instrument measurement units

Appendix C.3 Vickers Indentation Test Data

Sample ID			Equipment Parameters			Fracture Toughness	Standard Fracture Toughness Deviation
% MWCNTs	Sinter Temp	Number	Magnification	Force (g)	Indenter	GPa m^1/2	
0 MWCNTs	850C	1	50	500	Diamond	38.35	
0MWCNT	850C	1	50	500	Diamond	40.13	
0MWCNT	850C	1	50	500	Diamond	49.17	
0MWCNT	850C	1	50	500	Diamond	24.66	
0MWCNT	850C	1	50	500	Diamond	18.46	
0MWCNT	850C	1	50	500	Diamond	16.99	
0MWCNT	850C	1	50	500	Diamond	28.59	
0MWCNT	850C	1	50	500	Diamond	28.86	
0MWCNT	850C	1	50	500	Diamond	21.01	
0MWCNT	850C	1	50	500	Diamond	54.35	
0% MWCNTs						**32.06**	**12.93**
1MWCNT	850C	2	50	500	Diamond	10.71	
1MWCNT	850C	2	50	500	Diamond	14.52	
1MWCNT	850C	2	50	500	Diamond	8.41	
1MWCNT	850C	2	50	500	Diamond	20.69	
1MWCNT	850C	2	50	500	Diamond	10.51	
1MWCNT	850C	2	50	500	Diamond	15.87	
1MWCNT	850C	2	50	500	Diamond	15.07	
1MWCNT	850C	2	50	500	Diamond	12.53	
1MWCNT	850C	2	50	500	Diamond	12.61	
1MWCNT	850C	2	50	500	Diamond	12.79	
1% MWCNTs						**13.37**	**3.43**
2MWCNT	850C	2	50	500	Diamond	17.13	
2MWCNT	850C	2	50	500	Diamond	11.96	
2MWCNT	850C	2	50	500	Diamond	21.01	
2MWCNT	850C	2	50	500	Diamond	16.47	
2MWCNT	850C	2	50	500	Diamond	13.99	
2MWCNT	850C	2	50	500	Diamond	13.31	
2MWCNT	850C	2	50	500	Diamond	12.76	
2MWCNT	850C	2	50	500	Diamond	15.25	
2MWCNT	850C	2	50	500	Diamond	21.48	
2MWCNT	850C	2	50	500	Diamond	14.73	
2% MWCNTs						**15.81**	**3.28**
5MWCNT	850C	2	50	500	Diamond	16.88	
5MWCNT	850C	2	50	500	Diamond	15.93	
5MWCNT	850C	2	50	500	Diamond	10.88	
5MWCNT	850C	2	50	500	Diamond	8.86	
5MWCNT	850C	2	50	500	Diamond	11.28	
5MWCNT	850C	2	50	500	Diamond	8.51	
5MWCNT	850C	2	50	500	Diamond	17.81	
5MWCNT	850C	2	50	500	Diamond	7.96	
5MWCNT	850C	2	50	500	Diamond	8.10	
5MWCNT	850C	2	50	500	Diamond	7.89	
5% MWCNTs						**11.41**	**3.97**
10MWCNT	850C	2	50	200	Diamond	6.94	
10MWCNT	850C	2	50	200	Diamond	2.47	
10MWCNT	850C	2	50	200	Diamond	5.67	
10MWCNT	850C	2	50	200	Diamond	4.78	
10MWCNT	850C	2	50	200	Diamond	6.98	
10MWCNT	850C	2	50	200	Diamond	5.03	
10MWCNT	850C	2	50	200	Diamond	3.17	
10MWCNT	850C	2	50	200	Diamond	4.51	
10 MWCNT	850C	2	50	200	Diamond	3.15	
10 MWCNT	850C	2	50	200	Diamond	1.70	
10% MWCNTs						**4.44**	**1.80**

Notes:
[1]Micromet 5101 instrument measurement units

Appendix C.4 Oxidation Calculations

Oxidation calculations were derived from the ratio of net weight loss per sample following the sintering process and an estimated MWCNT oxidization loss from the outer 0.8mm sample surface. The post sintered MWCNT composition represents an estimated final concentration of MWCNTs within the sample during testing.

Post Sintering Disk Measurements at 1000°C		
Average Total Disk Diameter	0.71	inches
Average Total Disk Height	0.22	inches
Oxidized Ring Thickness	0.03	inches
Oxidized Ring Thickness	0.80	mm
Unoxidized Diameter	0.65	inches
Unoxidized Height	0.16	inches
Area		
Total Disk Area	0.39	inches^2
Unoxidized Disk Area	0.33	inches^2
Oxidized Disk Area	0.07	inches^2
Volume		
Total Volume	0.09	inches^3
Unoxidized Volume	0.05	inches^3
Oxidized Volume	0.04	inches^3

Pre-sintered MWCNT Composition	Pre-sintered MWCNT weight (g)	Estimated post-sintered MWCNT weight (g)	Measured post-sintered composite weight loss (g)	Measured post-sintered MWCNT weight (g)	Post-sintered unoxidized composite mass (g)	Post-sintered MWCNT Composition
0 wt%	0.00	0.00	0.10	-0.10	1.62	**0.00%**
1 wt%	0.03	0.01	0.01	0.00	1.66	**0.74%**
2 wt%	0.06	0.02	0.11	-0.09	1.56	**1.57%**
4 wt%	0.12	0.05	0.16	-0.11	1.50	**3.26%**
5 wt%	0.15	0.06	0.34	-0.28	1.50	**4.09%**
8 wt%	0.24	0.10	0.29	-0.19	1.50	**6.51%**
10 wt%	0.30	0.12	0.36	-0.24	1.45	**8.44%**

Assumptions:
Depth of MWCNT oxidation is 0.8mm in all samples
Post sintering weight loss of pure Bioglass is confined to outer shell

Appendix C.4 Oxidation Calculations

Post Sintering Disk Measurements at 850°C		
Average Total Disk Diameter	0.71	inches
Average Total Disk Height	0.22	inches
Oxidized Ring Thickness	0.03	inches
Oxidized Ring Thickness	0.80	mm
Unoxidized Diameter	0.64	inches
Unoxidized Height	0.16	inches
Area		
Total Disk Area	0.39	inches^2
Unoxidized Disk Area	0.32	inches^2
Oxidized Disk Area	0.07	inches^2
Volume		
Total Volume	0.09	inches^3
Unoxidized Volume	0.05	inches^3
Oxidized Volume	0.04	inches^3

Pre-sintered MWCNT Composition	Pre-sintered MWCNT weight (g)	Estimated post-sintered MWCNT weight (g)	Measured post-sintered composite weight loss (g)	Measured post-sintered MWCNT weight (g)	Post-sintered unoxidized composite mass (g)	Post-sintered MWCNT Composition
0 wt%	0.00	0.00	0.10	-0.14	1.58	**0.00%**
1 wt%	0.03	0.01	0.01	-0.08	1.60	**0.80%**
2 wt%	0.06	0.02	0.11	-0.27	1.42	**1.78%**
4 wt%	0.12	0.05	0.16	-0.28	1.35	**3.77%**
5 wt%	0.15	0.06	0.34	-0.11	1.45	**4.39%**
8 wt%	0.24	0.10	0.29	-0.19	1.31	**7.77%**
10 wt%	0.30	-[1]	-	-	-	-

Notes:

[1] Sample fractured before testing

Depth of MWCNT oxidation is 0.8mm in all samples

Post sintering weight loss of pure Bioglass is confined to outer shell

APPENDIX D: Photographic Log

APPENDIX D – Photographic Log

Figure D.1: 5wt% MWCNTs and Bioglass in 3-inch diameter zirconia bowl in preparation for ball mill mixing

Figure D.2: Retsch ball mill used for mixing MWCNT and Bioglass compositions

APPENDIX D – Photographic Log

Figure D.3: 5wt% MWCNT composite material after high energy ball mill mixing

Figure D.4: Profile view of die used for sample compression

APPENDIX D – Photographic Log

Figure D.5: Compression die with Bioglass composite sample prepared for 30,000 pound compression force

Figure D.6: Compressing samples in hydraulic press

APPENDIX D – Photographic Log

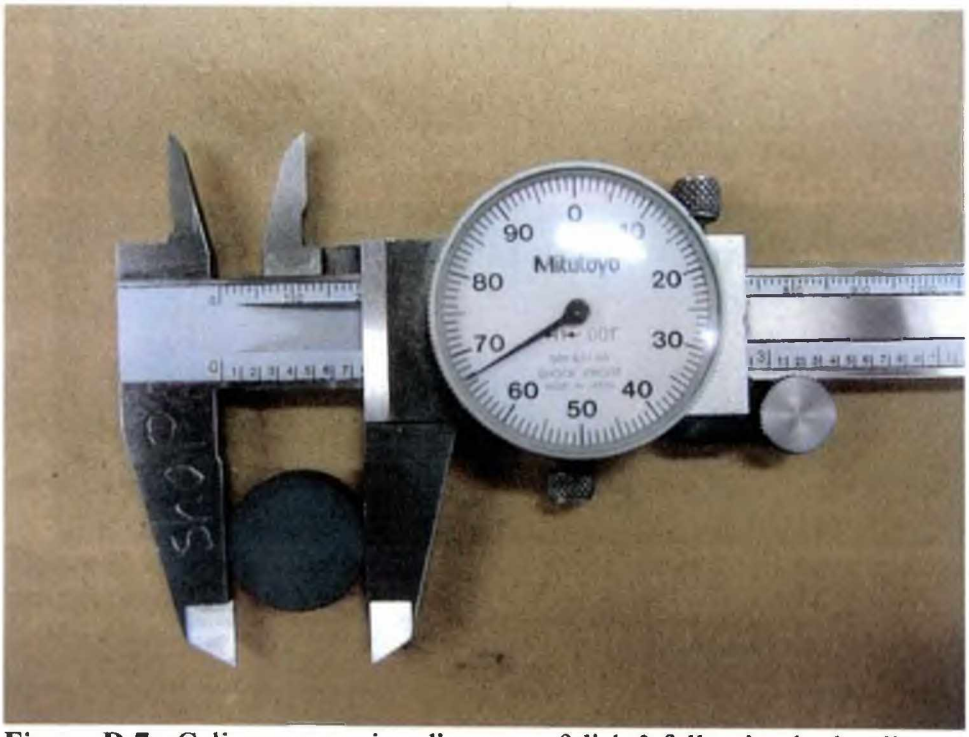

Figure D.7: Caliper measuring diameter of disk 3 following hydraulic compression

Figure D.8: Close up of disk 3 following hydraulic compression

APPENDIX D – Photographic Log

Figure D.9: MWCNT and Bioglass composite samples following hydraulic compression

Figure D.10: Control panel for Lucifer sintering furnace with argon environment

APPENDIX D – Photographic Log

Figure D.11: Lucifer sintering furnace

Figure D.12: View inside Lucifer sintering furnace

APPENDIX D – Photographic Log

Figure D.13: Pressed samples on firebrick prepared for sintering

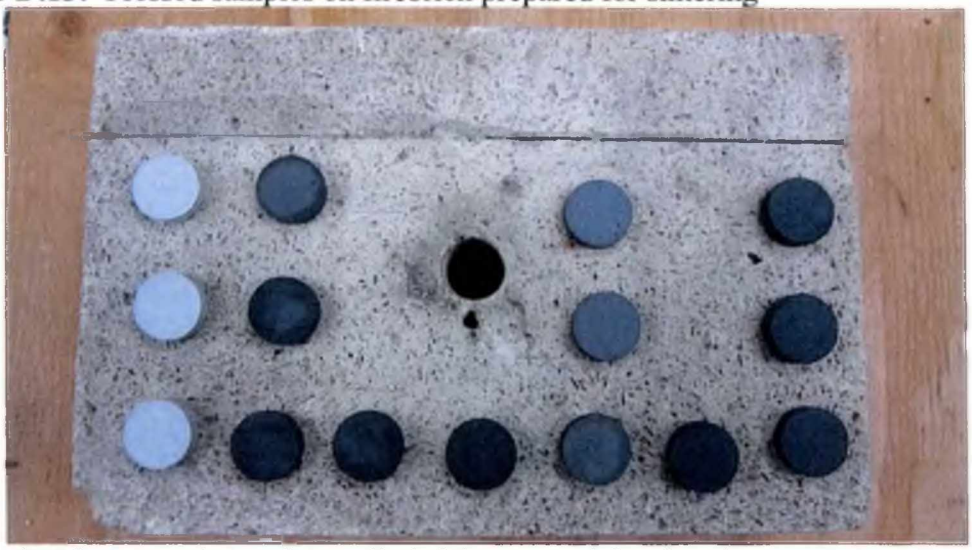

Figure D.14: Pressed samples on firebrick prepared for sintering

APPENDIX D – Photographic Log

Figure D.15: Samples placed in furnace prior to sintering. Indicator MWCNTs placed with samples to indicate nanotube integrity during sintering process

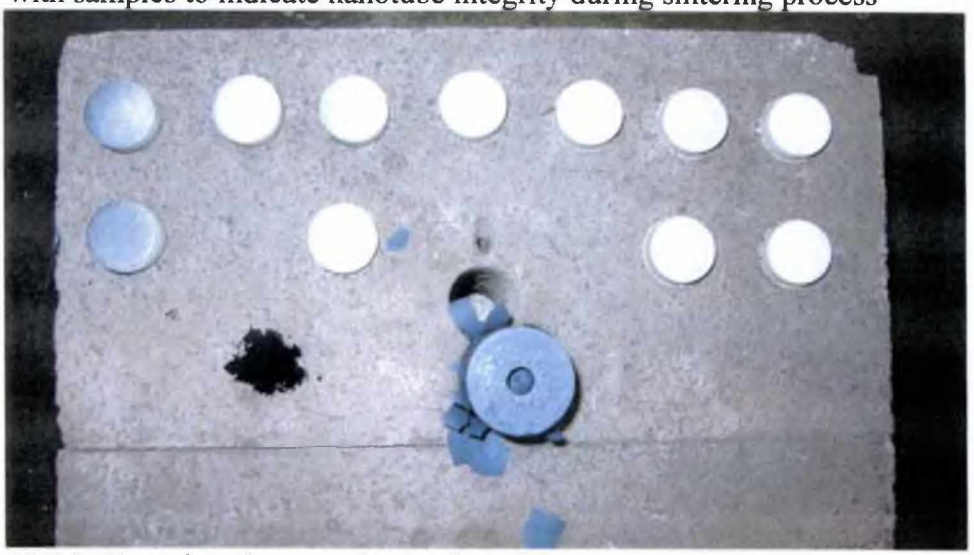

Figure D.16: Post sintering samples on firebrick

APPENDIX D – Photographic Log

Figure D.17: Cracks developed during processing and sintering at 850°C

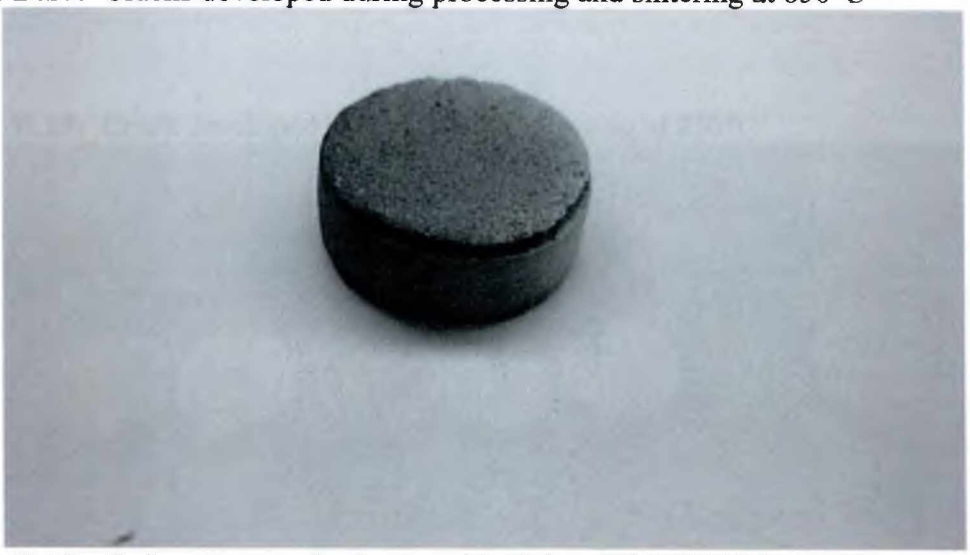

Figure D.18: Defects in samples larger with higher wt% MWCNTs

APPENDIX D – Photographic Log

Figure D.19: Crack developed in sample after sintering at 850°C

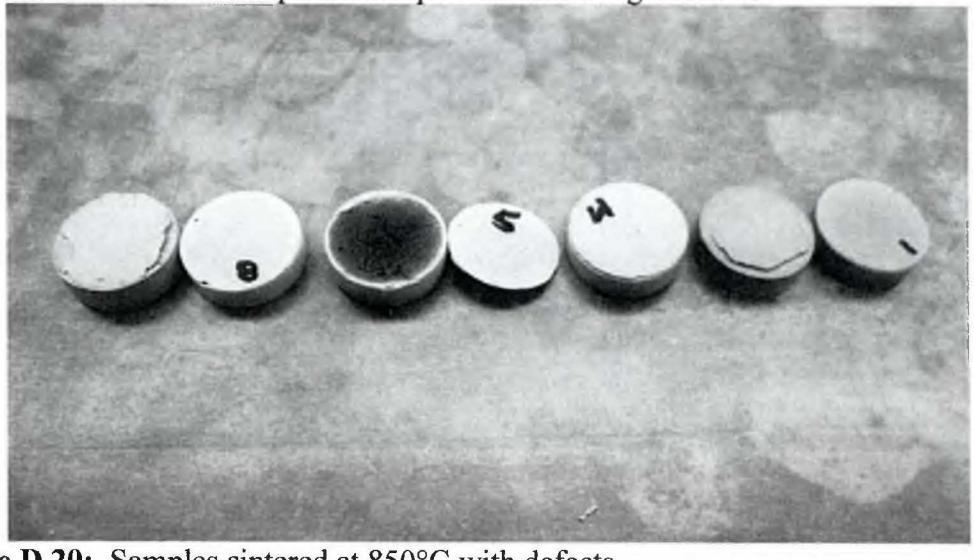

Figure D.20: Samples sintered at 850°C with defects

APPENDIX D – Photographic Log

Figure D.21: Pure Bioglass sample sintered at 850°C

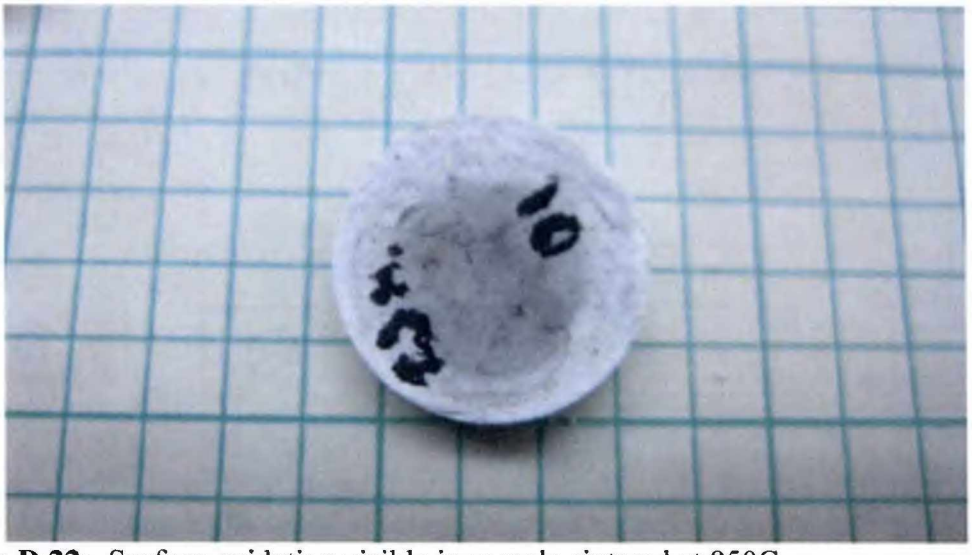

Figure D.22: Surface oxidation visible in sample sintered at 850C

APPENDIX D – Photographic Log

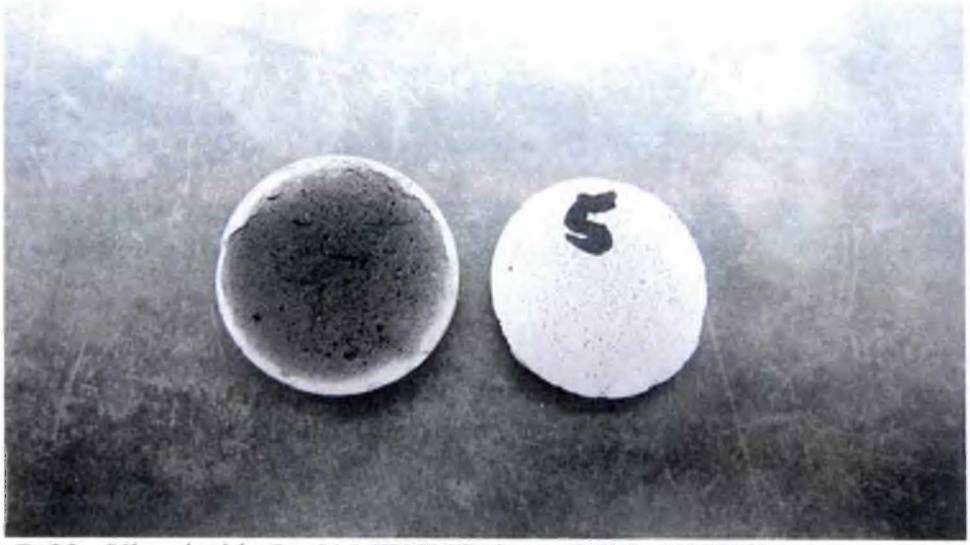

Figure D.23: View inside 5wt% MWCNT sintered disk at 850°C

Figure D.24: Samples mounted in epoxy for grinding, polishing, and testing

APPENDIX D – Photographic Log

Figure D.25: EcoMet 3 polisher with samples

Figure D.26: Polishing samples for testing

APPENDIX D – Photographic Log

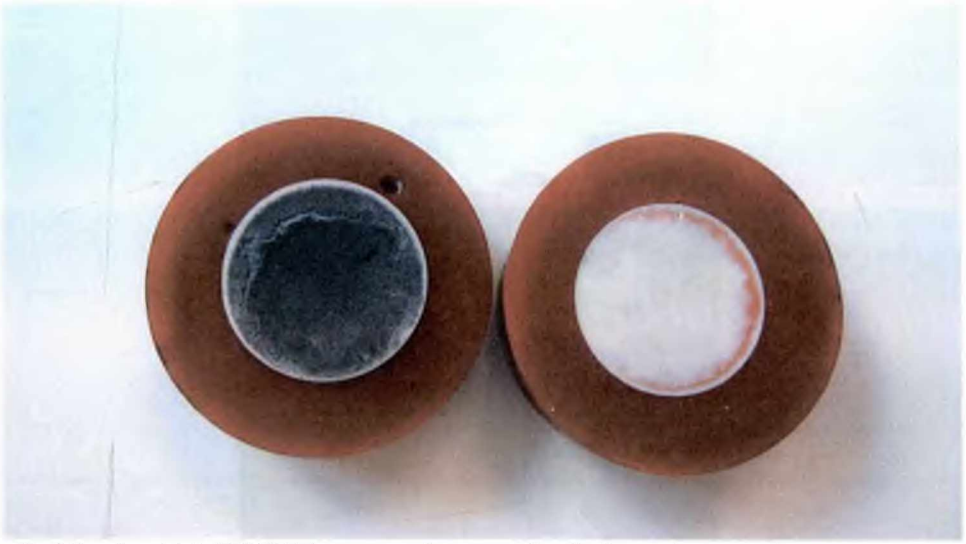

Figure D.27: 4wt% MWCNT composite sample (left) and pure Bioglass (right) sintered at 1000°C. Oxidation ring is visible on the outer perimeter of the composite sample

APPENDIX D – Photographic Log

Figure D.28: Buehler hardness tester with sample at 50x magnification

Figure D.29: Close up view of hardness testing with 500g force

APPENDIX D – Photographic Log

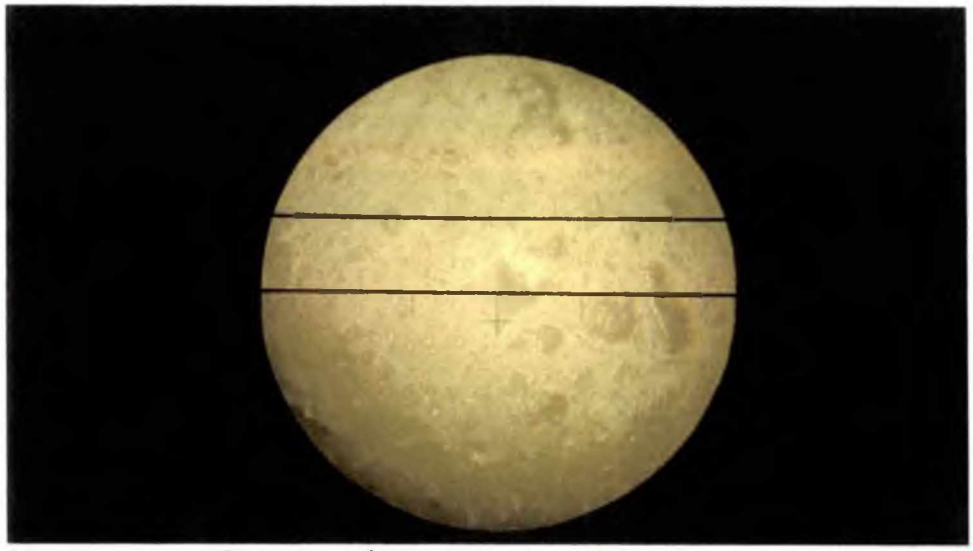

Figure D.30: 0wt% MWCNT and Bioglass composition sintered at 1000°C sample 01 showing vertical cracking following 500g indentation force and seen at 50x magnification. Field of view diameter is 0.29mm.

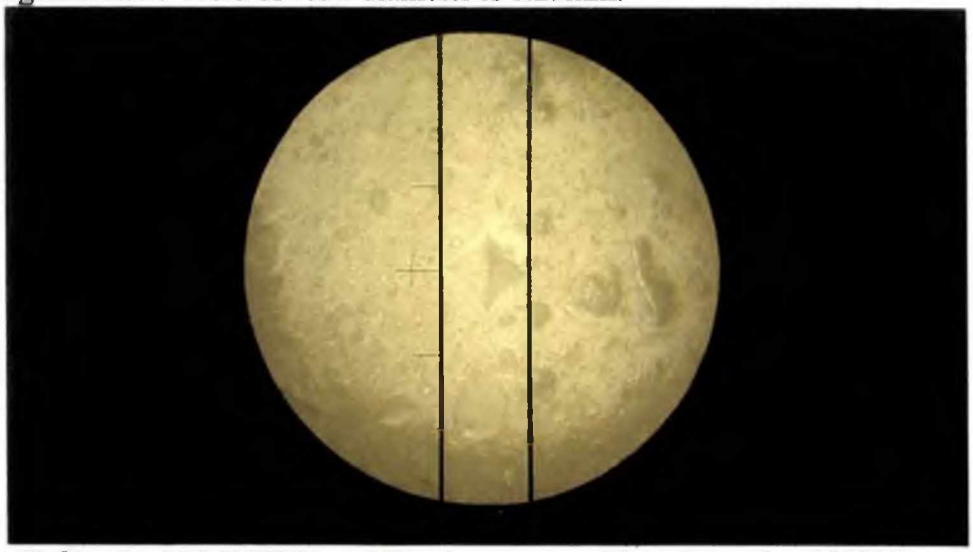

Figure D.31: 0wt% MWCNT and Bioglass composition sintered at 1000°C sample 02 showing indentation width following 500g indentation force and seen at 50x magnification. Field of view diameter is 0.29 mm

APPENDIX D – Photographic Log

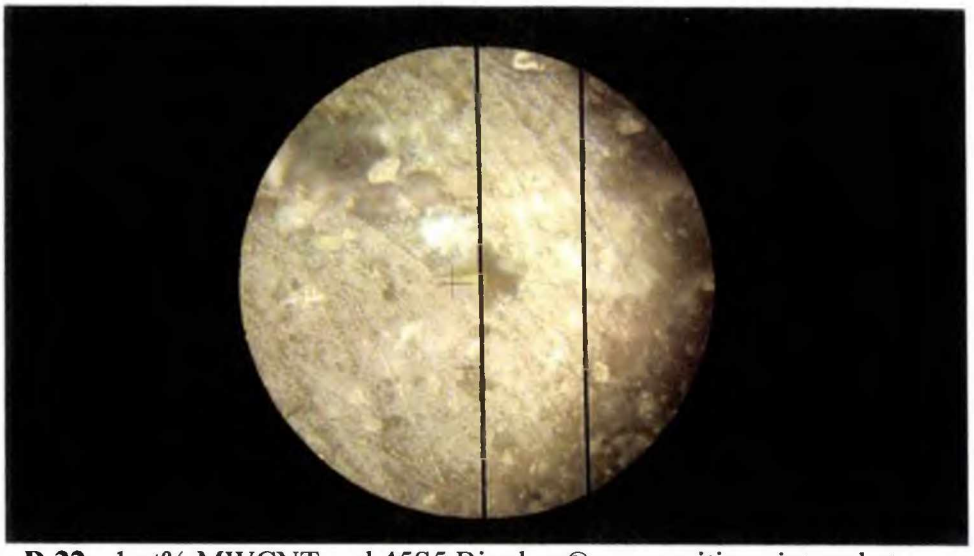

Figure D.32: 1wt% MWCNT and 45S5 Bioglass® composition sintered at 1000°C sample 01 showing horizontal cracking following 500g indentation force and seen at 50x magnification. Field of view diameter is 0.29 mm

Figure D.33: 1wt% MWCNT and Bioglass composition sintered at 1000°C sample 01 showing horizontal cracking following 500g indentation force and seen at 50x magnification. Field of view diameter is 0.29 mm

APPENDIX D – Photographic Log

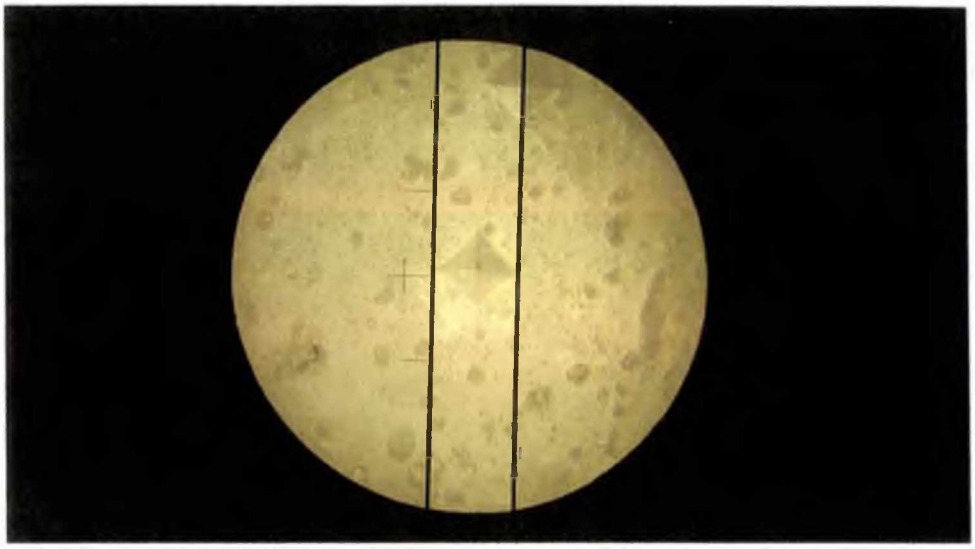

Figure D.34: 1wt% MWCNT and Bioglass composition sintered at 1000°C sample 02 showing indentation width following 500g indentation force and seen at 50x magnification. Field of view diameter is 0.29 mm

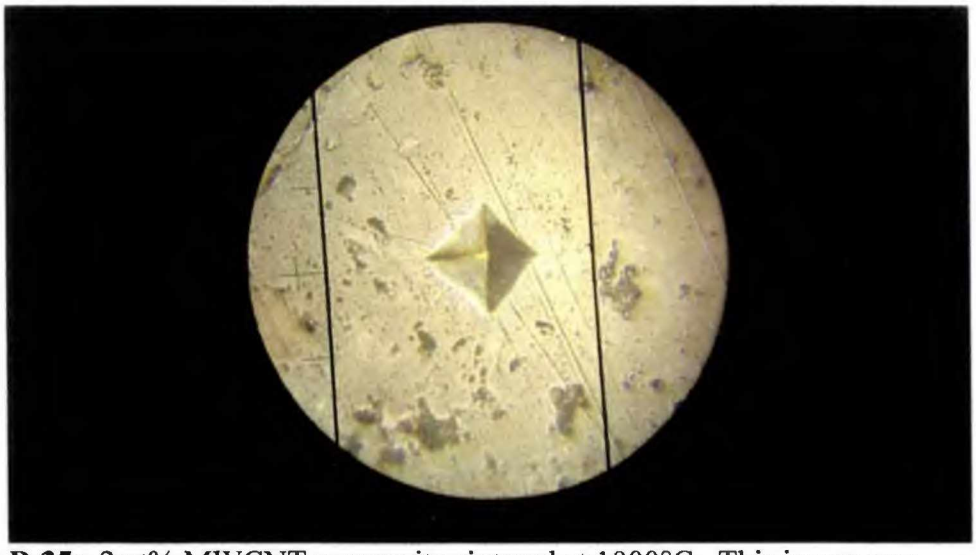

Figure D.35: 2wt% MWCNT composite sintered at 1000°C. This image was taken at 50x magnification and shows non uniform horizontal cracking following 500g indentation force. Field of view diameter is 0.29 mm

APPENDIX D – Photographic Log

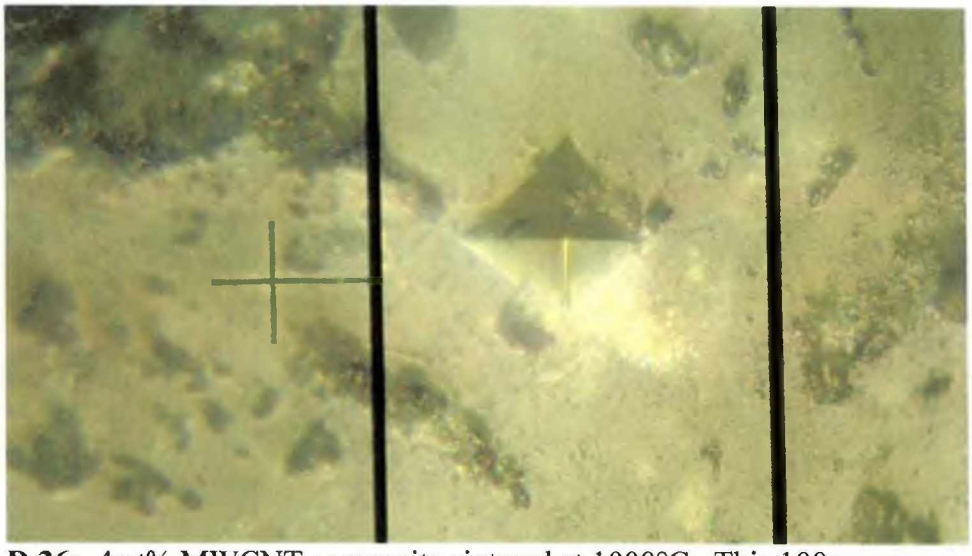

Figure D.36: 4wt% MWCNT composite sintered at 1000°C. This 100x magnified image shows minor horizontal cracking following 200g indentation force. Horizontal field of view is 0.27 mm

Figure D.37: 5wt% MWCNT and Bioglass composition sintered at 1000°C showing surface details and seen at 50x magnification. Field of view diameter is 0.29 mm

APPENDIX D – Photographic Log

Figure D.38: 8wt% MWCNT and Bioglass composition sintered at 1000°C showing surface texture and seen at 50x magnification. Field of view diameter is 0.29 mm

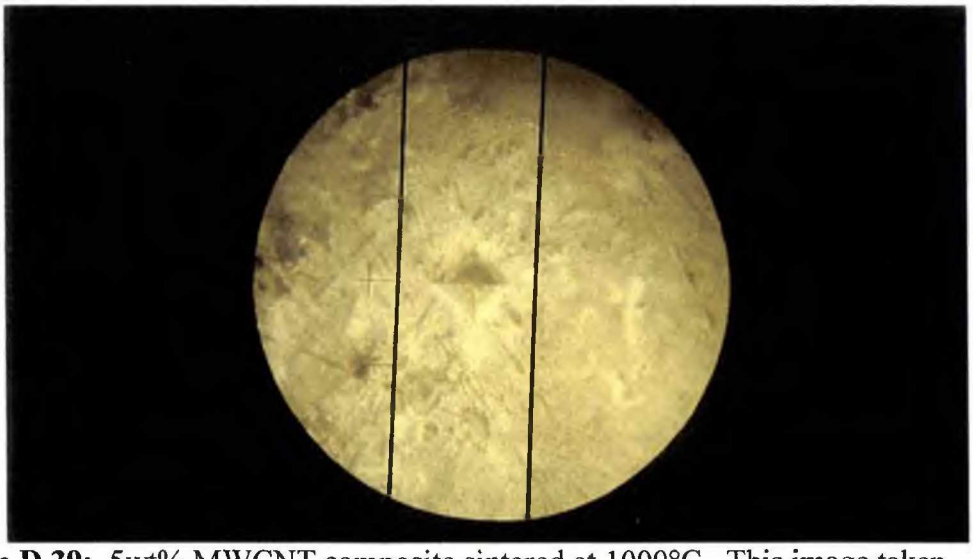

Figure D.39: 5wt% MWCNT composite sintered at 1000°C. This image taken at 50x magnification shows very little cracking in response to the 200g force indentation. Field of view diameter is 0.29 mm

APPENDIX D – Photographic Log

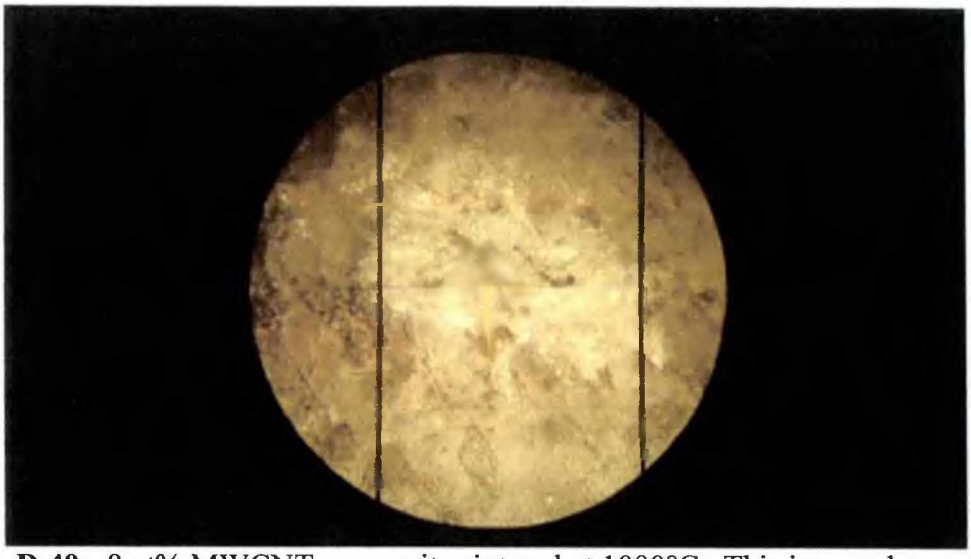

Figure D.40: 8wt% MWCNT composite sintered at 1000°C. This image shows the indentation resulting from a 200g force at 50x magnification. Field of view diameter is 0.29 mm

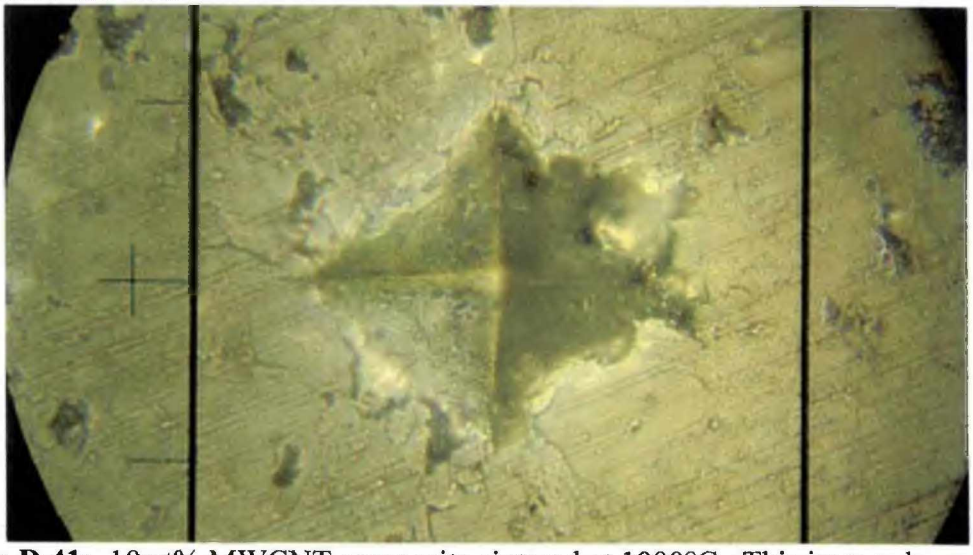

Figure D.41: 10wt% MWCNT composite sintered at 1000°C. This image shows cracking and deformation along the indentation edges at 65x magnification following the200g applied force. Horizontal field of view is 0.26 mm

APPENDIX D – Photographic Log

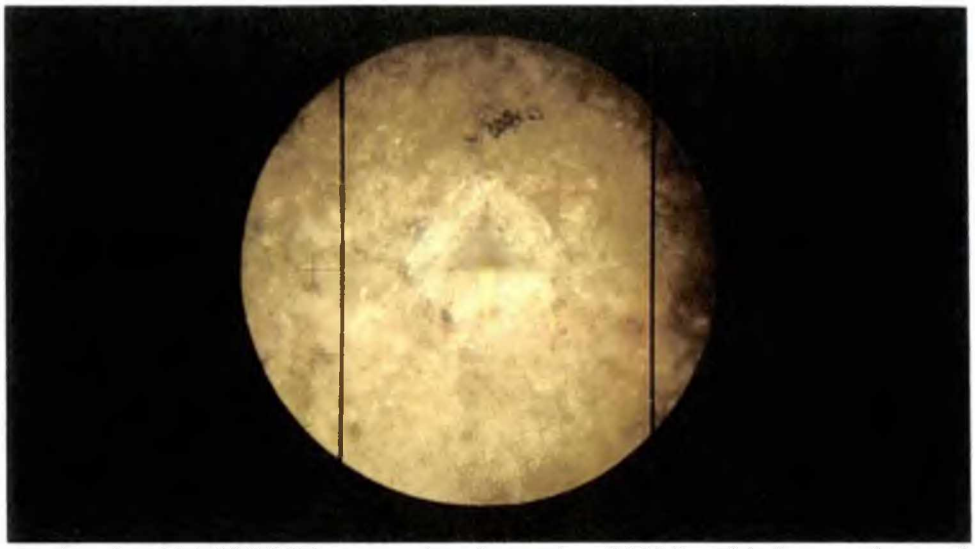

Figure D.42: 1wt% MWCNT composite sintered at 850°C. This image shows the indentation and cracking which followed the application of a 500g force at 50x magnification. Field of view diameter is 0.29 mm

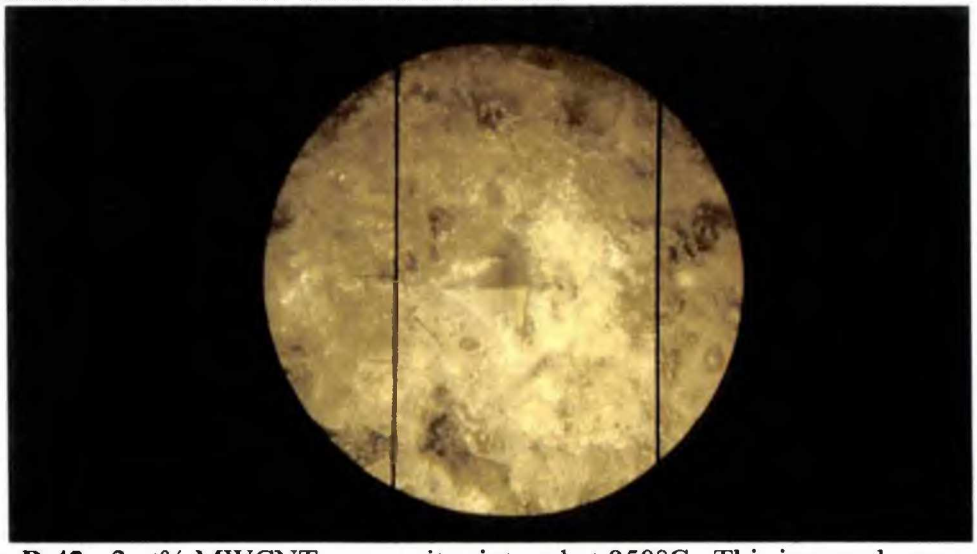

Figure D.43: 2wt% MWCNT composite sintered at 850°C. This image shows the indentation following 500g force and at 50x magnification. Field of view diameter is 0.29 mm

APPENDIX D – Photographic Log

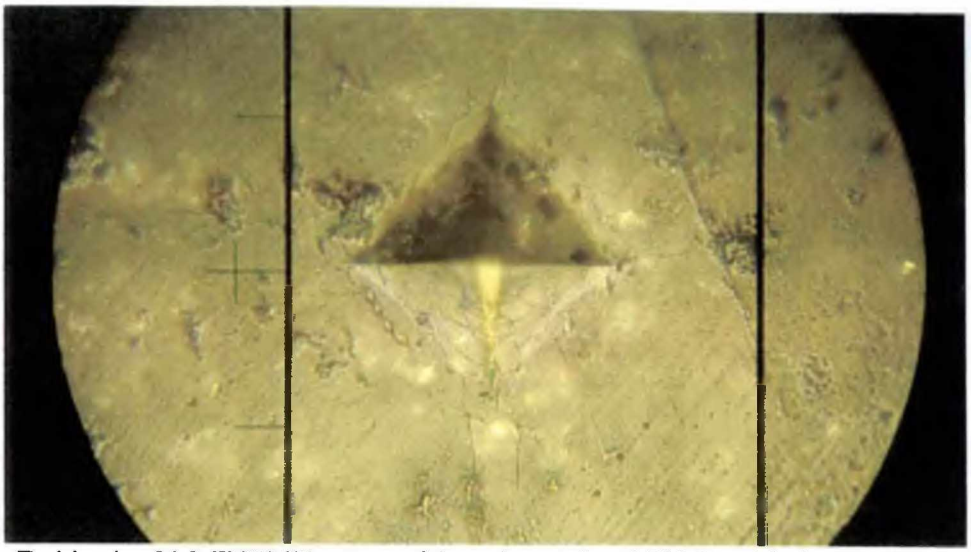

Figure D.44: 4wt% MWCNT composition sintered at 850°C. This image shows the indentation and cracking as a result of 500g force at 60x magnification. Field of view diameter is 0.29 mm

Figure D.45: 5wt% MWCNT composite sintered at 850°C. This image shows a 75x view of indentation and cracking caused by a 200g force. Horizontal field of view is 0.20 mm

APPENDIX D – Photographic Log

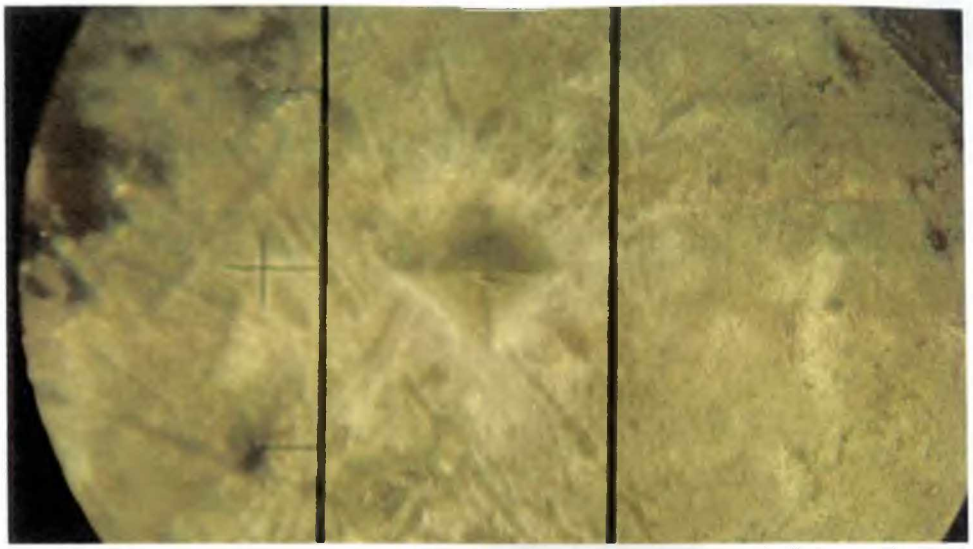

Figure D.46: 10wt% MWCNT composite sintered at 850°C. This image shows the indentation following 200g applied force at 50x magnification. Field of view is 0.28 mm

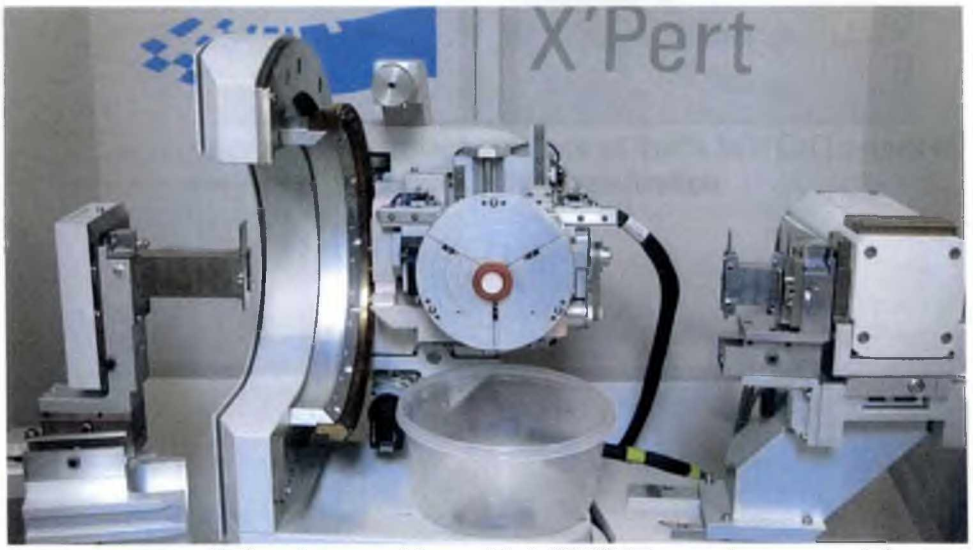

Figure D.47: X-Ray diffraction machine with MWCNT sample mounted for Analysis

APPENDIX D – Photographic Log

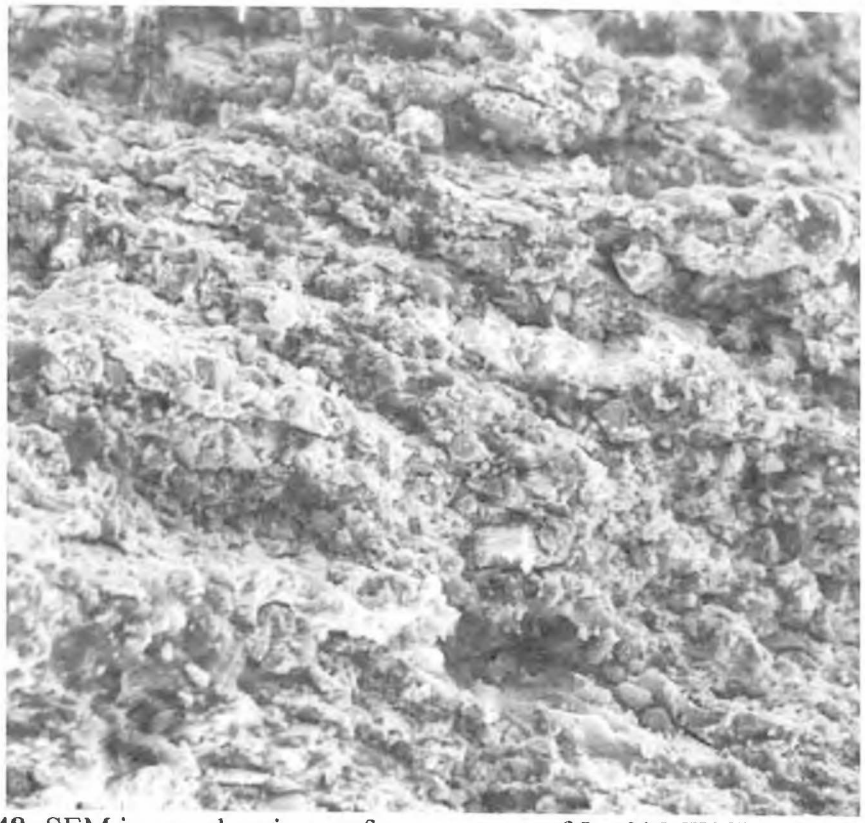

Figure D.48: SEM image showing surface structure of 8wt% MWCNTs sintered at 850°C. Field of view is 500 μm seen at 200x magnification